

3D-CRT vs. IMRT Technique – A Comparative Study In Breast Cancer Patients

José Mesquita

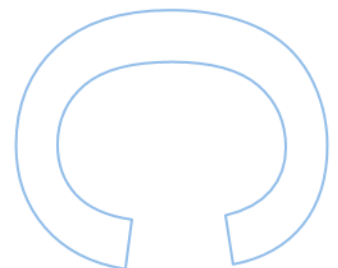
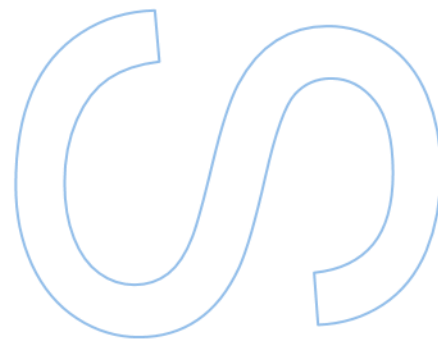
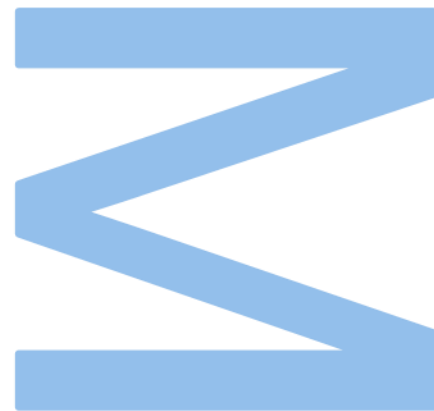
MSc in Medical Physics
Department of Physics and Astronomy
2021/2022

Supervisor

Anabela Gregório Dias, Assistente de Saúde, Instituto Português de Oncologia do Porto Francisco Gentil, EPE

Co-supervisor

Joana Lencart, Assessora de Saúde – Especialista em Física Médica, Instituto Português de Oncologia do Porto Francisco Gentil, EPE





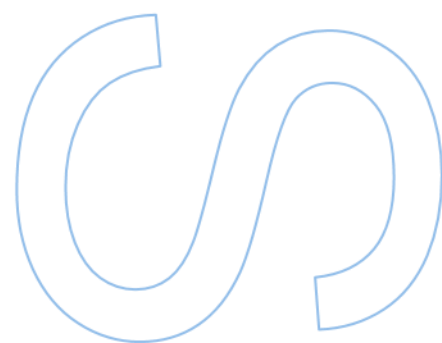
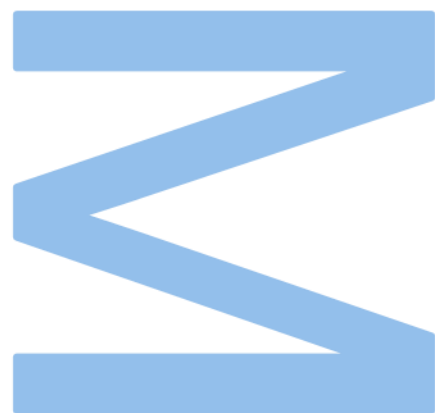
IPO PORTO
INSTITUTO PORTUGUÊS DE
ONCOLOGIA DO PORTO FG, EPE



Todas as correções determinadas
pelo júri, e só essas, foram efetuadas.

O Presidente do Júri,

Porto, ____/____/____



Sworn statement

I, José Carlos Cortês Mesquita, enrolled in the Master Degree in Medical Physics at the Faculty of Sciences of the University of Porto hereby declare, in accordance with the provisions of paragraph a) of Article 14 of the Code of Ethical Conduct of the University of Porto, that the content of this dissertation reflects perspectives, research work and my own interpretations at the time of its submission.

By submitting this dissertation, I also declare that it contains the results of my own research work and contributions that have not been previously submitted to this or any other institution.

I further declare that all references to other authors fully comply with the rules of attribution and are referenced in the text by citation and identified in the bibliographic references section. This dissertation does not include any content whose reproduction is protected by copyright laws.

I am aware that the practice of plagiarism and self-plagiarism constitute a form of academic offense.

José Carlos Cortês Mesquita

November 15th, 2022

Acknowledgements

This work wouldn't have come to fruition if my supervisor, Anabela Dias, my co-supervisor, Joana Lencart, and dosimetrists Nuno Pereira and Rita Pinho from IPO-Porto weren't so supportive throughout the entire process. I always felt welcome there and was encouraged to reach out to them for help. Besides that, I was given the opportunity to attend the European Congress in Medical Physics (Professor João also helped a lot and I want to thank him!) with an e-poster of our work, which was a very interesting experience that wouldn't have happened without their help. To them, HUGE THANKS; this is OUR work and, hopefully, an enriching one for all. Hopefully, we will continue this work and it will bring us good results and joy. Also, I want to thank Guilherme Campos for helping me with a software I was completely unfamiliarized with, making the whole experience much less complicated, and for providing his own time and resources to accelerate a process otherwise too slow to complete in useful time. In addition, I believe every professor taught me something in one capacity or another and all that culminated in who I was and what I knew about related subjects, making them also part of this work in an indirect way; I want to thank them and also highlight Professor Pedro Teles for his position as director of this masters program.

On a more personal note, I want to thank my close family, namely my mother, my father, my stepbrother, and stepmother; they made this possible. Also, thank you to every friend that was involved in my life in some way, for this past year.

Lastly, heartfelt thanks to my longtime friend Jorge, for being a constant and joyful presence in my life, for being the goofiest friend and such a delight to have around; to Daniela, who always has the nicest words to say, for being so close, kind, reassuring, and the best partner for a cup of tea; to Sofia, who was readily available to cheer me up and hold me during the hazy beginning of a dissertation, and her cat Mila, the prettiest creature alive; to Margarida, whom I met in this masters degree and quickly became a very present and kind partner, helpful, cheerful and the person I knew I could always count on; and to my therapist Margarida, for being a wonderful professional and an indispensable source of insight, encouragement and thoughtful sweet words that helped me take care of my mental health. All of them made me stand my ground and obliterated traces of Imposter Syndrome that would sneak up among insecurities, keeping me motivated and preventing me from sinking in despair.

Resumo

Várias técnicas de radioterapia para o tratamento conservador do cancro da mama são utilizadas, desde radioterapia conformal à radioterapia de intensidade modulada e de arco volumétrico. A 3D-CRT é a técnica mais comum para esse tipo de tratamento, mas não consegue o mesmo grau de cobertura do alvo possibilitado pelas mais modernas IMRT e VMAT e resulta em mais pontos quentes. Em contrapartida, a IMRT não é tão eficaz a poupar as regiões fora do alvo, que incluem os órgãos em risco, da absorção de baixas doses que pode potenciar malignidades induzidas por radiação. Numa tentativa de evitar estes aspetos negativos, uma técnica híbrida que funde campos de 3D-CRT e de IMRT foi desenvolvida. Planos 3D-CRT, IMRT e HT foram calculados para 20 doentes e os DVH e parâmetros dosimétricos foram comparados entre as três técnicas. Todos os 60 planos foram simulados no PRIMO e os DVH e parâmetros dosimétricos foram extraídos do software e comparados com os do TPS. Após a análise verificou-se um problema com os planos HT que envolviam cunha, o que levou ao comprometimento dos resultados do PRIMO referentes aos volumes alvo, tornando-os inconclusivos e não confiáveis. No sentido de apurar essa questão, um exemplo de um doente para quem foram calculados um plano sem cunha e um plano com cunha foi examinado para especificar que efeitos a presença de cunha pode ter na absorção de dose calculada pelo PRIMO. A HT apresenta-se como uma técnica que poderia ser implementada na prática clínica para doentes com critérios específicos.

Palavras-chave: cancro da mama, radioterapia, dose, 3D-CRT, IMRT, HT, TPS, PRIMO, DVH, homogeneidade, conformidade, órgãos em risco, PTV, CTV.

Abstract

There are several radiotherapy techniques for conservative breast cancer treatment, ranging from conformal radiotherapy to intensity modulated and volumetric arc. 3D-CRT is the most common technique for such treatments but lacks the degree of target coverage provided by the modern IMRT and VMAT and results in more *hot spots*. On the other hand, IMRT is not as good at sparing the non-target regions, including the OAR, from low dose absorption which may lead to radiation-induced malignancies. In an attempt to avoid these downsides, an hybrid technique fusing 3D-CRT and IMRT fields was designed. 3D-CRT, IMRT and HT plans were calculated for 20 patients and the DVH and dosimetric parameters were compared among the three techniques. All the 60 plans were simulated in PRIMO and DVH and dosimetric parameters were extracted from the software and further compared with the TPS outcome. An issue with HT plans which had wedges was found and that problem compromised the results regarding the target volumes results from PRIMO, making them unreliable and inconclusive; an example of a patient for whom a plan without wedge and one plan with wedge were calculated was examined to pinpoint exactly which effects in the absorbed dose as simulated by PRIMO the presence of a wedge can have. The HT seems to be a technique that could be implemented for clinical practice for patients with some specific criteria.

Keywords: breast cancer, radiotherapy, dose, 3D-CRT, IMRT, HT, TPS, PRIMO, DVH, dosimetric parameter, homogeneity, conformity, OAR, PTV, CTV.

Table of contents

Acknowledgements	i
Resumo	ii
Abstract	iii
List of figures	vi
List of graphs	viii
List of tables	x
List of abbreviations	xi
1 Introduction.....	1
1.1 Motivation and Purpose	1
1.2 Layout.....	1
2 Background	2
2.1 Overall picture of breast cancer.....	2
2.1.1 Demographics and Causes.....	2
2.1.2 Treatment.....	4
2.2 General Standards of Modern Radiotherapy.....	5
2.2.1 Ultimate Goal of a Radiotherapy Treatment and Concepts of Structure Volumes and Dose-Volume Histogram.....	5
2.2.2 Three-Dimensional Conformal Radiation Therapy (3D-CRT).....	10
2.2.3 Intensity Modulated Radiation Therapy (IMRT)	10
2.2.4 Volumetric Modulated Arc Therapy (VMAT).....	13
2.2.5 Hybrid Technique (HT)	14
2.3 Tools	16
2.3.1 Treatment Planning System (TPS).....	16
2.3.2 PRIMO.....	18
3 Materials and Methods	21
3.1 Materials	21
3.2 First Stage – TPS’s DVH Comparison.....	21
3.2.1 Planning	21
3.2.2 Analysis Procedure	23
3.3 Second Stage – TPS vs. PRIMO Comparison.....	27
3.3.1 Simulations	27
3.3.2 Analysis Procedure	31
4 Results and discussion.....	32

4.1 Results.....	32
4.1.1 TPS	32
4.1.2 PRIMO.....	44
4.1.3 TPS vs. PRIMO.....	55
4.2 Discussion.....	66
4.2.1 TPS	66
4.2.2 PRIMO.....	67
4.2.3 Comparison with the literature.....	69
4.2.4 TPS vs. PRIMO.....	71
4.2.5 The wedge issue.....	72
5 Conclusions and future work	76
References	78
Attachments.....	81
1. TPS results	81
2. PRIMO results.....	83
3. ECMP e-poster	85

List of figures

1 Estimated age-standardized incidence rates per 100 000 of breast cancer in women, by country, in 2020.	2
2 Estimated age-standardized mortality rates per 100 000 of breast cancer in women, by country, in 2020.	2
3 Estimated number of prevalent cases of cancer in women (diagnosed 5 years prior to the statistic assessment), by cancer site, in 2020.	3
4 Registered new cases, deaths and 5-year prevalence in Portugal, 2020, of the 5 most incident cancer types.	3
5 Tumour Control Probability (TCP) and Normal Tissue Complication Probability (NTCP) curves as a function of radiation dose.	6
6 Volume structures on a whole-breast irradiation treatment plan.	7
7 Differential and cumulative dose-volume histograms.	8
8 Dose distributions for two plans.	9
9 Beam dose profile comparison between CRT and IMRT.	11
10 Examples of low and high dose homogeneities and conformities.	11
11 Traditional and IMRT optimization processes workflow.	13
12 IMRT plan for breast cancer treatment, Eclipse.	17
13 Geometry of Varian Clinac 2100 C/D.	18
14 Phase-space and dose profile, PRIMO.	19
15 Different views of geometry, PRIMO.	20
16 Text file exported from Eclipse, plan info.	23
17 Text file exported from Eclipse, DVH.	24
18 DVH data, .csv format.	24
19 Paddick’s proposal for conformity index.	26
20 Defining water tank phantom in PRIMO.	27

21 Dose calibration window, PRIMO.	28
22 DICOM Image import window.	29
23 DICOM Structure import window.	29
24 DICOM RT plan import window; Variance Reduction; Configuration.	30
25 PRIMO procedure flowchart.	30
3.1 ECMP 2022 e-poster of this work.	85

List of graphs

1 Mean DVH of all structures, three techniques. TPS.	32
2 Mean DVH of PTV and CTV, three techniques. TPS.	33
3 Mean DVH of OAR, three techniques. TPS.	34
4 Box plots of PTV results. TPS.	35
5 Box plots of PTV results. TPS.	36
6 Box plots of CTV results. TPS.	37
7 Box plots of heart results. TPS.	38
8 Box plots of contralateral breast results. TPS.	39
9 Box plots of ipsilateral lung results. TPS.	40
10 Box plots of lungs results. TPS.	41
11 Box plots of spinal canal results. TPS.	42
12 Box plots of liver results. TPS.	42
13 Box plots of CI and HI results. TPS.	43
14 Box plots of MU results. TPS.	43
15 Mean DVH of all structures, three techniques. PRIMO.	44
16 Mean DVH of PTV and CTV, three techniques. PRIMO.	45
17 Mean DVH of OAR, three techniques. PRIMO.	46
18 Box plots of PTV results. PRIMO.	47
19 Box plots of PTV results. PRIMO.	48
20 Box plots of CTV results. PRIMO.	49
21 Box plots of heart results. PRIMO.	50
22 Box plots of contralateral breast results. PRIMO.	51
23 Box plots of ipsilateral lung results. PRIMO.	52
24 Box plots of lungs results. PRIMO.	53

25 Box plots of spinal canal results. PRIMO.54

26 Box plots of liver results. PRIMO.54

27 Box plots of CI and HI results. PRIMO.55

28 Mean DVH of all structures, three techniques. TPS vs. PRIMO.56

29 Mean DVH of PTV and CTV, three techniques. TPS vs. PRIMO.57

30 Mean DVH of OAR, three techniques. TPS vs. PRIMO.58

31 Box plots of PTV results. TPS vs. PRIMO.59

32 Box plots of PTV results. TPS vs. PRIMO.60

33 Box plots of CTV results. TPS vs. PRIMO.61

34 Box plots of heart results. TPS vs. PRIMO.62

35 Box plots of contralateral breast results. TPS vs. PRIMO.63

36 Box plots of ipsilateral lung results. TPS vs. PRIMO.63

37 Box plots of lungs results. TPS vs. PRIMO.64

38 Box plots of spinal canal results. TPS vs. PRIMO.64

39 Box plots of liver results. TPS vs. PRIMO.65

40 Box plots of CI and HI results. TPS vs. PRIMO.65

41 DVH of all structures, HT with and without wedge. TPS vs. PRIMO.73

42 Dose profiles along x from TPS and PRIMO, HT with and without wedge.74

43 Dose profiles along y from TPS and PRIMO, HT with and without wedge.74

44 Dose profiles along z from TPS and PRIMO, HT with and without wedge.75

List of tables

1	Extracted dosimetric parameters.	25
1.1	Dosimetric parameters for the PTV, TPS.	81
1.2	Dosimetric parameters for the CTV, TPS.	81
1.3	Dosimetric parameters for the heart, TPS.	81
1.4	Dosimetric parameters for the contralateral breast, TPS.	81
1.5	Dosimetric parameters for the ipsilateral lung, TPS.	82
1.6	Dosimetric parameters for the lungs, TPS.	82
1.7	Dosimetric parameters for the spinal canal, TPS.	82
1.8	Dosimetric parameters for the liver, TPS.	82
1.9	CI and HI, TPS.	82
1.10	MU, TPS.	82
2.1	Dosimetric parameters for the PTV, PRIMO.	83
2.2	Dosimetric parameters for the CTV, PRIMO.	83
2.3	Dosimetric parameters for the heart, PRIMO.	83
2.4	Dosimetric parameters for the contralateral breast, PRIMO.	83
2.5	Dosimetric parameters for the ipsilateral lung, PRIMO.	84
2.6	Dosimetric parameters for the lungs, PRIMO.	84
2.7	Dosimetric parameters for the spinal canal, PRIMO.	84
2.8	Dosimetric parameters for the liver, PRIMO.	84
2.9	CI and HI, PRIMO.	84

List of abbreviations

3D-CRT Three-Dimensional Conformal Radiation Therapy

IMRT Intensity Modulated Radiation Therapy

VMAT Volumetric Modulated Arc Therapy

HT Hybrid Technique

OAR Organs at risk

DVH Dose-volume histogram

TPS Treatment planning system

PTV Planning target volume

CTV Clinical target volume

GTV Gross tumour volume

ICRU International Commission on Radiation Units

TCP Tumour control probability

NTCP Normal tissue complication probability

CT Computed tomography

MLC Multi-leaf collimators

MU Monitor unit

LINAC Linear particle accelerator

DICOM Digital Imaging and Communication in Medicine Standard

HI Homogeneity index

CI Conformity index

1 Introduction

1.1 Motivation and Purpose

The purpose of this work was to analyse and compare dosimetric aspects, such as conformity and homogeneity in the target volume and discuss the resulting target volumes and OAR's DVH from plans of different techniques, namely: 3D-CRT, IMRT and a hybrid technique HT, for whole-breast irradiation. There was a search for certain worrying patterns, such as the low-dose regions outside the target which result from intensity modulated techniques, and the typical excessive *hot spots* that arise from treatments with 3D-CRT; having said that, there is clearly a balance to be thought carefully and the choice for some treatment modality instead of the others is tightly linked with the patient's health condition and body characteristics. The hybrid technique that was studied seems promising and may be able to gain popularity among tricky clinical cases, as it can be the key to solve the 3D-CRT vs. IMRT dilemma.

1.2 Layout

This work starts by presenting demographic statistics on breast cancer all over the world, zooming in to recent data in Portugal. Causes, symptoms, and treatment are discussed, and general standards of modern radiotherapy are introduced, with notions of important structures to be delineated, concepts of radiotherapy techniques, and useful tools such as planning, and simulation software being described. In later chapters, the materials and the methodology that were used in this work are enumerated and the whole experimental procedure well detailed. Finally, results are analysed and interpreted, and whether the goal of the dissertation was or was not met is assessed.

2 Background

2.1 Overall picture of breast cancer

2.1.1 Demographics and Causes

In 2020, 2.3 million women were diagnosed with breast cancer [Fig. 1] and 685 000 died as a consequence of the disease [Fig. 2], globally, according to WHO – *World Health Organization*¹. Data also points out that at the end of that same year, 7.8 million women who were diagnosed with breast cancer in the past 5 years still had the disease, leading to the conclusion that breast cancer is the world's most prevalent cancer [Fig. 3].

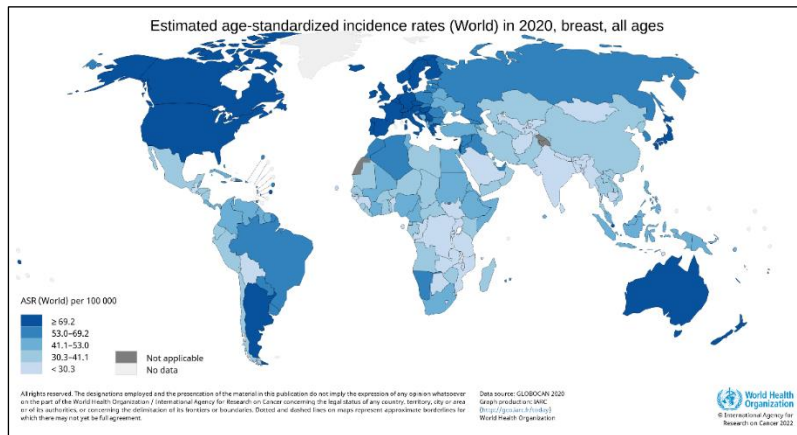


Figure 1 – Estimated age-standardized incidence rates per 100 000 of breast cancer in women, by country, in 2020. There seems to be a link between the development/income of a region, which in turn correlates with the life-expectancy of the population, and the appearance of new breast cancer cases; populations that live longer are more susceptible of having cancer (age is a key cause of the disease).

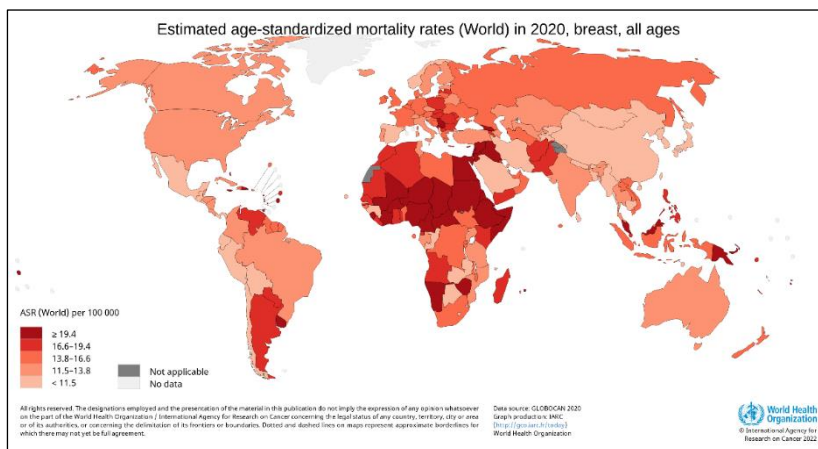


Figure 2 – Estimated age-standardized mortality rates per 100 000 of breast cancer in women, by country, in 2020. More uneducated populations, characteristic of poor and underdeveloped countries, present higher mortality rates due to the lack of access to quality medical resources and lower rates of early diagnoses, which results in late stage/advanced cancers, more difficult to treat.

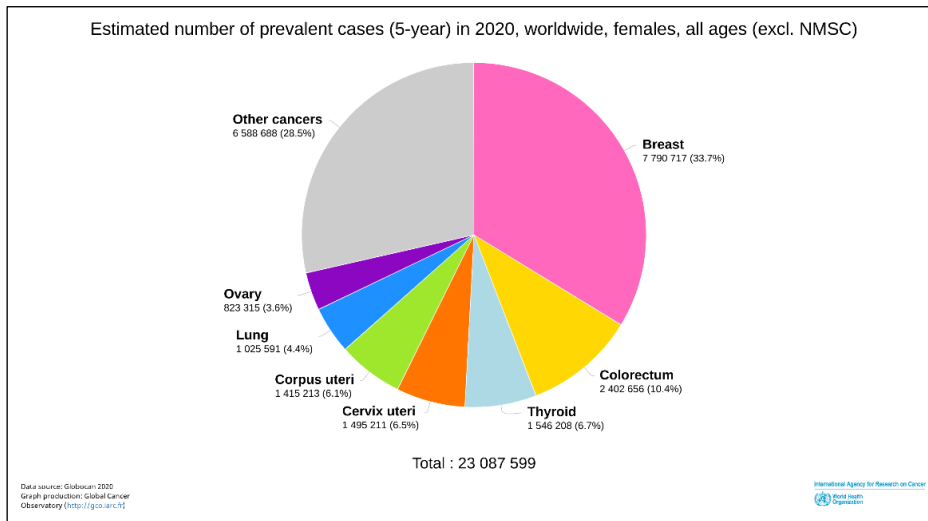


Figure 3 – Estimated number of prevalent cases of cancer in women (diagnosed 5 years prior to the statistic assessment), by cancer site, in 2020. Clearly, breast cancer was the most prevalent cancer in women, with 33.7% of all cancers.

That same year, 7041 new breast cancer cases were registered in Portugal (100% in women), making breast cancer the most incident cancer, 1864 died from the disease and 27051 who were diagnosed 5 years earlier still had the disease (503.49 per 100000) [Fig. 4].

Incidence, Mortality and Prevalence by cancer site										
Cancer	New cases				Deaths				5-year prevalence (all ages)	
	Number	Rank	(%)	Cum.risk	Number	Rank	(%)	Cum.risk	Number	Prop. (per 100 000)
Breast	7 041	1	11.6	7.43	1 864	5	6.2	1.32	27 051	503.49
Prostate	6 759	2	11.2	7.86	1 917	4	6.4	0.71	25 602	530.72
Lung	5 415	3	9.0	2.68	4 797	1	15.9	2.27	6 213	60.93
Colon	5 367	4	8.9	2.29	2 972	2	9.9	0.90	14 809	145.23
Rectum	4 954	5	8.2	2.28	1 303	8	4.3	0.43	14 967	146.78

Figure 4 – Registered new cases, deaths and 5-year prevalence in Portugal, 2020, of the 5 most incident cancer types.

In our local institution, IPO-Porto - *The Portuguese Oncology Institute of Porto Francisco Gentil, EPE*, the latest available report², from 2018, states that 1422 cases of breast cancer out of a total of 7566 malignant tumours were admitted here (18.8% of all cases, the second most incident overall), with 13 of them being diagnosed in men (0.3% of all cases in men) and 1409 in women (38.3% of all cases in women), making the breast the second least incident cancer site in men, only more incident than eye and lacrimal gland cancer (0.2% of all cases in men), and the most incident type of cancer in women, above peritoneum and digestive organs cancer (18.4% of all cases in women). Of those 1422 tumours, 834 were stage-I, 309 stage-II, 141 stage-III, 68 stage-IV and 70 not classified, expressing the highly successful screening program, able to detect the

disease early. Unfortunately, from 2020 onwards, the menacing *SARS-CoV-2* pandemic drove some national health facilities to collapse and forced the Portuguese government and health experts to take precautionary measures and mobilize the majority of attentions to the prevention and treatment of *COVID-19*, leaving many cancer screening programs compromised and those which were not, saw a decrease in attendance due to a generalized sense of dread in the population; this amalgamation of factors led many patients to have their cancers diagnosed in later stages, which is expected to lead to an increase in mortality rate.³

There is evidence of increasing breast cancer incidence rates in **older women**, but precautions should be taken by every woman who have gone past puberty, joining screening programs for early detection of the disease in order to prevent the metastization of the cancer and, therefore, boost the treatment success probability.

The development of breast cancer may be triggered by one's behaviour and lifestyle, but about half of them seem to arise from unavoidable, natural factors such as **sex** (larger incidence in women) and **age** (the disease tends to appear in the adult/elder age group). Obesity, excessive alcohol drinking, family history of breast cancer (despite the lack of such occurrence in the majority of diagnosed cases), age of first pregnancy and age at which menstrual periods began, tobacco use, postmenopausal hormone therapy and **radiation exposure** are risk-enhancing factors; however, even if an effort were made to avoid some of these behaviours, the risk of developing breast cancer would only go down by 30% at most, since sex is, simultaneously, the strongest risk factor and uncontrollable. Specific gene mutations in BRCA1, BRCA2 and PALB-2 are the most dominant incidence risk-enhancing mutations and may require an invasive safety approach, such as a mastectomy. Men make up approximately 0.5-1% of all breast cancers.

2.1.2 Treatment

Breast cancer treatment perspectives are highly positive, with nearly 90% survival rate or more, always benefiting from an early diagnosis. Presently, the first stage of treatment may consist solely of the cancerous lump extraction - **lumpectomy** – if it is diagnosed early and its volume is not considered very large, reducing detrimental aesthetic outcomes; on the other hand, larger tumours most likely require whole-breast removal – **mastectomy**. Following the former (but not exclusively), it is common practice

for the patient to undergo radiation therapy as a means to control the disease (and prevent recurrence), by killing potential residual cancer cells that remain adjacent to the tumour bed and may or may have multiplied and spread to previously healthy tissues, such as the lymph nodes. Suppressing these cells may be achieved by Intraoperative Radiotherapy (IORT), either with photons or electrons, immediately after surgery as a short-range high-dose boost that provides the patient with the benefit of a short-time radiation treatment, in contrast with the standard whole-breast irradiation (WBI) which generally requires weeks of treatment; as stated, post-operative irradiation is not exclusive to breast-conserving surgery cases and irradiation to the chest-wall can be a solution to ensure the same control in patients who had a mastectomy.⁴⁻⁷ Other procedures include extending the removal area to the lymph nodes the cancer can reach, chemotherapy, hormonal treatment and others, but these fall out of the scope of this work. Regarding cancers in advanced stages, radiotherapy may not be able to irradiate the disease, but can prevent the patient from dying from it.

On the following sections, a brief description of the most used external beam radiotherapy (EBRT) techniques in breast cancer treatment, Three-Dimensional Conformal Radiation Therapy (3D-CRT) and Intensity Modulated Radiation Therapy (IMRT), as well as attempts of a hybrid technique (HT) approach will be made, addressing some literary reports on the matter.

2.2 General Standards of Modern Radiotherapy

2.2.1 Ultimate Goal of a Radiotherapy Treatment and Concepts of Structure Volumes and Dose-Volume Histogram

The whole conception of an external radiotherapy treatment, albeit employed following detailed guidelines such as the ones reported by ICRU – *International Commission on Radiation Units*, is susceptible to a certain degree of variability depending on many factors, namely the team involved throughout the entire process, from patient admission in the institution to the delivery of the treatment and follow-up, the patient, inherent characteristics of the tumour and the available equipment at the facility. However, one single aspect is key, and all treatments should gravitate towards its realization – an external radiation therapy treatment should be one that delivers the most radiation possible to the target (in accordance with the prescribed dose) while

avoiding healthy tissue irradiation, to guarantee the treatment's success with the highest malignant cells/healthy cells ratio achievable. This idea is in line with concepts like Tumour Control Probability (TCP) and Normal Tissue Complication Probability (NTCP) and a favourable treatment outcome is accomplished when the dose delivery curve falls somewhere between these two, illustrated in [Fig. 5]. It becomes apparent that the larger the difference between the two - the so-called therapeutic window, the easier the task, and these can be spread apart by conforming the dose delivery to the target while sparing normal tissues, as well as other methods like the use of radiosensitizers, since these would shift the TCP curve to the left and widen the therapeutic window, allowing one to lower the prescribed dose and still manage to get a good outcome, but such radiobiological aspects fall on other areas of expertise and so are beyond the scope of this study.⁸

Once three-dimensional images of the patient are acquired, using computed tomography (CT), the oncologist and the dosimetrist delineate the target and organs at risk volume structures according to guidelines established by ICRU; the ones in practice are described by the ICRU Reports 62⁹ and 83¹⁰.

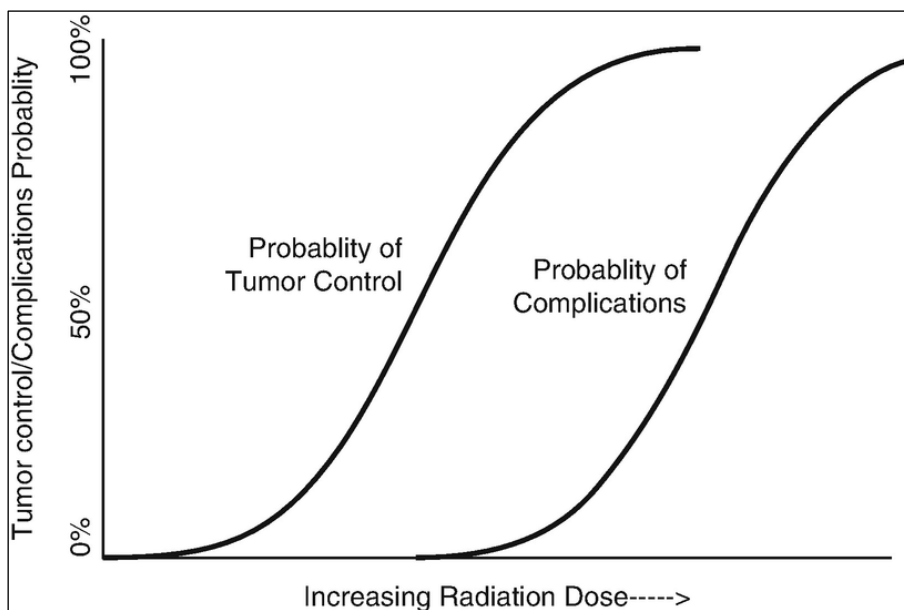


Figure 5 – Tumour Control Probability (TCP), left, and Normal Tissue Complication Probability (NTCP), right, curves as a function of radiation dose. The larger their separation, the better.

The gross tumour volume (GTV) corresponds to the detectable primary tumour region, but metastatic regional nodes (nodal GTV) and distant metastases (metastatic GTV) may also be delineated, if present. In post-operative irradiation scenarios, such as

the ones that will be treated in this work, the lack of a malignant primary tumour implies the absence of a GTV.

The clinical target volume (CTV) is an expansion of the GTV, adding a margin to account for subclinical malignancy assessed by a probabilistic ponderation; microscopic tumour spread near the tumour boundary, possible infiltration into lymph nodes or even overlap with other volumes due to metastazition into other organs are probable issues that are considered by this margin.

The planning target volume (PTV) enters the realm of geometrical concepts, since it is based on the addition of a safety three-dimensional layer wrapping the CTV, taking in consideration possible involuntary organ movement and uncertainties related to the setup (patient positioning and beam alignment). This conservative concept tries to ensure the clinically appropriate irradiation of the whole CTV and is the volume structure for which the absorbed dose is prescribed and reported. Initially, it was suggested that the PTV delineation could be compromised by the proximity of critical organs or even by overlapping of other delineated structures, but it is not considered a good practice anymore because the resulting reduced margin could look deceptively acceptable, but ineffective in practice.

The organs at risk (OAR) are non-target tissues (+ margin) that require special attention on the planning process, as absorbed dose to these structures could be the cause of these organs' damage or failure. Typically, this concept applies to organs in the vicinity of the target and organs that might be covered by radiation fields and hit by scattered radiation, but irradiation to every non-target tissue should be avoided. OAR may have their architecture in series or in parallel; in the former scenario, if a functional subunit¹¹ i.e., a portion of a tissue that performs a certain function, absorbs an

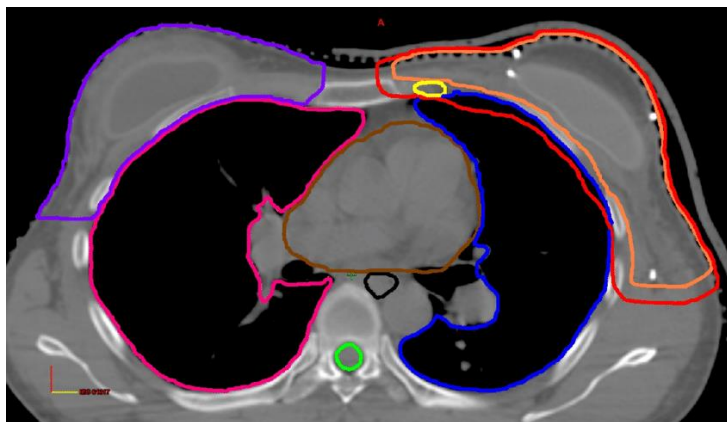


Figure 6 – Volume structures (targets and OAR) on a whole-breast irradiation treatment plan. The following example displays the following structures: CTV (orange), heart (brown), ipsilateral lung (blue), internal mammary nodes (yellow), PTV (red), oesophagus (black), contralateral breast (purple), contralateral lung (pink), spinal canal (green).¹²

overwhelming amount of dose, the organ ceases to function, whereas in the latter case the organ can withstand damage to subunits and still maintain a reasonable degree of vitality. With this idea in mind, the adequate treatment planning parameter to evaluate the damage to a series organ is the maximum dose to that structure, while the appropriate one to assess the deterioration in parallel organs is the mean dose or integral dose. Therefore, the existence of such structures has a huge influence on the treatment planning.

One useful way of evaluating and reporting a treatment plan is by assessing the dose-volume histogram (DVH), more specifically the cumulative DVH. This histogram plots the volume of a structure (relative, in % of total structure volume, or absolute, usually in CC) receiving at least a certain amount of dose (relative, in % of prescribed dose, or absolute, usually in Gy or cGy) [Eq. 1, Fig. 7] and allows for a thorough comparison between plans; still, this tool does not provide positional information, meaning it can give information about the volume receiving at least a certain amount of dose, but it does not tell the planner where that happens; that visually information can be gathered by isodose curves on a colourwash view in the TPS.[Fig. 8]

$$DVH_{rel\ cum}(D) = 1 - \frac{1}{V} \int_0^{D_{max}} \frac{dV(D)}{dD} dD \tag{Eq. 1}$$

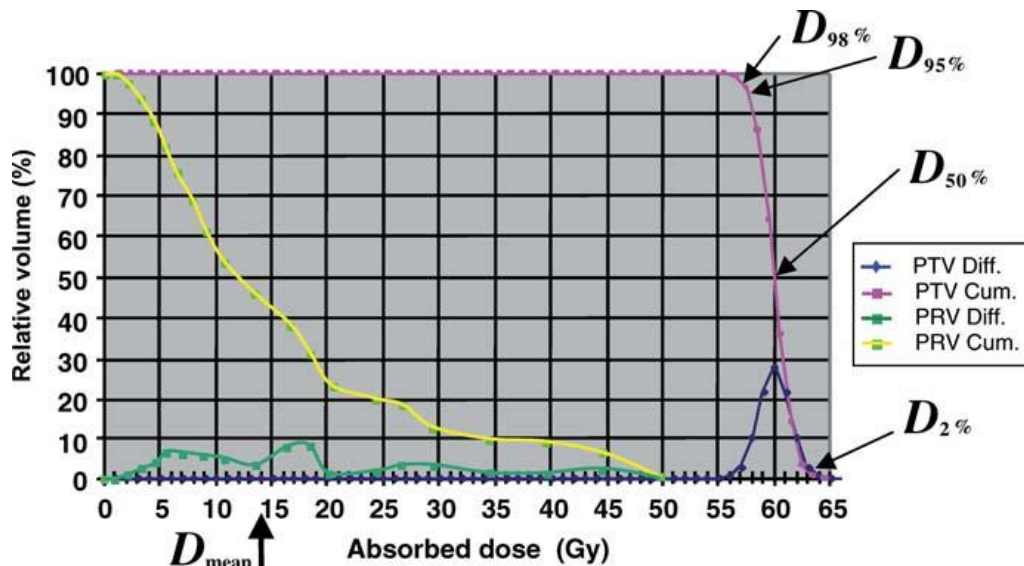


Figure 7 – Differential and cumulative dose-volume histograms, with examples of dosimetric parameters.¹⁰

The need for the elaboration of DVH corroborates the idea that the base reporting level, *Level 1*, is inadequate in the realm of conformal and intensity modulated

radiotherapy, with *Level 2* becoming the minimum requirement for these modalities. Treatment planning systems employ dose-volume calculation algorithms (mainly *Monte Carlo* simulations) with heterogeneity corrections on CT-reconstructed 3D images instead of focusing on the old ICRU Reference Point, a point typically centred on the field axes' intersection and located on a central part of the PTV that may misrepresent the absorbed dose on the organ if the PTV has steep gradients or if an OAR is present within an imaginary spherical volume around the PTV i.e., if the PTV is concave and surrounds the OAR in question (refer to Fig. 9 for an example of the hypothesized distribution).^{9, 10, 14} DVH for all volumes of interest are expected to be reported and a regular QA program to be performed in the institution, to ensure that the treatment is accurately delivered. Further updates on a developing research or technique can be provided, as well as radiobiological quantitative parameters such as the TCP, NTCP, the Equivalent Uniform Dose (EUD) i.e., the absorbed dose that would result in the same biological response as the delivered dose distribution, and the Homogeneity and Conformity Indices (HI & CI, to be defined in later sections); this intensive reporting is said to reach *Level 3*.

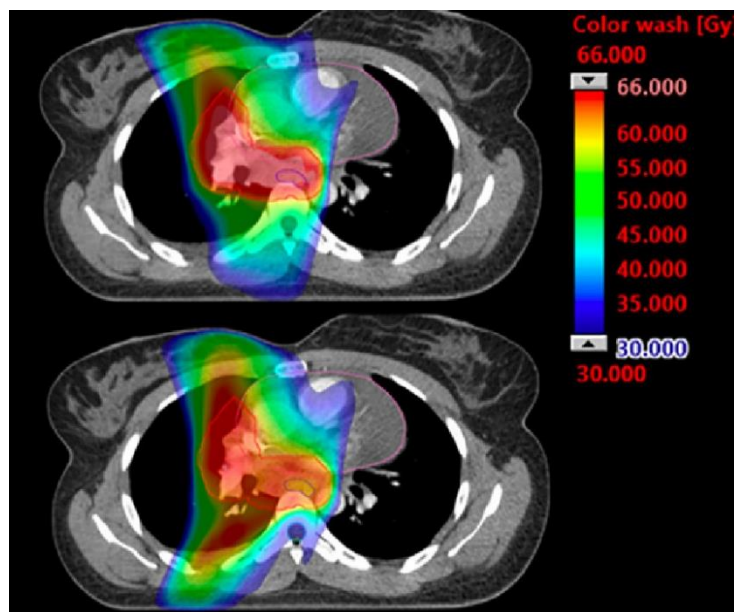


Figure 8 – Dose distributions for two plans. In this case, the colour bar indicates that the shown dose range is [30.000 Gy, 66.000 Gy], with colder colours in the lower-end and hotter colours on the upper-end of the dose interval.¹³ In fact, a limitation arises from the absorbed-dose computation: each voxel (or pixel, if a slice is shown) has a dose value assigned to it and so this distribution is discrete, not continuous; higher dose definition with smoother voxel-to-voxel dose transitions can be obtained by reducing the calculation bin size (in effect, the size of the voxel).

2.2.2 Three-Dimensional Conformal Radiation Therapy (3D-CRT)

Three-Dimensional Conformal Radiation Therapy is a radiotherapy modality which revolutionized the field, proving to be a step forward compared with conventional frameworks. This technique is a milestone in terms of dose conformity to the target volume, owing in part to the versatility the treatment planner has at his disposal during the treatment planning. A 3D-CRT plan may employ many fields of uniform intensity (even though each beam is assigned a weighting factor) in a wide range of possible directions, with variable shapes attained with wedges or compensators and even multi-leaf collimators (MLC), a system with typically 80 to 120 paired lead blocks that can move independently, becoming a highly sophisticated mechanism that allows the beam to match the target with high precision, sparing critical organs. The planning is carried out in an iterative fashion as the planner defines the necessary set of parameters for each field, judges the computed absorbed dose to the existing structures and based on that evaluation, which is biased by their own experience, decides whether to optimize the plan by adjusting some of the previously defined parameters e.g., a field direction, weight or shape, and a new absorbed dose map is calculated; this procedure can be looped the necessary amount of times and, when the planner is confident with the outcome, the oncologist may or may not approve the plan; an experienced dosimetrist or medical physicist is of high importance because this whole process may be time-consuming, but can be reduced if each iteration is guessed relatively well. The described planning method is called *forward-planning* [Fig. 11].

2.2.3 Intensity Modulated Radiation Therapy (IMRT)

The main difference between 3D-CRT and IMRT is the latter's ability to discretize each beam into a grid of beamlets with varying fluences, something the less sophisticated planning modality 3D-CRT is unable to achieve, being limited to the use of MLC and wedges to shape the field. Although 3D-CRT is still widely used and a good technique overall, IMRT is more advanced and its efficiency in shaping concave-like dose profiles is sufficient for it to be regarded as a superior choice in certain clinical cases, with evidently better resulting conformity and homogeneity.

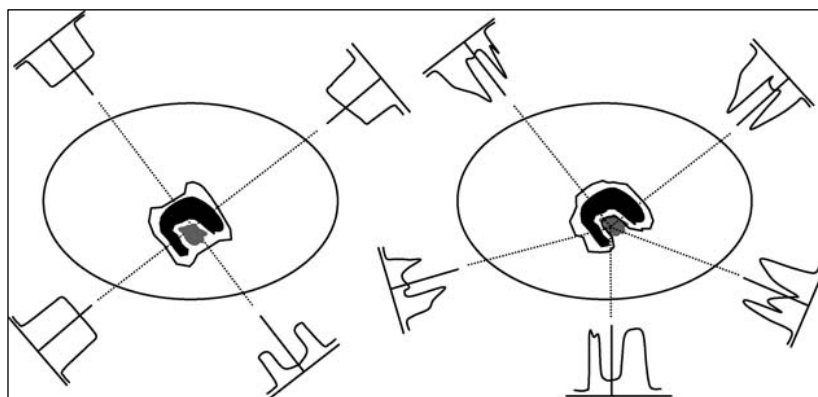


Figure 9 – Beam dose profile comparison between CRT (left) and IMRT (right). IMRT can achieve better conformity to the PTV (black), being more successful at sparing the organs at risk (grey) than CRT, due to the capability of having non-uniform dose profiles in each field; IMRT is more appropriate when dealing with concave shapes.¹⁰

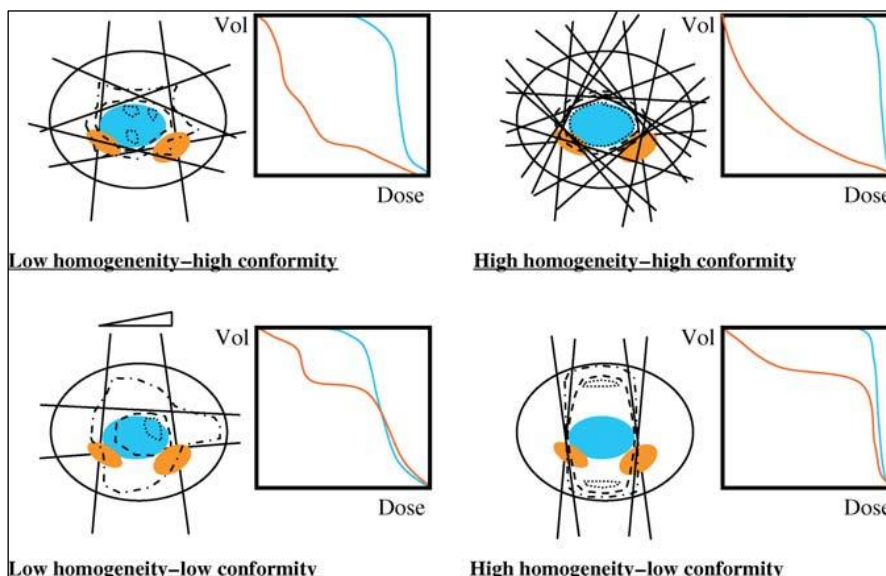


Figure 10 – Examples of low and high dose homogeneities and conformities. The PTV is depicted in blue and the OAR in orange. The dashed lines are isodose lines. A largely homogeneous case is associated with a rapidly decaying curve of the PTV's DVH, meaning the low and high doses encompass approximately the same volume. A highly conformal case is characterized by a rigorous overlap of the dose absorption region and the PTV.¹⁰

An IMRT plan can follow a forward-planning fashion, as the one used in 3D-CRT, but can also recur to an *inverse-planning* method [Fig. 11]. With this optimization novelty, the treatment planner defines dose-volume constraints e.g., $D_{xx\%} \leq yy \text{ Gy}$, meaning the minimum dose received by xx% of the total structure volume cannot exceed yy Gy, and $V_{xx \text{ Gy}} \leq yy\%$, restricting the volume that receives at least xx Gy to a maximum of yy%, and, by doing so, the optimization software iteratively searches for an optimal set of beamlet weights and general beam parameters, and the absorbed-dose is computed.

Despite the apparently automatic workflow, the planner still has an important role, as the optimization process is quite facilitated and faster the more dose-volume constraints the planner provides, resulting in the tightening of the possible outcome space; the optimization can be tracked in real-time, and the planner may decide to apply changes to the constraints with the intention of obtaining a better cumulative dose-volume histogram.

One unfortunate downside of IMRT is the increase in monitor units (MU) when compared with conventional radiotherapy and 3D-CRT. Even if the beam is shaped according to the planner's desire by the primary collimators, MLC and other necessary wedges, the MU refer to the LINAC output and more MU implies more projected radiation, independently of what might come after the LINAC target. This becomes a problem because there is an increase in leakage through the gantry's head and the collimators end up working as scatterers; both these factors contribute to an overall rise in absorbed dose to the body, with possible consequences such as the occurrence of second malignancies. Strategies to reduce this undesired additional absorbed-dose to the body can consist in shielding enhancement and removal of the field-flattening filter, since its presence contributes to more scattering and the modulation achievable by IMRT is perfectly capable of flattening the field, excluding the need for the filter.

Additionally, the ICRU 83 Report recommends the transition from maximum and minimum doses to near-maximum ($D_{2\%}$) and near-minimum ($D_{98\%}$) doses, not based on single-point computations and, hence, more feasible; still, both the maximum and minimum doses can be reported if the oncologist finds them relevant.

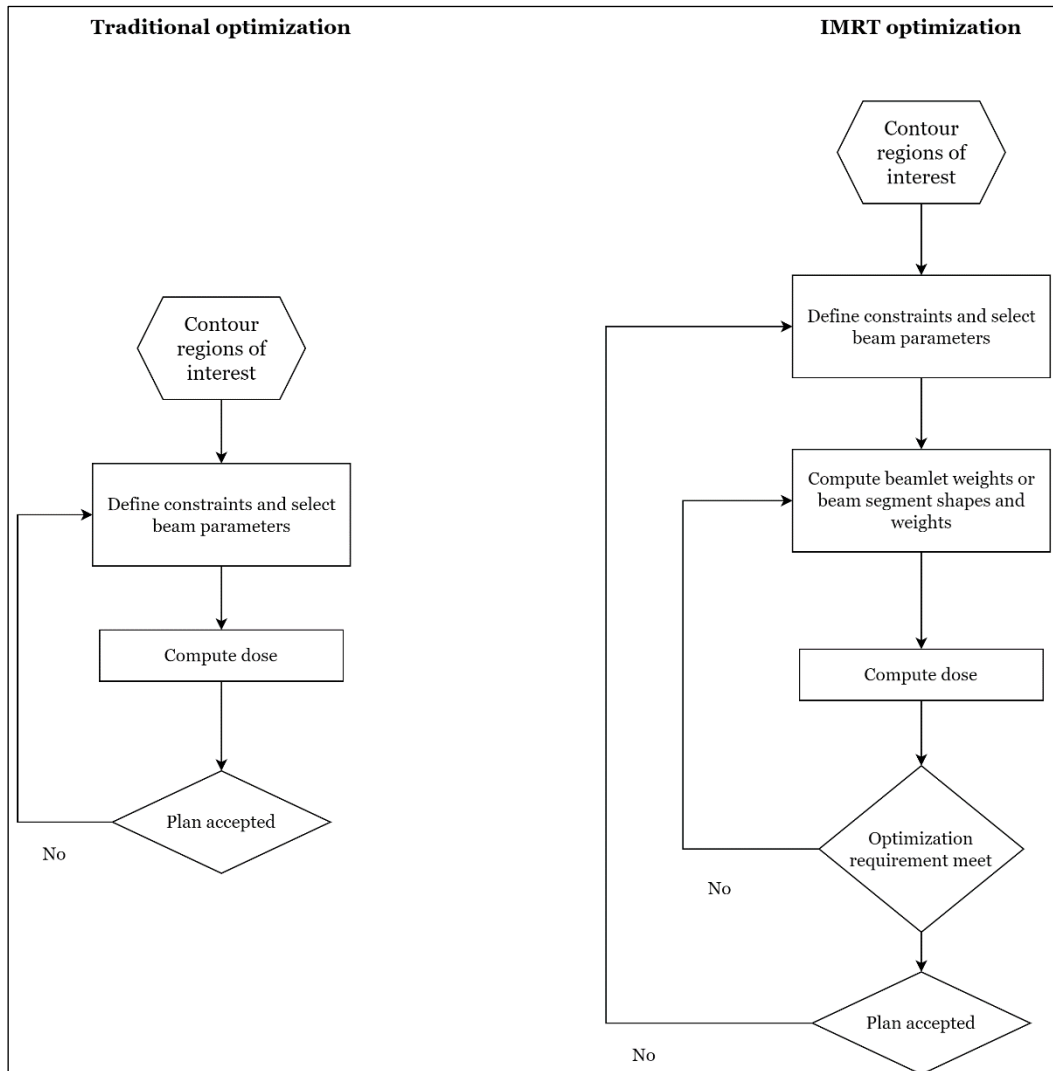


Figure 11 – Traditional and IMRT optimization processes workflow.¹⁰

2.2.4 Volumetric Modulated Arc Therapy (VMAT)

Despite the usefulness of IMRT, the number of required beam directions and the increase in MU contribute to the increase in treatment delivery time. *Otto*¹⁵ presented a novel plan optimization platform with an aperture-based algorithm capable of designing a treatment which delivers the dose during a single gantry arc of up to 360 degrees, with high dose conformity and with high-resolution sampling of beam directions during planning; this platform is called Volumetric Modulated Arc Therapy (VMAT).

VMAT incorporates MLC leaf positions and MU weights as optimization parameters. Minimum and maximum dose-volume constraints are specified for both the target and healthy structures, individually, and each constraint is linked to an importance value. Then, a cost function is calculated for each constraint using the product of a

standard quadratic dose difference function and the respective importance value of the constraint, culminating in a total cost that is equal to the sum of all individual constraint cost values.

MLC leaf positions and MU weights constraints are set so the optimization is performed considering only the physically achievable aperture shapes e.g., excluding scenarios in which opposing leaves overlap, and MU values e.g., non-negative values; continuity of the treatment delivery is ensured by assigning constraints to the MLC leaf motion and MU variation. Referred to as *efficiency constraints* and defined in terms of gantry rotation angle, these are

$$\frac{\Delta x}{\Delta \theta} \leq \left(\frac{dx}{d\theta}\right)_{max} \quad \text{Eq. 2}$$

$$\frac{\Delta MU}{\Delta \theta} \leq \left(\frac{dMU}{d\theta}\right)_{max} \quad \text{Eq. 3}$$

- x – MLC leaf position, [cm]
- MU – MU weight
- Θ – gantry angle, [deg]

and the threshold quantities $(dx/d\Theta)_{max}$ and $(dMU/d\Theta)_{max}$ are chosen according to the delivery system's specifications and features, so as to avoid complications and inefficiency during treatment. An available gantry sample is randomly selected in each iteration of the optimization process and either the MU weight or a MLC leaf position is changed; if this set of parameters does not violate a mechanical or efficiency constraint, the dose distribution and cost function are calculated. Only changes resulting in a reduction of the cost function are accepted.

2.2.5 Hybrid Technique (HT)

A hybrid plan may be thought of as a rather loose concept of a plan mixing the 3D-CRT and IMRT techniques. Some studies have been conducted to assess the usefulness of such a type of plan. There is some variability among studies because,

although mixing 3D-CRT and IMRT beams is part of the definition, the way the relative weights are attributed to the 3D-CRT and IMRT beams depends on the planner and even on the plan itself.

Xiaoxue Xie *et al.*¹⁶ designed 3D-CRT, *inverse planning* IMRT and hybrid plans for 8 left-sided breast cancer patients who underwent breast conserving surgery. All plans were performed using 6 MV photon beams, with a prescribed dose of 50 Gy to the PTV, which was delineated as the CTV plus a 1 cm margin in the superior and inferior directions, 0.5 cm in the other directions and further adjustments to exclude 0.5 cm of the build-up region near the skin, pushing the high-dose gradient away from the PTV boundary and, thus, reducing the variability in patient setup. Breast volumes ranged from 304 to 1633 cc, with an average of 812.75 ± 444.93 cc.

The hybrid plans mixed two 3D-CRT and four IMRT beams. The 3D-CRT component comprised standard medial and lateral primary beams, without wedges. The IMRT component consisted of four fields focused on angles of about 45° anterior from the nearest tangent beams in an attempt to reduce *hot spots* outside the breast, especially in the entrance regions of these tangent fields. 3D-CRT and IMRT had 60 and 40% relative weight, respectively.

Jackie Yim *et al.*¹⁷ studied differences between 3D-CRT and a hybrid IMRT (hIMRT) technique in a 25 early breast cancer patients sample, out of which 13 had left-sided tumours and the other 12 had right-sided tumours; their mean age was 58.6 years, the median PTV breast volume was 655.37 cc and the median separation was 21.84 cm. All plans aimed to deliver 50 Gy to the PTV. The initial PTV was adapted to a new structure, the PTV Breast Eval, which excludes the pectoralis major and the skin surface, 5 mm from the body contour, because the authors find it to be a more appropriate volume delineation for the evaluation of dose to the breast alone. A planning volume, which they called IMRT PTV, was generated for optimization purposes by converting the 50% isodose line from the open field plan into a structure; then, this structure was cropped 0.2 cm from the body and 0.3 cm from the posterior field edge. The PTV structures were delineated by the radiation oncologist and the OAR by the planner.

The hybrid IMRT technique was half 3D-CRT, half IMRT, consisting of up to six opposing tangential fields; two to four open beams and two inversely optimised IMRT beams. All these fields were partially blocked at the lung. The IMRT component only used 6 MV photon energies and the 3D-CRT component used both 6 and 18 MV.

In another study, Yi-Chi Liu *et al.*¹⁸ designed IMRT, Hybrid 3D-CRT/IMRT, Continuous Partial Arc, and Non-Continuous Partial Arc plans for right breast cancer after breast-conserving surgery, but the last two won't be discussed since they are VMAT methods. The prescription dose was 50.4 Gy in 28 fractions to the PTV and the photon energy was 6 MV. The study was conducted in a RANDO phantom. The CTV included the whole breast tissue, lymph nodes, front border of 0.5 cm beneath the skin, and area of tumour metastasis. The PTV extended the CTV by 0.7 cm, except for the front border, and considers the distance error during breath or positioning.

The hybrid technique plan combined 3D-CRT and IMRT fields. The 3D-CRT field was set with two tangential angles. The MLC, lead blocks, and collimator angles were adjusted manually. Additionally, there was an optimized lung shield, to decrease radiation dose to the organ. Then, two IMRT fields were added with increment of tangential angles, each separated 20°. 3D-CRT's contribution was 70% of the prescription dose (so, 126 cGy per fraction), and IMRT's was 30% (the remaining 54 cGy per fraction).

2.3 Tools

2.3.1 Treatment Planning System (TPS)

After admission to a medical institution, a patient is assisted by an oncologist who later recurs to various tools and other medical staff to provide a thorough diagnosis of the disease. The patient is submitted to the imaging installations and a set of computed tomography (CT) images, which provide high-resolution slice-wise information on tissue electronic density (coded by greyscale pixel intensities) and can be stacked through interpolations to construct a three-dimensional view of the patient, is acquired.

The set of images gathered from the patient are imported into a **treatment planning system (TPS)**, the treatment planner delineates all the relevant target volumes and OAR, by demand of the oncologist, either manually for every slice or taking advantage of an interpolation algorithm that can predict and bound the structure in slice **N** by analysing the manually delineated structure in e.g. slices **N-1** and **N+1**, begins to idealize how the treatment will be performed and proceeds to elaborate the plan, step by step, by inserting all the necessary beam modifiers, such as jaws, compensators, MLC, wedges, etc., and fields, with a prescribed dose and fractionation scheme in mind. As previously mentioned on sections **2.2.2** and **2.2.3**, the beams are generated and

iteratively adjusted to achieve the best treatment outcome, whether the optimization process is carried out in a *forward* or *inverse* way. Three-dimensional absorbed dose calculation algorithms based on physical properties and phenomena of radiation interaction with matter, mathematical models and e.g., stochastic and iterative algorithms such as Monte Carlo, use tissue and volumetric data from the image set to construct a voxel-wise dose matrix that is capable of matching absorbed dose to specific structures and a dose normalization is made, typically to the isocentre; elaboration of DVH and dosimetric parameters can be extracted and a conversion to MU, a concept related to both the LINAC's energy output and reading on the ion chamber, is computed so the treatment machine can model the radiation beams according to the prediction of what these beams' properties need to be so that a certain field irradiates the patient and, consequently, a certain (likely) dose is absorbed by the PTV. When acceptable and ready, the plan is approved and sent to the treatment workstation.¹⁹



Figure 12 – IMRT plan for the treatment of breast cancer elaborated with the Eclipse treatment planning system (TPS) Varian Medical Systems, Palo Alto, CA, version 13.5. Slices are shown with three perspectives - transversal, frontal and sagittal, along with the fields, structures and isodose lines; a reconstructed 3D model is also displayed.

A, anterior; F, foot; H, head; L, left; P, posterior; R, right.

2.3.2 PRIMO

PRIMO²⁰ is a free interactive, graphical software that can carry out Monte Carlo simulations with premade clinical LINAC models, excluding the need to code them in the conventional way, which is harder and more prone to error, in a way that a relatively deep knowledge on radiation transport and physical properties of matter would be needed otherwise to achieve accurate simulations; PRIMO uses the PENELOPE code.

Firstly, the user needs to choose an accelerator model and operation mode [Fig. 13] i.e., photons or electrons; Varian and Elekta linacs are available and e.g., the Varian TrueBeam can be obtained by importing the phase-space files distributed by the manufacturer, in the IAEA format. Then, the nominal energy and other primary beam parameters are indicated by the user, who also defines the beam's shape with modifiers i.e., the jaws, MLC, etc., or electron applicators. Even though the users can control most of these parameters and adjust them as they will, PRIMO suggests premade definitions that, in general, are considered adequate. One special feature of the software is the ability to skip the first part of the simulation i.e., the one starting from the primary electron source of the linac, and import a previously tallied phase-space file, as long as it is written in the IAEA format, and, thus, save valuable time. Dose distributions can be estimated inside a user-constructed virtual phantom or in a voxelized geometry constructed from CT images, imported in the DICOM-CT (Digital Imaging and Communication in Medicine Standard) format. The Hounsfield Units (HU) are converted into mass density values and materials are assigned to the segmented structures, such as target volumes and OAR; then, DVH can be created for each structure. Alternatively, structures that were

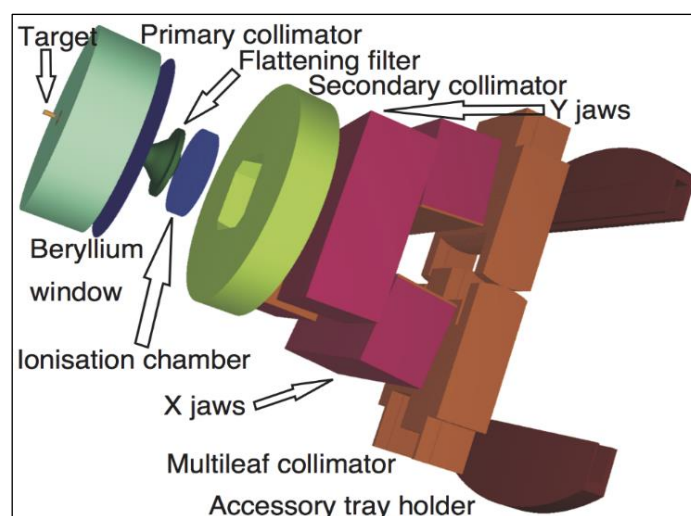


Figure 13 – Simulated geometry of the Varian Clinac 2100 C/D operating in photon mode at 18 MV in PRIMO.²¹

delineated in a TPS before can be imported if they are stored in a DICOM RT-STRUCT file.

The simulation can be layered in three segments, from top to bottom: the fixed upper components, the movable components of the linac, and the dose tallying geometry (supposed to emulate the patient or a phantom for research purposes). Ultimately, a 3D dose map is acquired.

When the simulation is finished, the user can analyse the outcome of the phase-space file [Fig. 14], which lets the user view 2D plots of the spatial distribution of particles and the energy spectrum in the phase-space plane. 3D dose distributions superimposed to the tallied volumes are also available for the user to navigate through, with axial, coronal, and sagittal perspectives [Fig. 15], and the DVH are displayed in case the simulation was performed in a CT volume. These results can be compared with experimental data e.g. from the TPS and graphic representation of both dose profiles and their difference can be plotted, a spatial dose difference distribution can be generated with a gradient colour bar indicating which dose file dominates in each region, and gamma analysis can be performed with the possibility of exporting a summary report on a .pdf file.

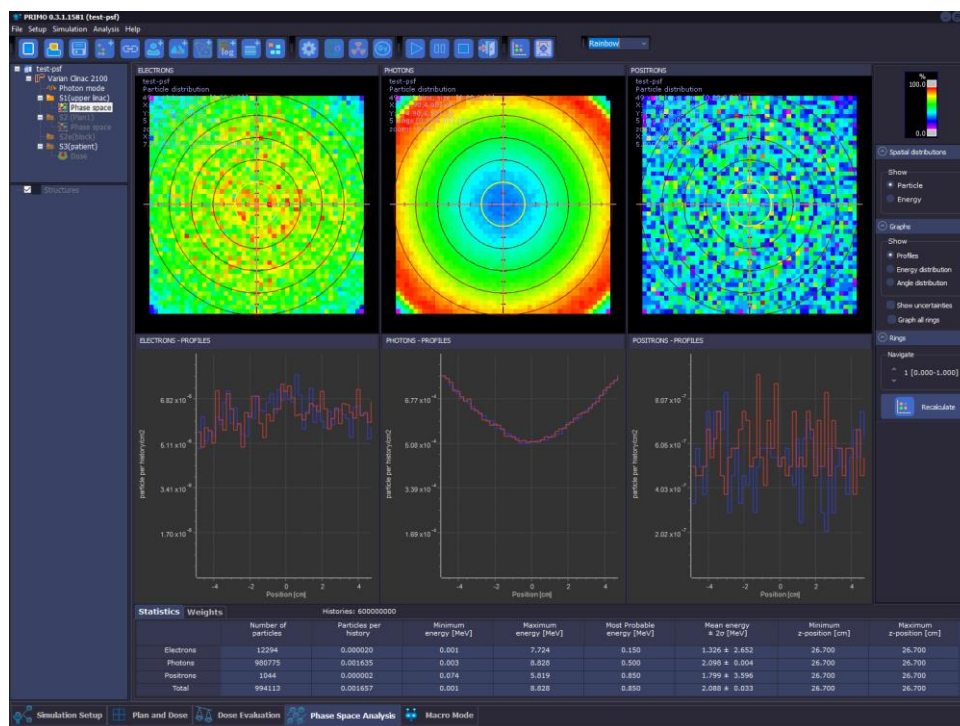


Figure 14 – Phase-space and dose profile analysis window, on PRIMO.²¹

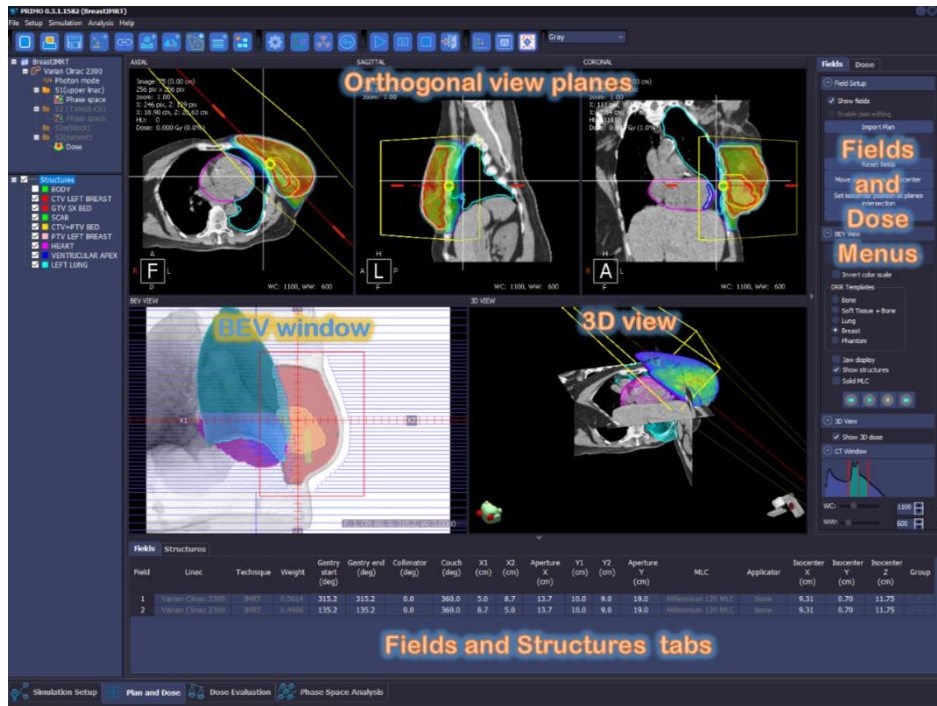


Figure 15 – Different views of the geometry, including the beam's eye view (BEV). Also, dose per region is shaded in different colours, the hotter the higher the dose.²¹

3 Materials and Methods

3.1 Materials

The preparation of the treatment plans to be analysed in this comparative work was carried out on the **Varian Eclipse v13.5**¹⁹ TPS, using the AAA dose calculation algorithm.

Then, a package named *DVHmetrics*²², developed by Daniel Wollschlaeger and Heiko Karle for the *R (R Core Team 2021)* programming language²³ and *Python*²⁴, having imported many mathematical and data-driven packages, such as *NumPy*, *Pandas*, *Matplotlib*, etc., were used for the first phase of this dissertation.

For the second stage, PRIMO v0.3.64.1814 (64-bit) was added as the Monte Carlo simulation environment and was ran in a computer with Intel(R) Xeon(R) CPU E5–2660 v3 @ 2.60GHz 2.60GHz with 16GB of RAM, 32 CPU cores available.

3.2 First Stage – TPS's DVH Comparison

3.2.1 Planning

The first stage of this work was done on the TPS. The dosimetrists imported CT image sets from 20 left breast cancer patients who underwent breast conserving surgery. The patient selection was restricted to left breast cancer because the proximity of the heart requires more attention during planning; therefore, studying the effects of these treatment techniques on left breasts is more interesting and reliable than on right breasts. With indications by two radiation oncologists, they contoured the relevant structures for the dosimetric study of whole-breast irradiation, and these structures were: contralateral breast, ipsilateral lung, lungs (both lungs as one structure), heart, spinal canal, liver, an auxiliary virtual structure called shell, which is used in the optimization process to push the dose delivery to the PTV, and body. Then, they proceeded to elaborate 3D-CRT, IMRT and hybrid plans for each patient, so a comparative study could be done. Both oncologists prescribed a total dose of 50 Gy in 25 fractions to the PTV and even though an oncologist can be more or less conservative regarding volume delineation and dosimetric objectives and constraints, the fact that only two doctors prescribed all the treatments greatly reduces undesired human-caused variability. Also, the optimization is an iterative process that is dependent on many factors, some related to the patients

themselves, such as geometric irregularities or tumour location; this prevents the dosimetrists to strictly follow dosimetric constraints for breast cancer treatment, like the ones recommended by RTOG-1005²⁵, and with that in mind such a list was consulted, but not ultimately followed.

The 3D-CRT plans were started by defining two opposing tangential fields taking most of the weight, one internal and one external, centred in the PTV, and angled in the best possible way to avoid OAR irradiation, primarily the heart, ipsilateral lung and contralateral breast. In some cases where the breast's location might be very close to the armpit, the external tangential field may be cranio-caudal and noncoplanar (the bed is slightly rotated). A first calculation is computed and *hot spots* on the surface are expected. Then, some *field-in-field* segments are created to improve the dose at depth and reduce the superficial *hot spots*. These segments need to employ more than 10 MU each and have around 10% of the weight of the principal fields.

By experience, starting IMRT plans by letting the optimizer define the beams' angulation does not end up well; in our institution, the beams and their respective directions are manually created, but in this case, there are two internal tangential, two external tangential and one anterior oblique fields. The anterior oblique beam is adjusted to the volume and lowers the existing prescription dose outside the PTV. ICRU recommends a minimum of 95% of the prescription dose to the PTV and a maximum of 107% of the prescription dose. In addition to minimum and maximum doses to the PTV, a mean dose to the PTV and constraints to the OAR are also defined. An optimization is made, followed by a first calculation. The DVH is checked and, if needed (which most likely will be after just one calculation), dose objectives' priorities and constraints are adjusted, in a trial by error manner.

The HT plans' starting point was the IMRT plan: the best two fields at sparing the OAR were kept from one plan onto the other. An optimization and calculation were computed with these two beams; then, static fields were added and make up to 80% of the weight, keeping the IMRT beams with 20% of the weight. Finally, further segments are created to improve the dose at depth and reduce superficial *hot spots*.

3.2.2 Analysis Procedure

Once all the plans were complete, the DVH data was exported from the TPS in a tabular format with additional information. [Fig. 16, 17] The data layout is not suitable to deal with, hence the need to clean the DVH files and formatting them to a .csv type file. Although doable, the number of patients and the number of structures per patient make the extraction of all the tables by hand virtually impossible to handle in a reasonable amount of time. To tackle this issue, *DVHmetrics* was used. *DVHmetrics* is an extensive tool that comes across as a quite useful way to deal with DVH data from many different TPS, providing the ability to plot a patient-wise average DVH of all the structures, extract dosimetric parameters, and compute some radiobiological concepts; however, none of this was used because full control of the data was intended to be owned in this work, so all statistical treatment could be done from scratch. *DVHmetrics* and *R* overall were solely used to clean the exported DVH files, and the outcome is a .csv file like the one displayed below. [Fig. 18]

```

Patient Name      : anonymized patient
Patient ID       : ██████████
Comment          : DVHs for one plan
Date             : quarta-feira, 23 de fevereiro de 2022 12:20:39
Exported by      : 137312
Type             : Cumulative Dose Volume Histogram
Description      : The cumulative DVH displays the percentage (relative)
                  or volume (absolute) of structures that receive a dose
                  equal to or greater than a given dose.

Plan: MAMA ESQ1
Course: HIBRIDO
Plan Status: Unapproved
Prescribed dose [Gy]: 50.000
% for dose (%): 100.0

Structure: Breast Right
Approval Status: Unapproved
Plan: MAMA ESQ1
Course: HIBRIDO
Volume [cm³]: 339.2
Dose Cover. [%]: 100.0
Sampling Cover. [%]: 100.0
Min Dose [Gy]: 0.000
Max Dose [Gy]: 3.051
Mean Dose [Gy]: 0.318
Modal Dose [Gy]: 0.005
Median Dose [Gy]: 0.137
STD [Gy]: 0.431
Equiv. Sphere Diam. [cm]: 8.7
Conformity Index: N/A
Gradient Measure [cm]: N/A

```

Figure 16 – Example of a text file exported from the Eclipse TPS, with patient information, date, plan, prescribed dose, normalization, and one of the structures: in this case, the contralateral breast "Breast Right", along with some dosimetric information of a 3D-CRT plan.

The most convenient strategy to organize the data was to average the DVH so that for each treatment technique i.e., 3D-CRT, IMRT, and hybrid, and for each structure there was a plot that corresponded to the average of all patients. This way, comparisons between the three techniques for all structures are possible. These average DVH and further statistical treatment and analysis were done with *Python*²⁴ tool.

Dose [Gy]	Relative dose [%]	Ratio of Total structure volume [%]
0	0	100
0.051	0.102	68.1203
0.102	0.204	55.7042
0.153	0.306	47.8027
0.204	0.408	41.856
0.255	0.51	37.1081
0.306	0.612	33.1123
0.357	0.714	29.6525
0.408	0.816	26.5966
0.459	0.918	23.9124
0.51	1.02	21.4947
0.561	1.122	19.3403
0.612	1.224	17.4054
0.663	1.326	15.6558
0.714	1.428	14.0723
0.765	1.53	12.6866
0.816	1.632	11.406
0.867	1.734	10.2925
0.918	1.836	9.25374
0.969	1.938	8.3367
1.02	2.04	7.51446
1.071	2.142	6.80652
1.122	2.244	6.14599
1.173	2.346	5.59705

Figure 17 – Example of a table from the same text file and the same structure shown on [Fig. dvhtxt1]. The relative structure volume, in percentage, corresponds to the upper limit of a dose bin, in Gy.

```
"patID", "dose", "volumeMEAN", "volumeReMEAN", "volumeMEDIAN", "volumeReMEDIAN", "volumeMIN", "volumeReMIN", "volumeMAX", "volumeReMAX", "volumeSD", "volumeReSD", "structure"
"55991602", 0.1994, 5.100, 1994, 5.100, 1994, 5.100, NA, NA, "Breast_R"
"55991602", 0.051, 368.372183, 18.4694, 368.372183, 18.4694, 368.372183, 18.4694, NA, NA, "Breast_R"
"55991602", 0.102, 265.2625165, 13.2997, 265.2625165, 13.2997, 265.2625165, 13.2997, NA, NA, "Breast_R"
"55991602", 0.153, 216.056207, 10.8326, 216.056207, 10.8326, 216.056207, 10.8326, NA, NA, "Breast_R"
"55991602", 0.204, 181.13949275, 9.08195, 181.13949275, 9.08195, 181.13949275, 9.08195, NA, NA, "Breast_R"
"55991602", 0.255, 154.71755345, 7.75721, 154.71755345, 7.75721, 154.71755345, 7.75721, NA, NA, "Breast_R"
"55991602", 0.306, 134.8792592, 6.76256, 134.8792592, 6.76256, 134.8792592, 6.76256, NA, NA, "Breast_R"
"55991602", 0.357, 119.85808135, 6.00943, 119.85808135, 6.00943, 119.85808135, 6.00943, NA, NA, "Breast_R"
"55991602", 0.408, 107.76941685, 5.40333, 107.76941685, 5.40333, 107.76941685, 5.40333, NA, NA, "Breast_R"
"55991602", 0.459, 97.5206786, 4.88948, 97.5206786, 4.88948, 97.5206786, 4.88948, NA, NA, "Breast_R"
"55991602", 0.51, 88.4987573, 4.43714, 88.4987573, 4.43714, 88.4987573, 4.43714, NA, NA, "Breast_R"
"55991602", 0.561, 80.4318026, 4.03268, 80.4318026, 4.03268, 80.4318026, 4.03268, NA, NA, "Breast_R"
"55991602", 0.612, 73.1435007, 3.66726, 73.1435007, 3.66726, 73.1435007, 3.66726, NA, NA, "Breast_R"
"55991602", 0.663, 66.5413068, 3.33624, 66.5413068, 3.33624, 66.5413068, 3.33624, NA, NA, "Breast_R"
"55991602", 0.714, 60.521108, 3.0344, 60.521108, 3.0344, 60.521108, 3.0344, NA, NA, "Breast_R"
"55991602", 0.765, 55.00611605, 2.75789, 55.00611605, 2.75789, 55.00611605, 2.75789, NA, NA, "Breast_R"
"55991602", 0.816, 49.96122775, 2.50495, 49.96122775, 2.50495, 49.96122775, 2.50495, NA, NA, "Breast_R"
"55991602", 0.867, 45.36191075, 2.27435, 45.36191075, 2.27435, 45.36191075, 2.27435, NA, NA, "Breast_R"
"55991602", 0.918, 41.13835755, 2.06259, 41.13835755, 2.06259, 41.13835755, 2.06259, NA, NA, "Breast_R"
"55991602", 0.969, 37.26424075, 1.86835, 37.26424075, 1.86835, 37.26424075, 1.86835, NA, NA, "Breast_R"
"55991602", 1.02, 33.7493334, 1.69212, 33.7493334, 1.69212, 33.7493334, 1.69212, NA, NA, "Breast_R"
"55991602", 1.071, 30.52402745, 1.53041, 30.52402745, 1.53041, 30.52402745, 1.53041, NA, NA, "Breast_R"
"55991602", 1.122, 27.59490475, 1.38355, 27.59490475, 1.38355, 27.59490475, 1.38355, NA, NA, "Breast_R"
"55991602", 1.173, 24.9460093, 1.25074, 24.9460093, 1.25074, 24.9460093, 1.25074, NA, NA, "Breast_R"
"55991602", 1.224, 22.5370522, 1.12996, 22.5370522, 1.12996, 22.5370522, 1.12996, NA, NA, "Breast_R"
"55991602", 1.275, 20.3578615, 1.0207, 20.3578615, 1.0207, 20.3578615, 1.0207, NA, NA, "Breast_R"
"55991602", 1.326, 18.387754235, 0.921923, 18.387754235, 0.921923, 18.387754235, 0.921923, NA, NA, "Breast_R"
"55991602", 1.377, 16.604631345, 0.832521, 16.604631345, 0.832521, 16.604631345, 0.832521, NA, NA, "Breast_R"
"55991602", 1.428, 14.98938552, 0.751536, 14.98938552, 0.751536, 14.98938552, 0.751536, NA, NA, "Breast_R"
"55991602", 1.479, 13.51880078, 0.677804, 13.51880078, 0.677804, 13.51880078, 0.677804, NA, NA, "Breast_R"
"55991602", 1.53, 12.187252635, 0.611043, 12.187252635, 0.611043, 12.187252635, 0.611043, NA, NA, "Breast_R"
"55991602", 1.581, 10.97322043, 0.550174, 10.97322043, 0.550174, 10.97322043, 0.550174, NA, NA, "Breast_R"
"55991602", 1.632, 9.86834721, 0.494778, 9.86834721, 0.494778, 9.86834721, 0.494778, NA, NA, "Breast_R"
"55991602", 1.683, 8.86285992500001, 0.444365, 8.86285992500001, 0.444365, 8.86285992500001, 0.444365, NA, NA, "Breast_R"
"55991602", 1.734, 7.94676613, 0.398434, 7.94676613, 0.398434, 7.94676613, 0.398434, NA, NA, "Breast_R"
"55991602", 1.785, 7.114880125, 0.356725, 7.114880125, 0.356725, 7.114880125, 0.356725, NA, NA, "Breast_R"
"55991602", 1.836, 6.35699007, 0.318726, 6.35699007, 0.318726, 6.35699007, 0.318726, NA, NA, "Breast_R"
```

Figure 18 – DVH data of a 3D-CRT plan, for the contralateral breast. This .csv is ready to be imported into a statistics software.

The extracted dosimetric parameters, obtained via linear interpolation between existing data points (linear interpolation is accurate enough for this case, as the bin width is pretty narrow compared with the data range), are indicated in Table 1.

Table 1 – Extracted dosimetric parameters.

PTV	CTV	Heart	Contralateral breast	Ipsilateral lung	Lungs	Spinal canal	Liver	Shell	Body
D _{mean}	D _{mean}	D _{mean}	D _{mean}	D _{mean}	D _{mean}	D _{max}	D _{mean}	D _{max}	D _{max}
D _{50%}	D _{max}	D _{max}	D _{max}	V _{30 Gy}	V _{30 Gy}				V _{95%}
D _{max}	D _{min}	V _{30 Gy}		V _{20 Gy}	V _{20 Gy}				
D _{min}	V _{98%}	V _{20 Gy}		V _{10 Gy}	V _{10 Gy}				
D _{2%}		V _{5 Gy}							
D _{95%}									
D _{98%}									
V _{107%}									
V _{95%}									

Other computed quantities were the homogeneity and conformity indices. These concepts have evolved throughout the years and still are somewhat arbitrary and largely dependent on the author's choice of definition. In this work, the HI was defined according to the ICRU 83 Report i.e.,

$$HI = \frac{D_{2\%} - D_{98\%}}{D_{50\%}} \tag{Eq. 4}$$

- $D_{2\%}, D_{50\%}, D_{98\%}$ – least amount of absorbed dose received by 2%, 50% and 98% of the PTV, respectively, [Gy]

The more alike the near-minimum and near-maximum doses are, the more the HI converges to 0; hence, 0 is its ideal value. For the CI, Ian Paddick's definition²⁶ was used, as it seems to be an appropriate way to measure conformity without obtaining misleading results. Choosing the 95% isodose as a guideline, Paddick's proposal becomes:

$$CI = \frac{(V_{PTV}^{95\%D})^2}{V_{PTV} \times V_{TOTAL}^{95\%D}} \tag{Eq. 5}$$

- $V_{PTV}^{95\%D}$ – portion of the PTV covered by the 95% isodose, [cc]

- $V_{TOTAL}^{95\%D}$ – portion of the total volume covered by the 95% isodose, [cc]
- V_{PTV} – PTV volume, [cc]

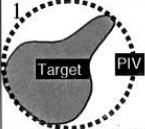
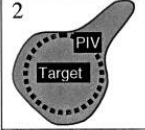
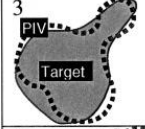
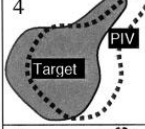
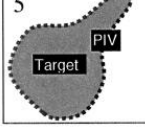
Isodose Plan	Parameters	PITV	RCl _i	Proposed Index
		$\frac{PIV}{TV}$	$\frac{TV_{PIV}}{TV}$	$\frac{TV_{PIV}^2}{TV \times PIV}$
	TV = 5cm ³ TV _{PIV} = 5cm ³ PIV = 10cm ³	2.00	1.00	0.50
	TV = 5cm ³ TV _{PIV} = 3cm ³ PIV = 3cm ³	0.60	0.60	0.60
	TV = 5cm ³ TV _{PIV} = 4cm ³ PIV = 5cm ³	1.00	0.80	0.64
	TV = 5cm ³ TV _{PIV} = 3cm ³ PIV = 5cm ³	1.00	0.60	0.36
	TV = 5cm ³ TV _{PIV} = 5cm ³ PIV = 5cm ³	1.00	1.00	1.00

Figure 19 – Rationale behind the proposal of the new model (last column). It is shown that previous models were not excellent at avoiding misleading results, with some poorly conformal plans wrongly presenting typical values of high conformity. TV_{PIV} is the intersection of the target volume TV with the volume bounded by the isodose, PIV.

The number of total MU of the plans was also compared between the three techniques.

Validity and significance of the differences found in dosimetric parameters and MU between techniques was verified with a statistical hypothesis test. The appropriate test for this analysis is the Friedman test, a non-parametric alternative to the repeated-measures ANOVA, because it does not rely on the assumption of normality and can withstand the existence of outliers. This is a global test and assesses if at least one technique is different from the others, but it does not give information about which one(s). For further detail, the Nemenyi test, which is a *post-hoc* test, was used to pinpoint the significantly different technique(s). The chosen significance level was $p < 0.05$.

3.3 Second Stage – TPS vs. PRIMO Comparison

3.3.1 Simulations

The phase-space for the Trilogy 1 was created in PRIMO using the Varian Clinac 2300, with energy 6X, for 2×10^8 particles. The simulation time was about 75 hours.

The dose is given in eV/g by default and a calibration factor is needed to convert the dose in Gy. At our institution, the calibration is done by adjusting the linac’s output, for 6X beam energy mode, to reach 1.00 cGy/MU (SSD = 100 cm, 10x10 cm² field, at 1.60 cm depth in a 40x40x40 cm³ water tank phantom) or 0.66 cGy/MU at a 10 cm depth, knowing the number of MU. A 40x40x40 cm³ water phantom was generated in a PRIMO project, as shown in Figure 20, and a simulation was performed in the reference conditions above described (PRIMO has an SID = 100 cm by default, so the isocentre must have coordinates (x, y, z) = (0, 0, 0) cm in order to set SSD = 100 cm). After the simulation was finished, the dose in eV/g at (0, 0, 10) cm was extracted, being **0.3902 ± 0.0019 eV/g (uncertainty of 0.50%)** with 100 MU in 1 fraction. This small uncertainty was achieved with a splitting factor of 1000 at the phantom.

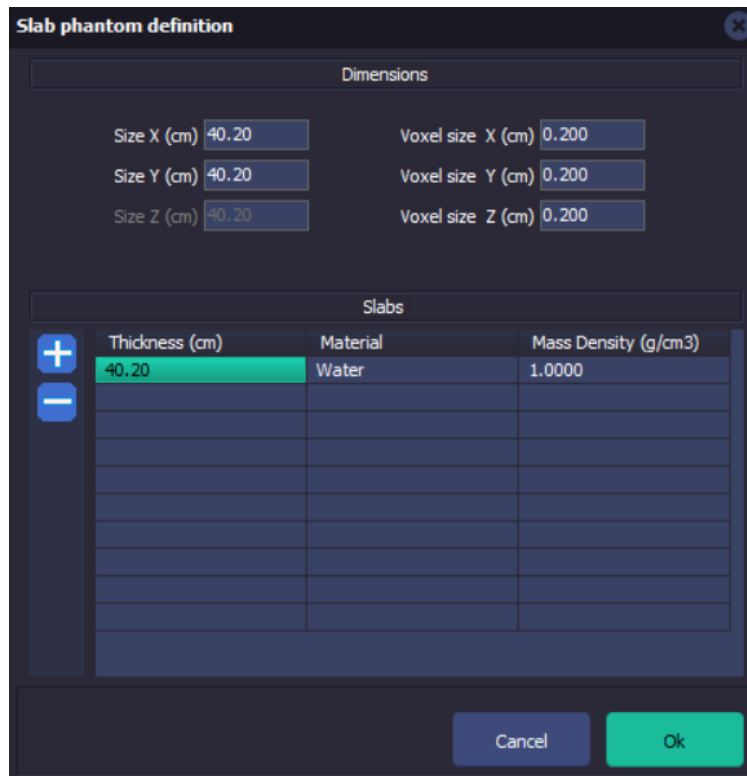


Figure 20 – Definition of the water tank phantom with dimensions 40.20 x 40.20 x 40.20 cm³, with voxel size 0.200 x 0.200 x 0.200 cm³.

The dose conversion follows the following expression:

$$D = \frac{D_{exp}^{ref}}{MU^{ref}} \frac{D_{MC}}{D_{MC}^{ref}} MU \tag{Eq.6}$$

- D – dose, [Gy]
- D_{exp}^{ref} – dose measured in reference conditions, [Gy]
- MU^{ref} – monitor units used to obtain the measured reference dose
- D_{MC} – simulated dose for the treatment plan, [eV/g per history]
- D_{MC}^{ref} – dose estimated by a Monte Carlo simulation in reference conditions, [eV/g per history]
- MU – monitor units of the treatment plan

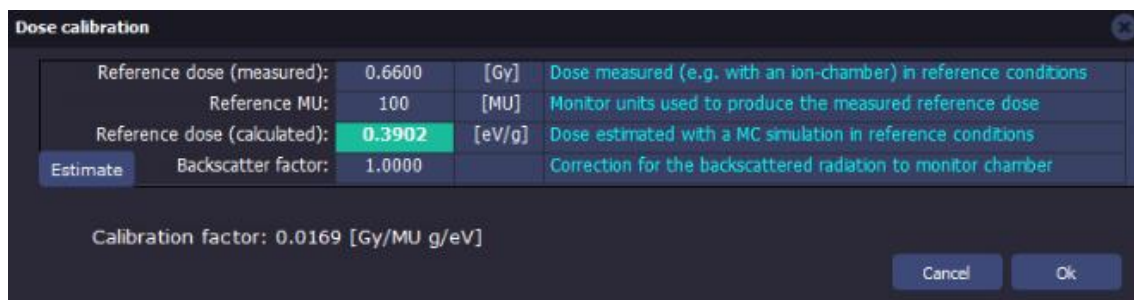


Figure 21 – Dose calibration window. This is set to correspond to a measured dose of 0.6600 Gy at 10.0 cm depth on the central axis, with reference MU of 100 MU and a calculated reference dose of 0.3902 eV/g. The backscatter factor stays at 1.0000.

A project was created for each treatment plan i.e., three projects per patient, one for each technique. The sequence of actions executed to run the simulations began with linking the phase-space file to the project; then, the DICOM CT files with the settings ticked as displayed in Figure 22, the DICOM Structure file with the medium outside structure volumes set to emulate air, as shown in Figure 23, and the DICOM Plan file, as shown in Figure 24, were imported.

To run the simulation, the configurations were changed so the used engine was the **Dose Planning Method (DPM)**, a new seed was generated and the number of histories, determined by the plan, was set as the simulation stop condition. [Fig. 24] Then, a splitting factor of 2500 was applied in the phantom. [Fig. 24] A flowchart that summarizes this entire process is shown in Figure 25.

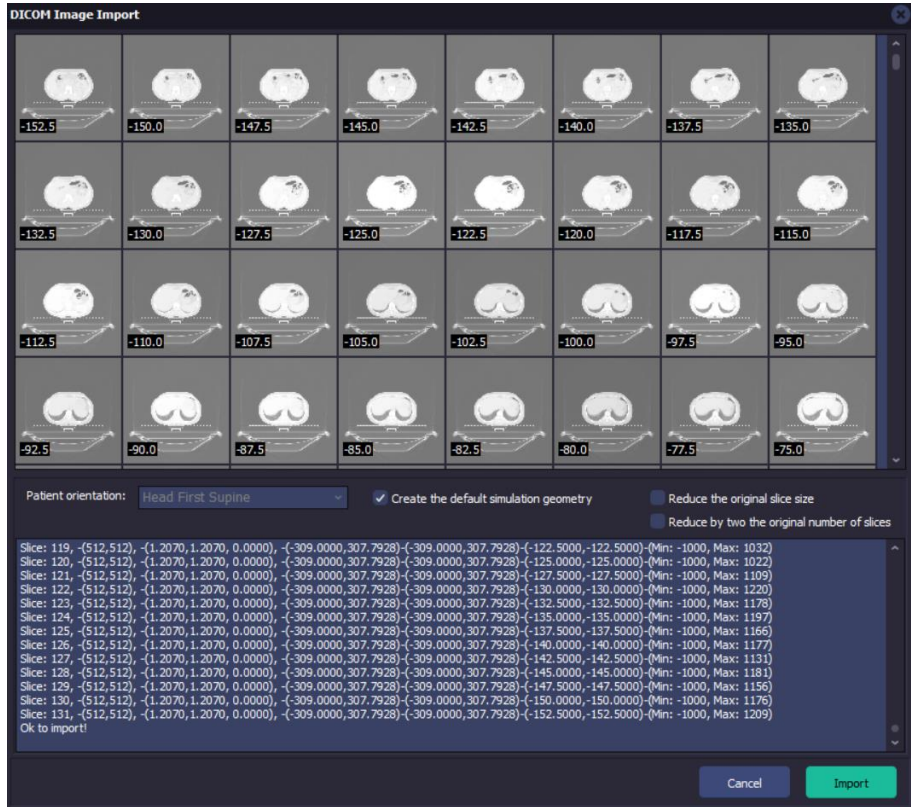


Figure 22 – DICOM Image Import window.

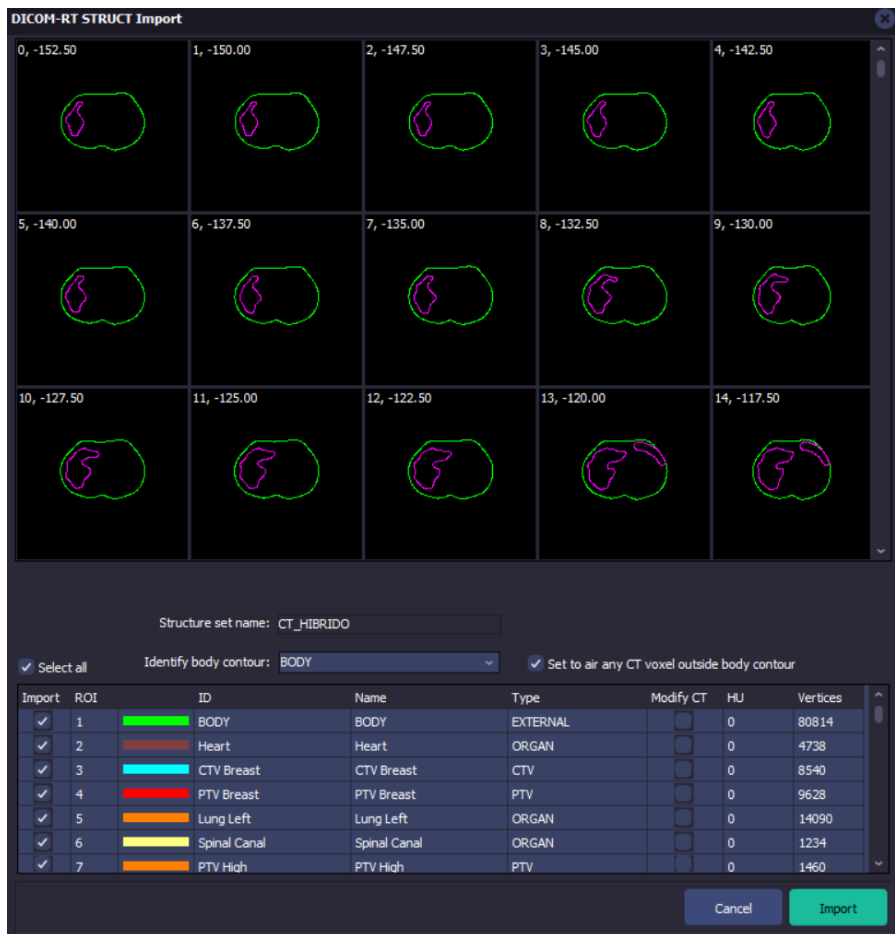


Figure 23 – DICOM Structure Import window. Any CT voxel outside of the body contour is set to air.

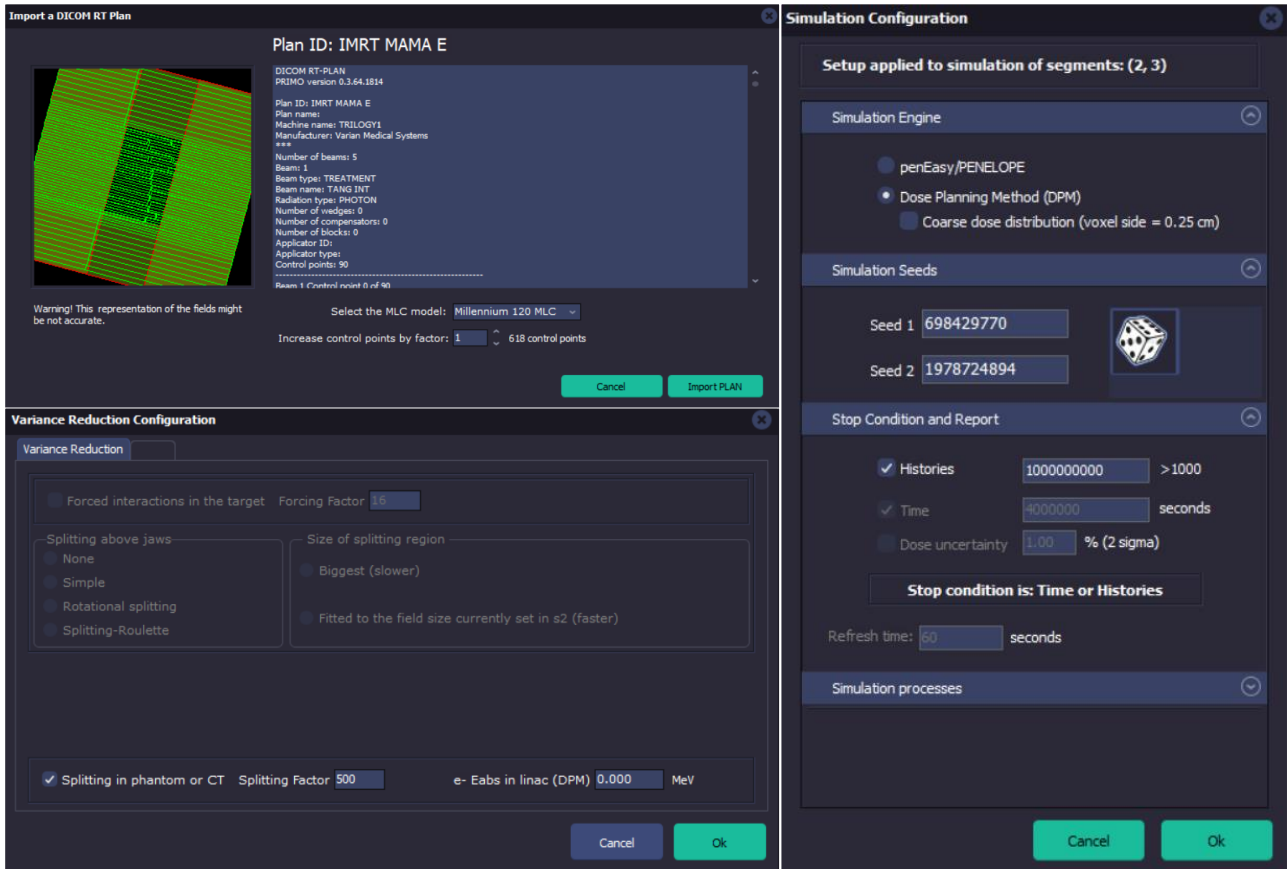


Figure 24 – Top left: DICOM RT Plan Import window. The chosen MLC was the Millennium 120 MLC. Bottom left: Variance Reduction Configuration window. Right: Configuration Window. DPM was used as the simulation engine, a new seed was generated for each simulation and histories was the limiting parameter.

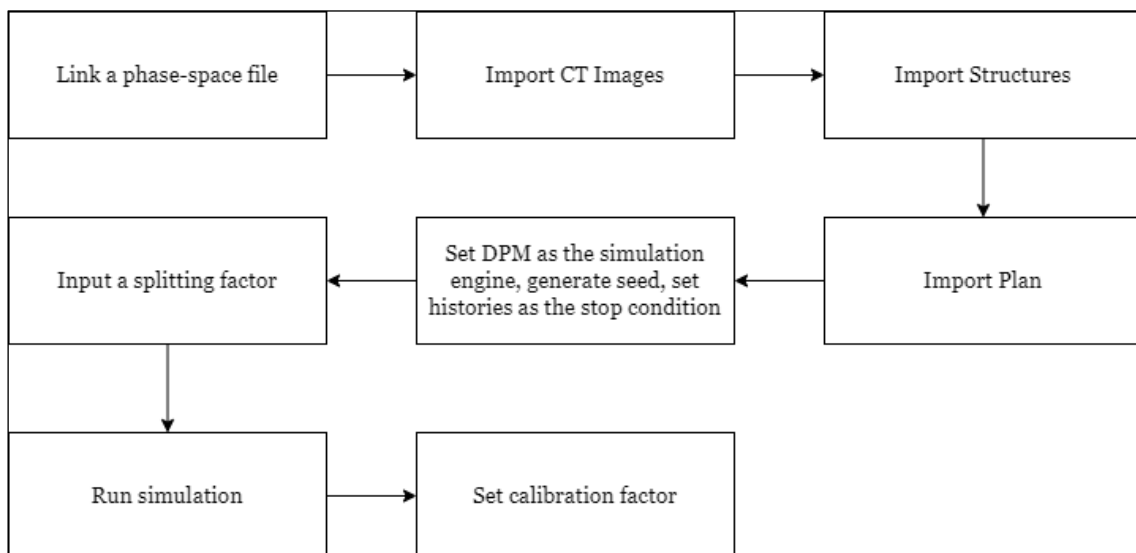


Figure 25 – PRIMO procedure flowchart.

3.3.2 Analysis Procedure

The DVH that resulted from the PRIMO simulations were exported as files readable by *R + DVHmetrics* and all the data preparation was conducted in a similar fashion as in section 3.2.2, even though a prior linear interpolation of the values with *Python* was needed to set the DVH dose bin widths of all the patients and structures to 0.051 Gy, so a direct comparison with the data acquired from the TPS could be made.

All the dosimetric parameters and the CI and HI determined in the analysis of the TPS data were also determined in this section, this time with the PRIMO data, and a similar comparison between techniques was performed with the same tools. Furthermore, the simulation times were compared between techniques.

Following, the DVH and the dosimetric parameters determined so far with the data from the TPS and PRIMO were compared to assess agreement between tools; to check statistical significance, three Wilcoxon signed-rank tests were performed (one for each technique) instead of one Friedman test as was the case until this point. The chosen significance level was $p < 0.05$.

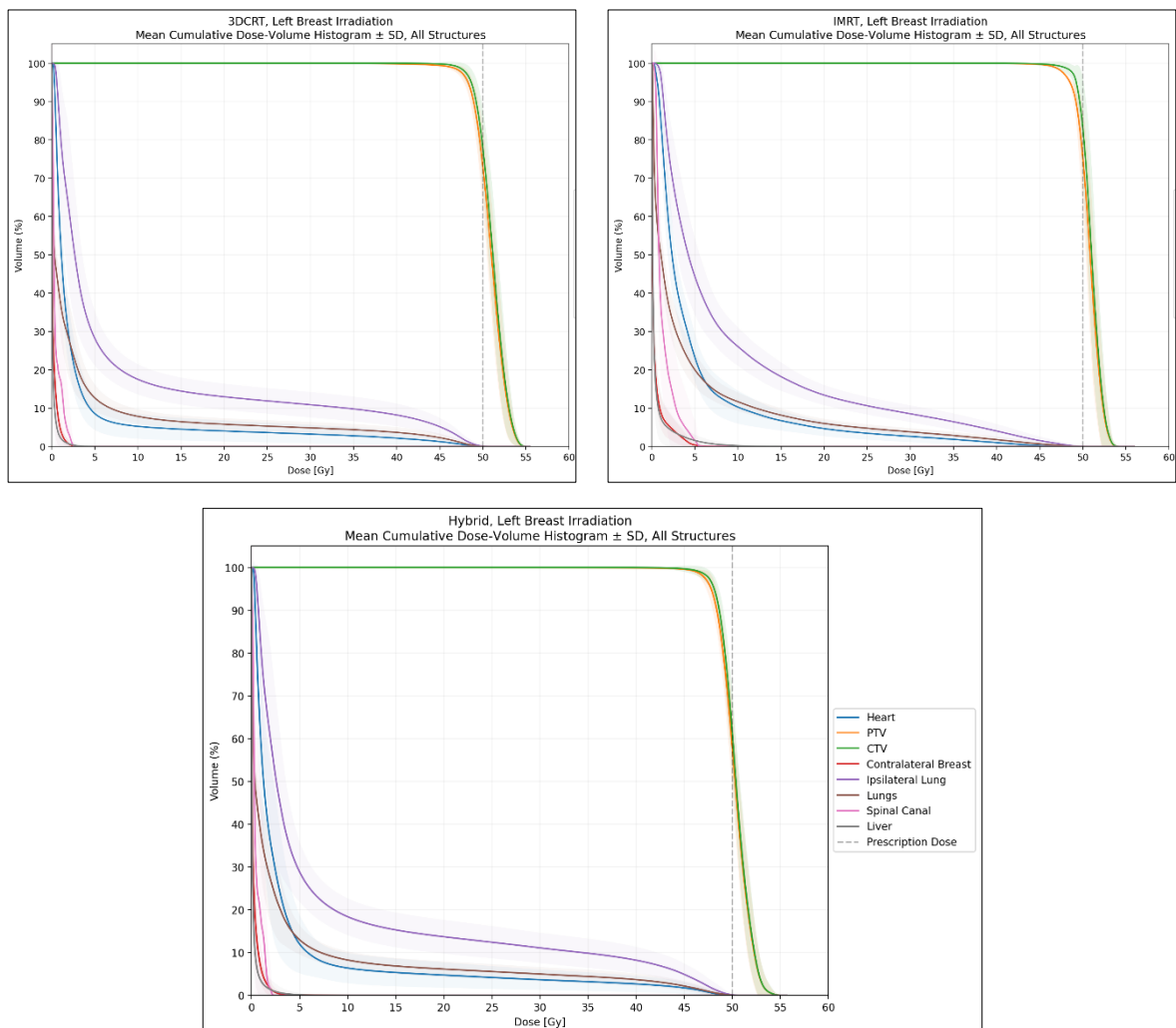
4 Results and discussion

4.1 Results

4.1.1 TPS

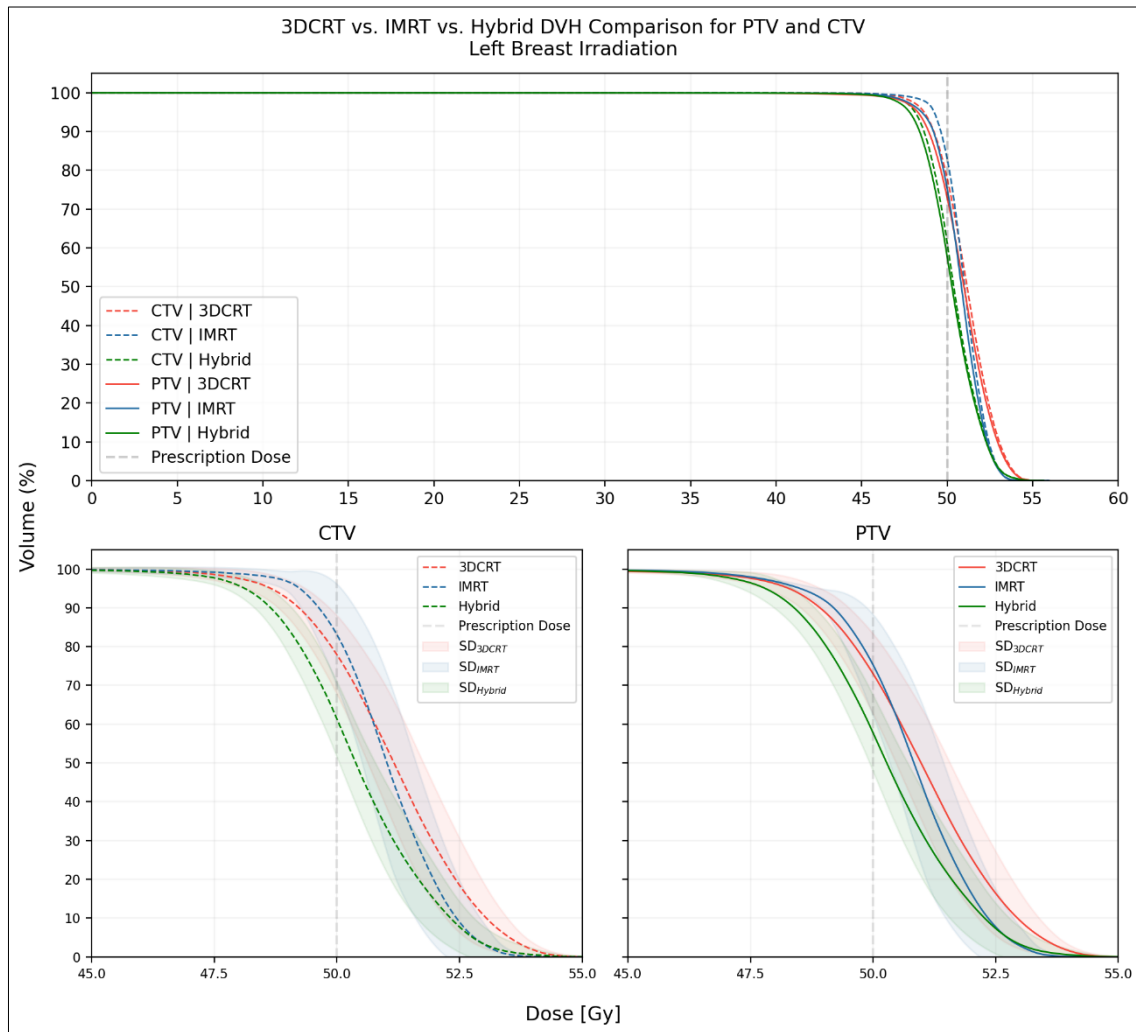
In this section, the resulting DVH plotted from the data acquired from the TPS, as well as box plots for some dosimetric parameters are presented in a comparative manner. The results will give some insight about possible advantages of one technique over the others.

The mean DVH for all structures for 3D-CRT, IMRT and HT are shown below.
[Graph. 1]

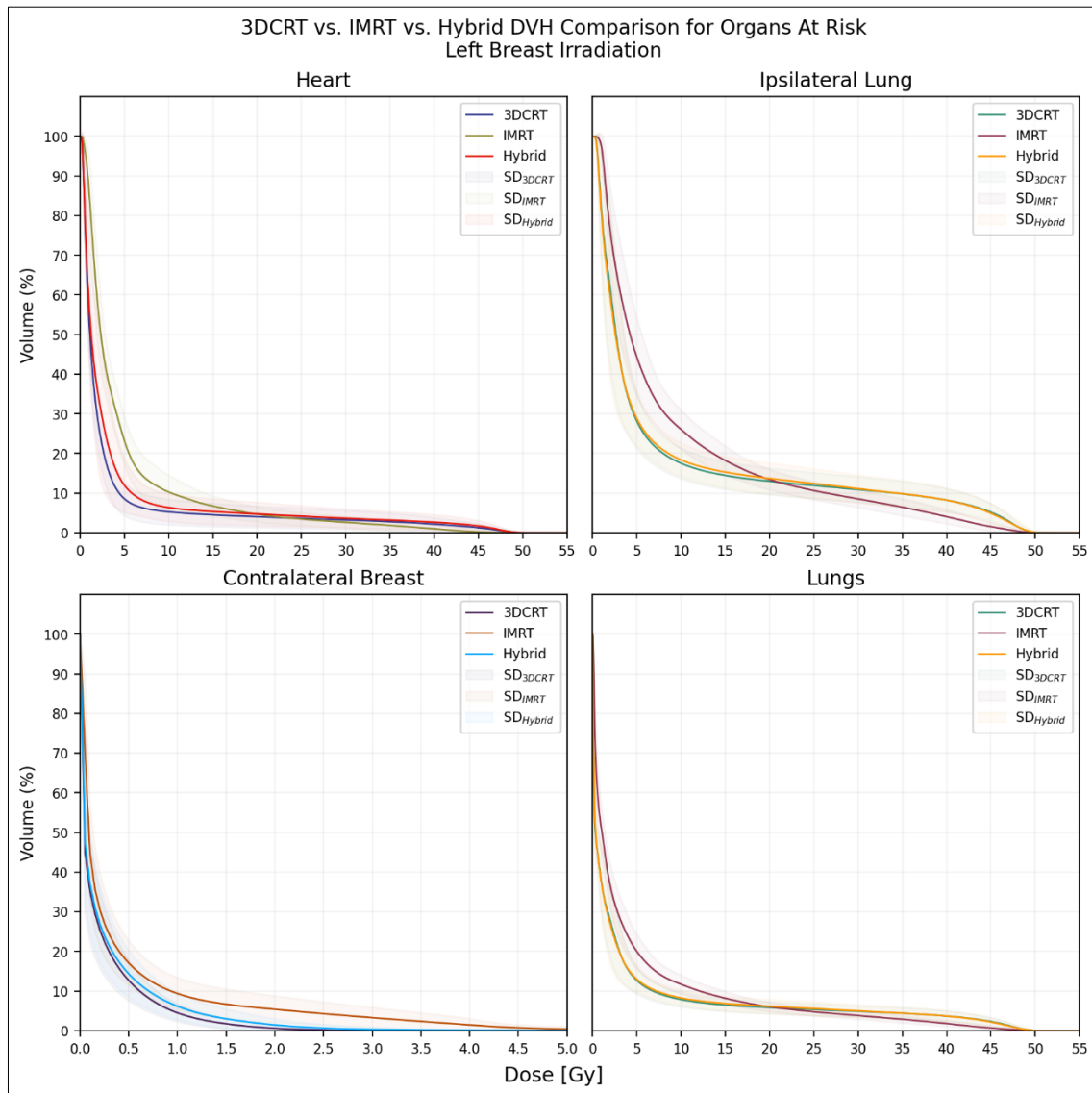


Graph 1 – Mean DVH of all structures, (a) 3D-CRT, (b) IMRT and (c) HT technique.

The mean DVH comparison between techniques for the PTV and CTV, as well as for some OAR, namely the heart, contralateral breast, ipsilateral lung and both lungs, are presented below. [Graph 2, 3]

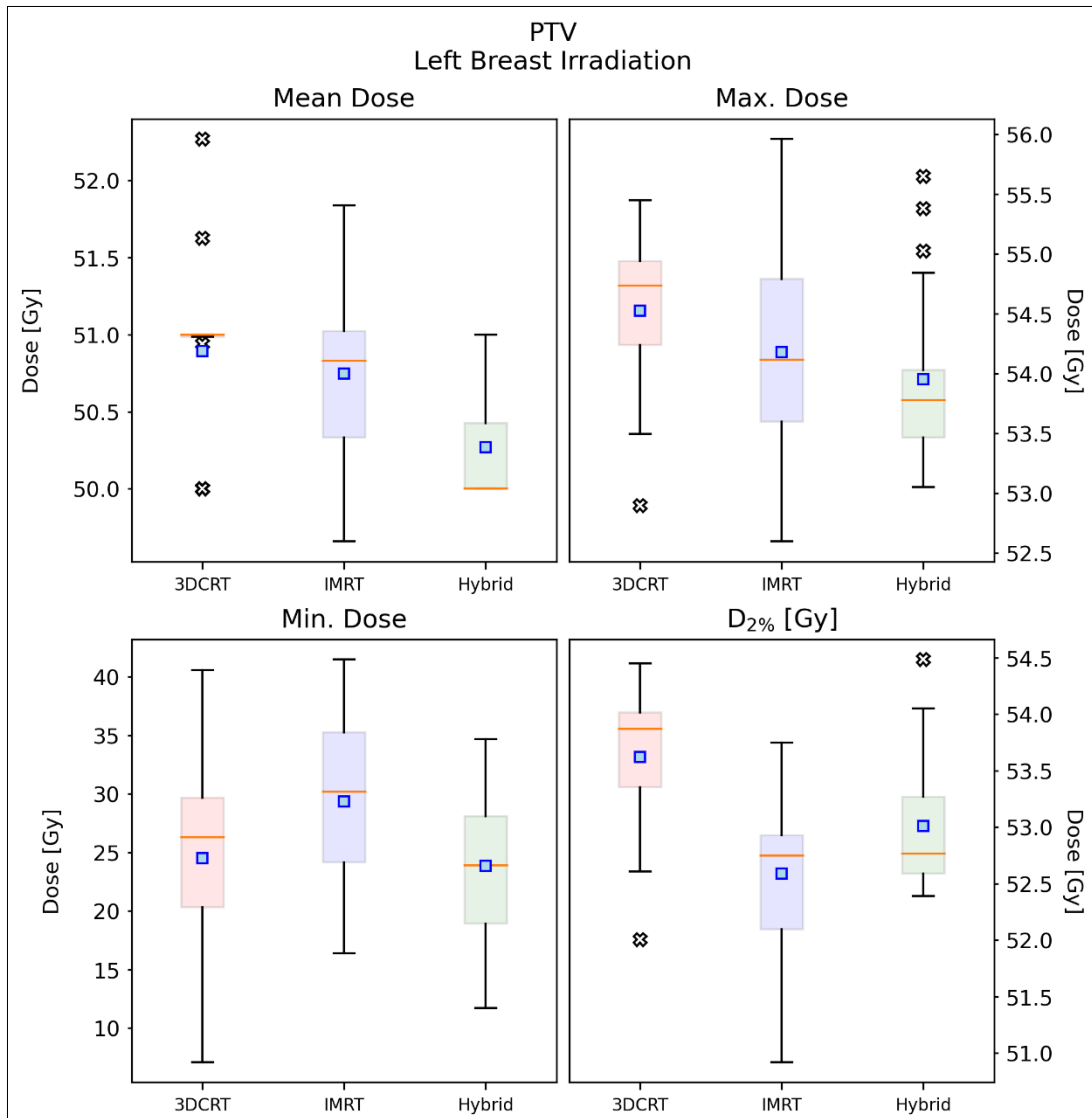


Graph 2 – Comparison of the mean DVH of the PTV and CTV between the three techniques; the bottom graphs are extracted from the graph on the top, separated by structure, zoomed in and centered on the prescribed dose of 50 Gy.



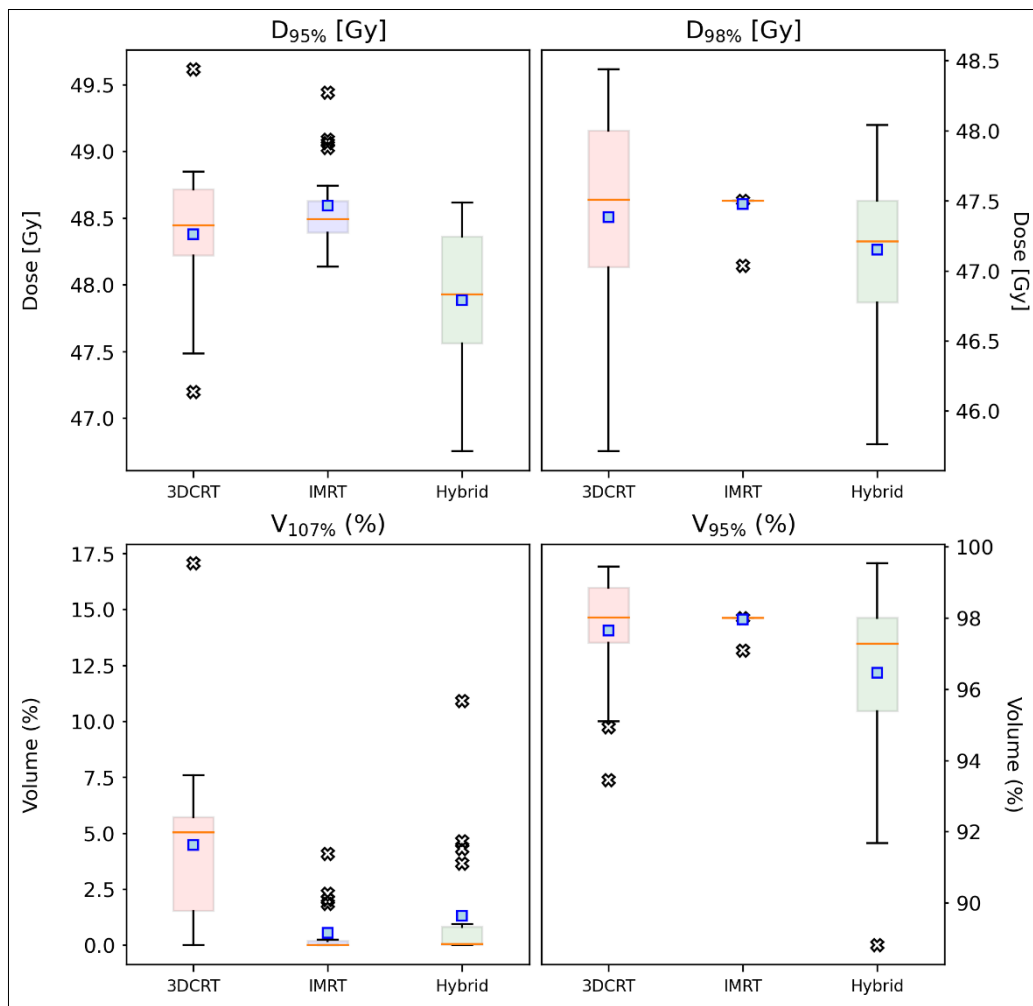
Graph 3 – Comparison of the mean DVH of the heart, contralateral breast, ipsilateral lung and both lungs, between the three techniques.

For the PTV, the dosimetric parameters that were determined were the mean dose, maximum dose, minimum dose, $D_{2\%}$, $D_{95\%}$, $D_{98\%}$, $V_{107\%}$, and $V_{95\%}$. Box plots showing the distributions of the results for the three techniques are presented below. [Graph 4, 5][Table 1.1]



Graph 4 – Comparison of the box plots of the mean, maximum, and minimum doses and D_{2%} results for the PTV.

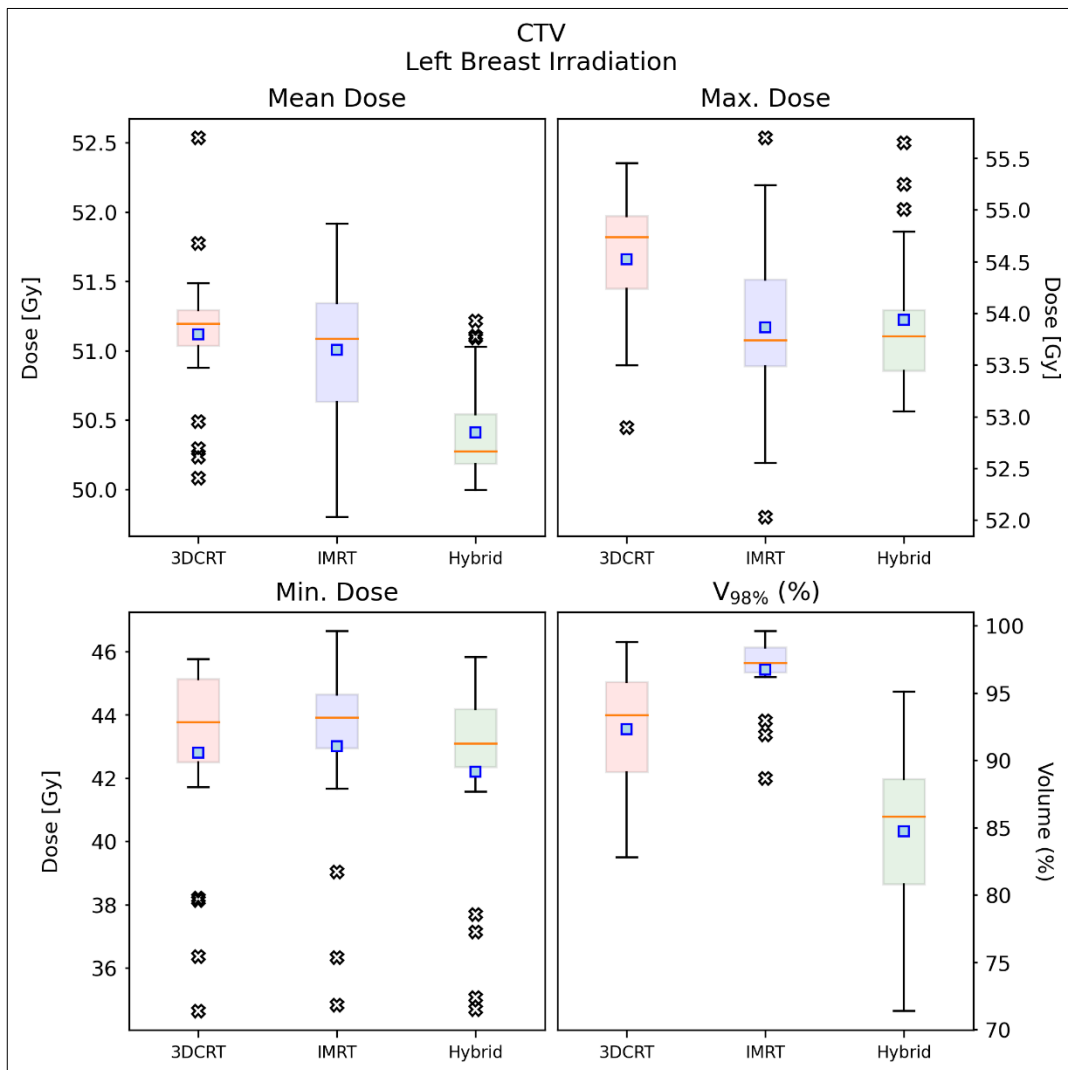
Orange dash: median; **blue square:** mean; **x mark:** outliers (points ∉ [Q1 – 1.5 IQR, Q3 + 1.5 IQR])



Graph 5 – Comparison of the box plots of D_{95%}, D_{98%}, V_{107%}, and V_{95%} results for the PTV.

Orange dash: median; **blue square:** mean; **x mark:** outliers (points ∉ [Q1 – 1.5 IQR, Q3 + 1.5 IQR])

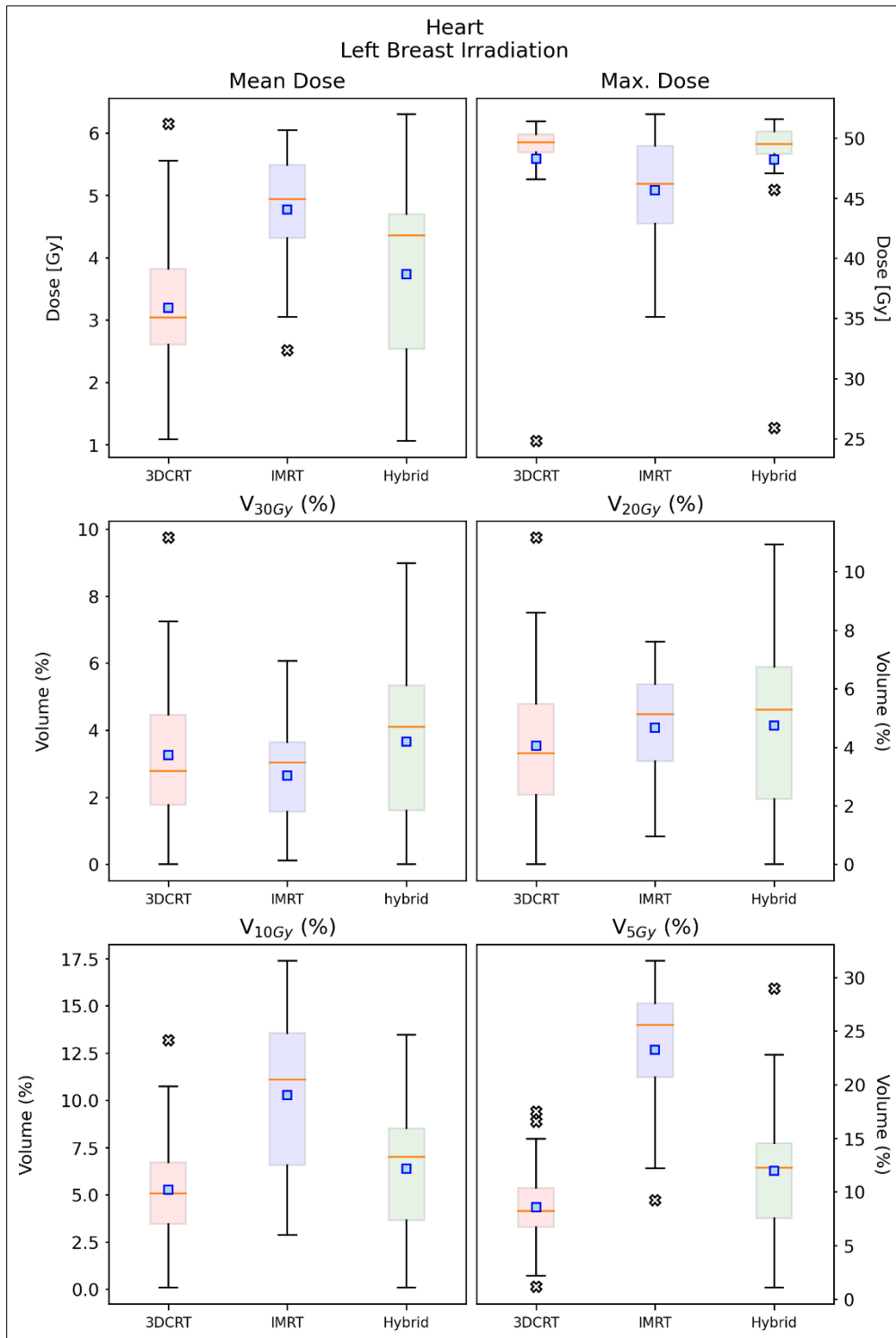
For the CTV, the dosimetric parameters that were determined were the mean dose, maximum dose, minimum dose, and V_{98%}. Box plots showing the distributions of the results for the three techniques are presented below. [Graph 6][Table 1.2]



Graph 6 – Comparison of the box plots of the results for the CTV.

Orange dash: median; **blue square:** mean; **x mark:** outliers (points \notin [Q1 – 1.5 IQR, Q3 + 1.5 IQR])

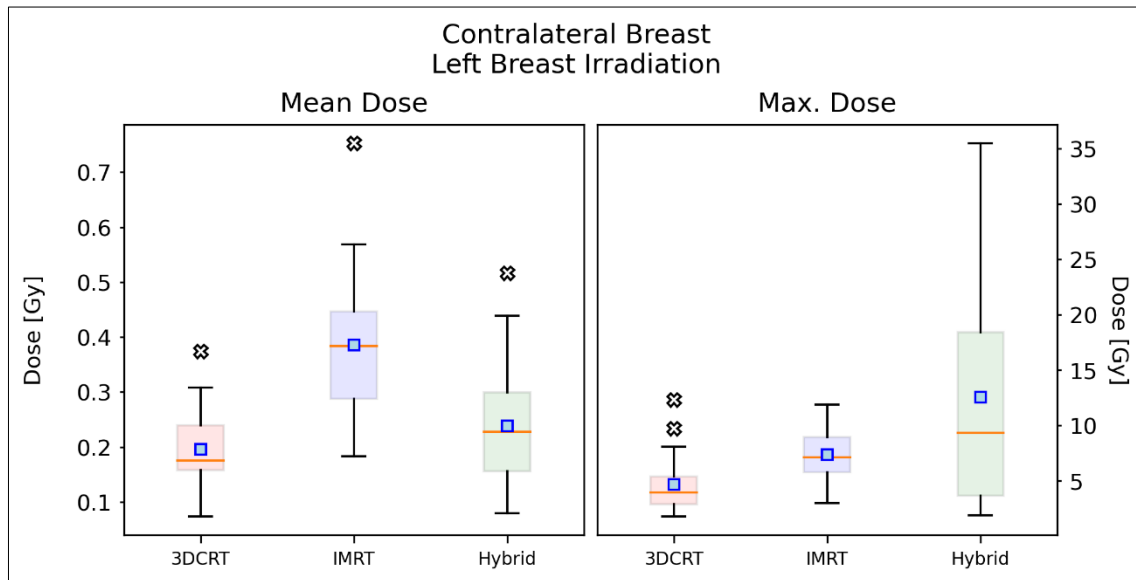
For the heart, the dosimetric parameters that were determined were the mean dose, maximum dose, V_{30Gy} , V_{20Gy} , V_{10Gy} , and V_{5Gy} . Box plots showing the distributions of the results for the three techniques are presented below. [Graph 7][Table 1.3]



Graph 7 – Comparison of the box plots of the results for the heart.

Orange dash: median; **blue square:** mean; **x mark:** outliers (points \notin [Q1 – 1.5 IQR, Q3 + 1.5 IQR])

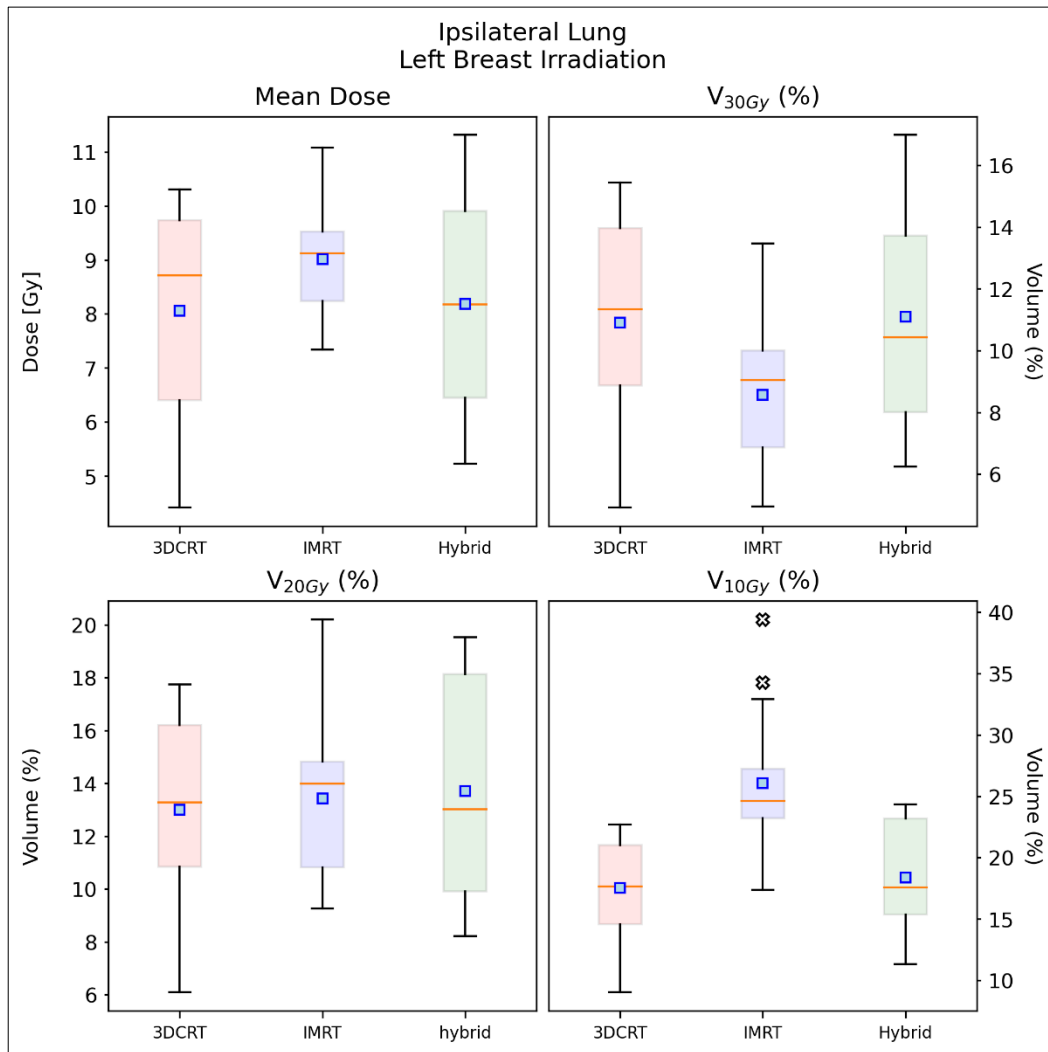
For the contralateral breast (right), the dosimetric parameters that were determined were the mean dose and maximum dose. Box plots showing the distributions of the results for the three techniques are presented below. [Graph 8][Table 1.4]



Graph 8 – Comparison of the box plots of the results for the contralateral breast.

Orange dash: median; **blue square:** mean; **x mark:** outliers (points \notin [Q1 – 1.5 IQR, Q3 + 1.5 IQR])

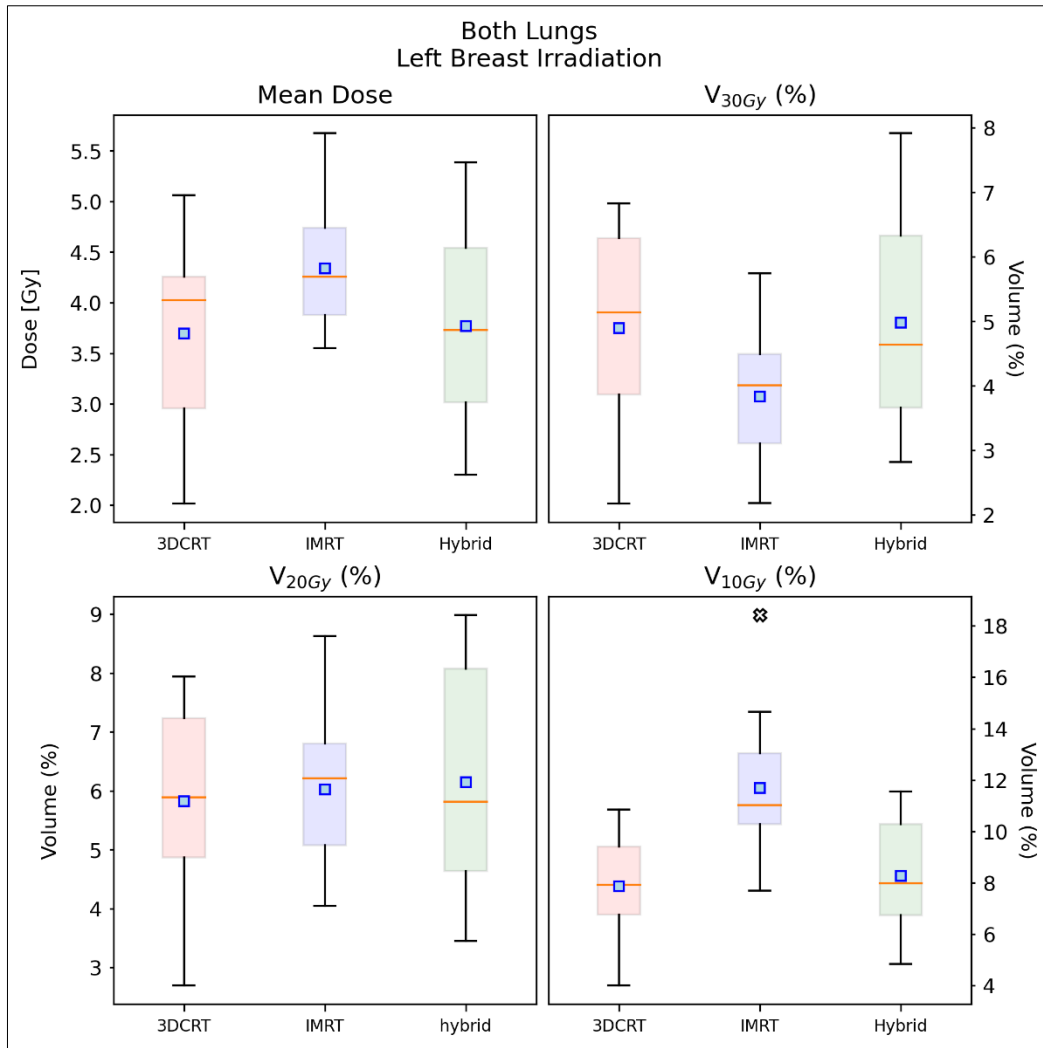
For the ipsilateral lung, the dosimetric parameters that were determined were the mean dose, V_{30Gy} , V_{20Gy} , and V_{10Gy} . Box plots showing the distributions of the results for the three techniques are presented below. [Graph 9][Table 1.5]



Graph 9 – Comparison of the box plots of the results for the ipsilateral lung.

Orange dash: median; **blue square:** mean; **x mark:** outliers (points $\notin [Q1 - 1.5 IQR, Q3 + 1.5 IQR]$)

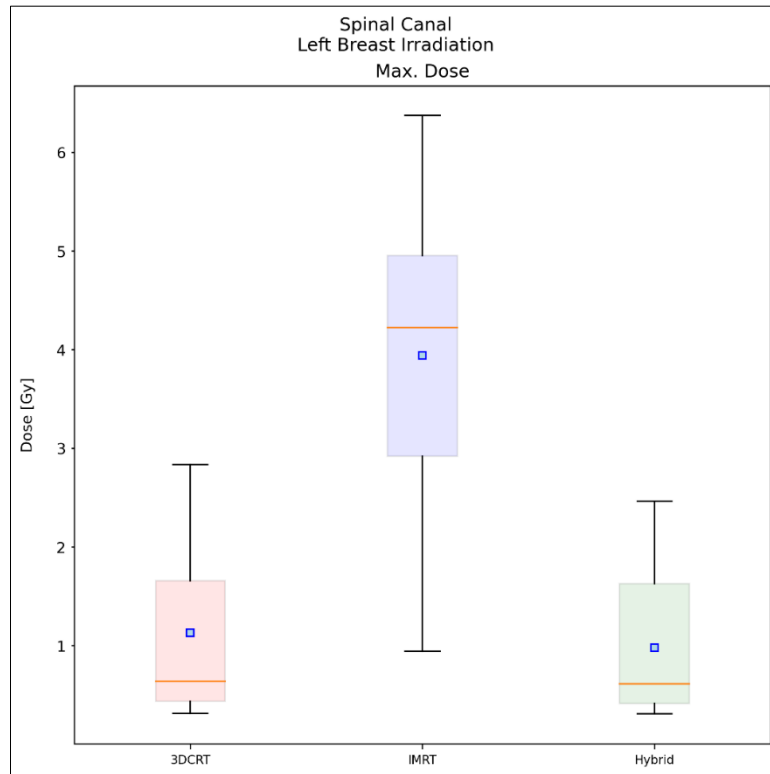
For the lungs, the dosimetric parameters that were determined were the mean dose, V_{30Gy} , V_{20Gy} , and V_{10Gy} . Box plots showing the distributions of the results for the three techniques are presented below. [Graph 10][Table 1.6]



Graph 10 – Comparison of the box plots of the results for the lungs.

Orange dash: median; **blue square:** mean; **x mark:** outliers (points \notin [Q1 – 1.5 IQR, Q3 + 1.5 IQR])

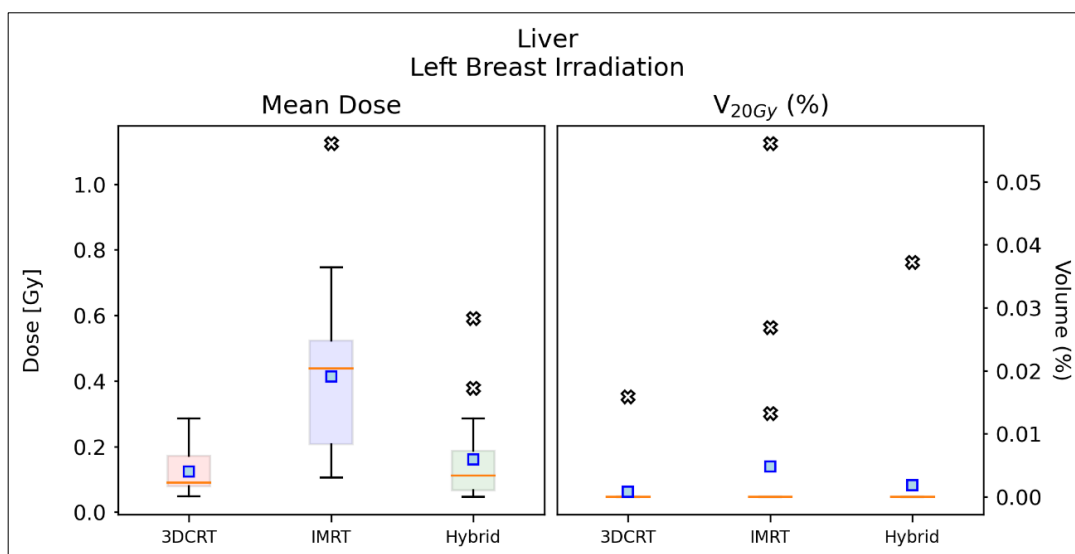
For the spinal canal, the dosimetric parameter that was determined was the maximum dose. Box plots showing the distributions of the results for the three techniques are presented below. [Graph 11][Table 1.7]



Graph 11 – Comparison of the box plots of the results for the spinal canal.

Orange dash: median; **blue square:** mean; **x mark:** outliers (points \notin [Q1 – 1.5 IQR, Q3 + 1.5 IQR])

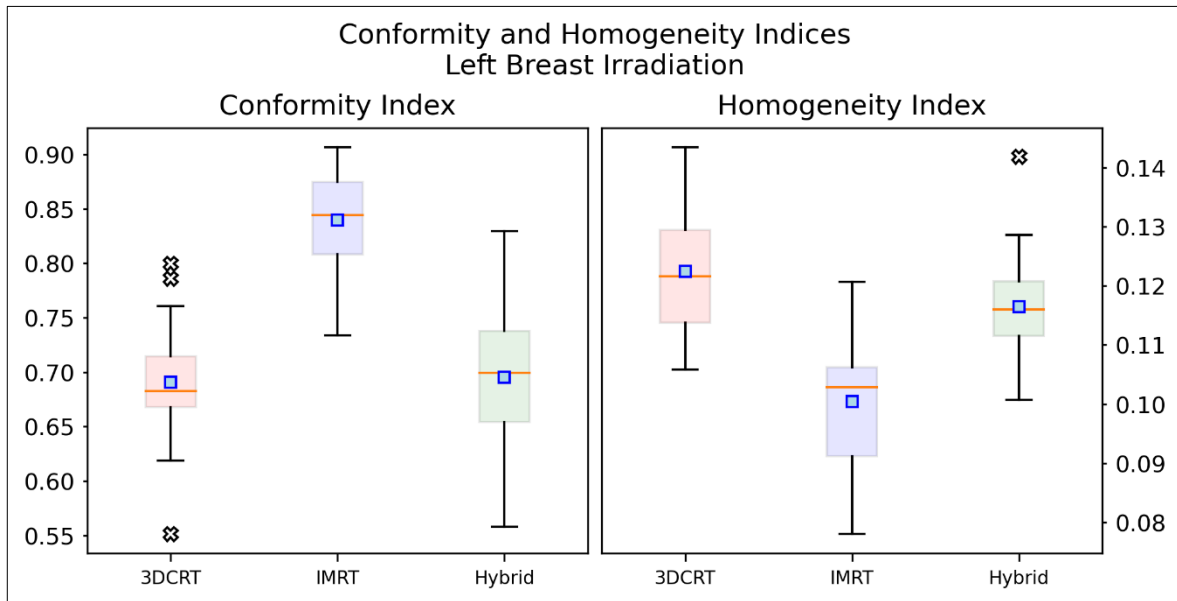
For the liver, the dosimetric parameters that were determined were the mean dose and V_{20Gy} . Box plots showing the distributions of the results for the three techniques are presented below. [Graph 12][Table 1.8]



Graph 12 – Comparison of the box plots of the results for the liver.

Orange dash: median; **blue square:** mean; **x mark:** outliers (points \notin [Q1 – 1.5 IQR, Q3 + 1.5 IQR])

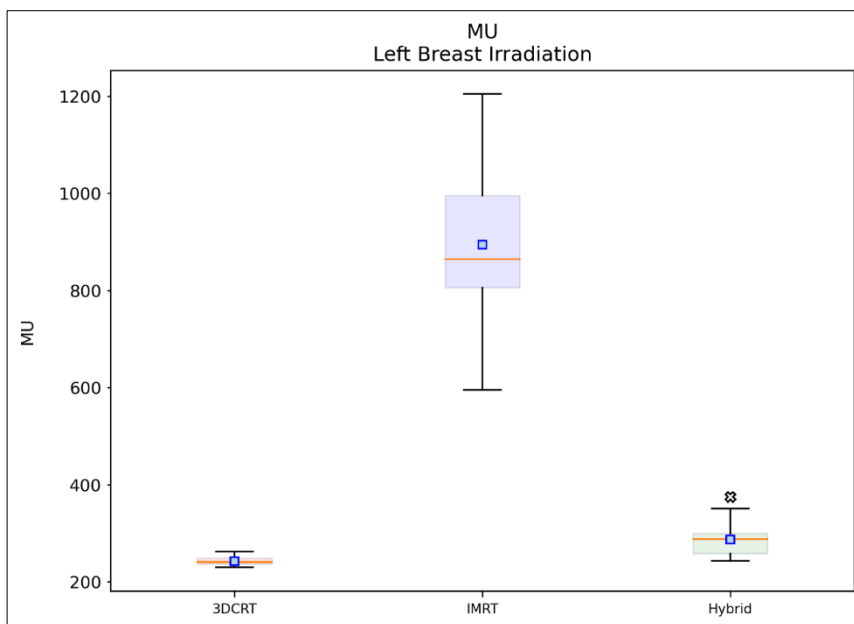
Box plots showing the distributions of the CI and HI for the three techniques are presented below. [Graph 13][Table 1.9]



Graph 13 – Comparison of the box plots of the results for the CI and HI.

Orange dash: median; blue square: mean; x mark: outliers (points \notin [Q1 – 1.5 IQR, Q3 + 1.5 IQR])

Box plots showing the distributions of MU for the three techniques are presented below. [Graph 14][Table 1.10]



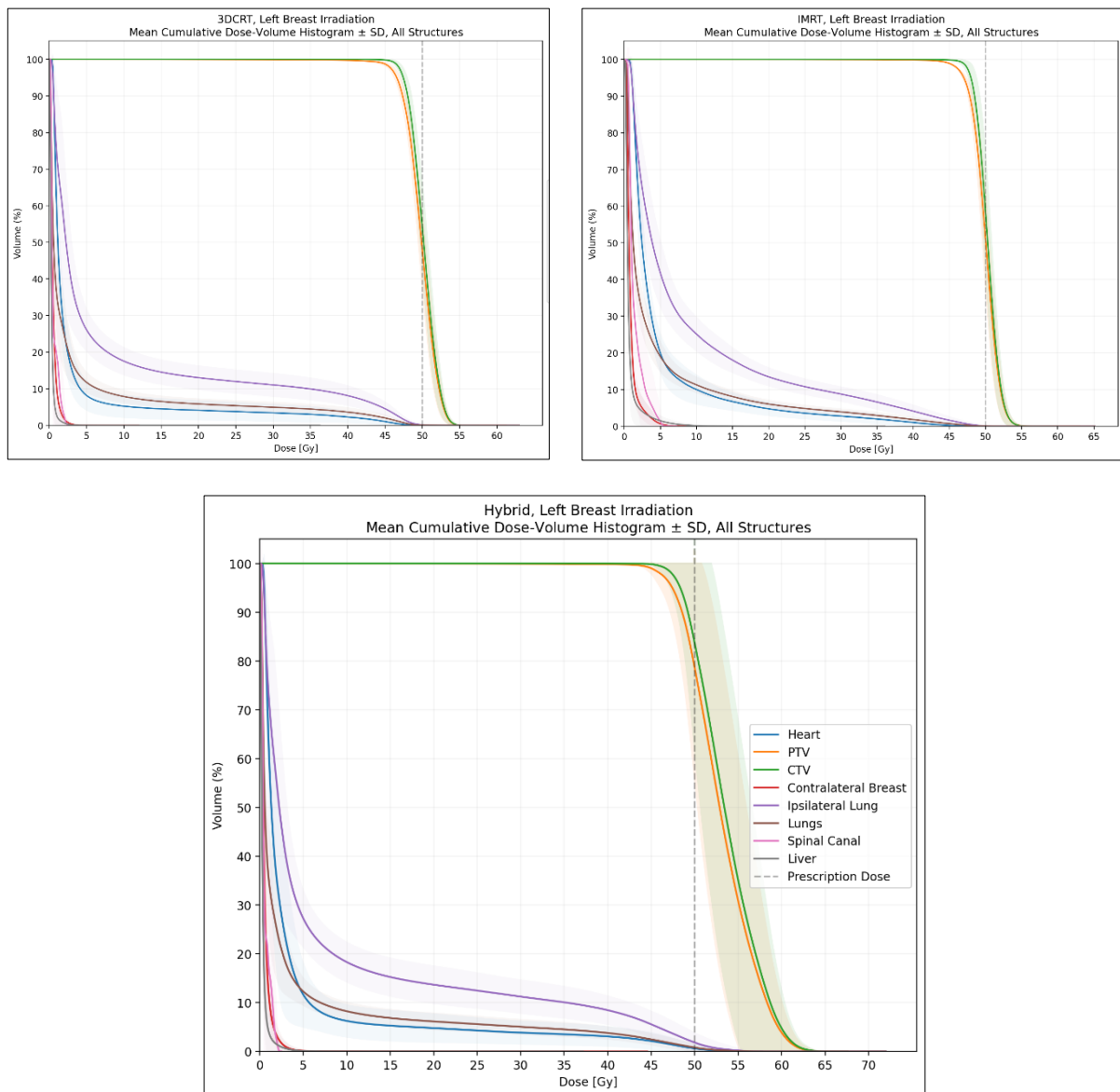
Graph 14 – Comparison of the box plots of the results for the MU.

Orange dash: median; blue square: mean; x mark: outliers (points \notin [Q1 – 1.5 IQR, Q3 + 1.5 IQR])

4.1.2 PRIMO

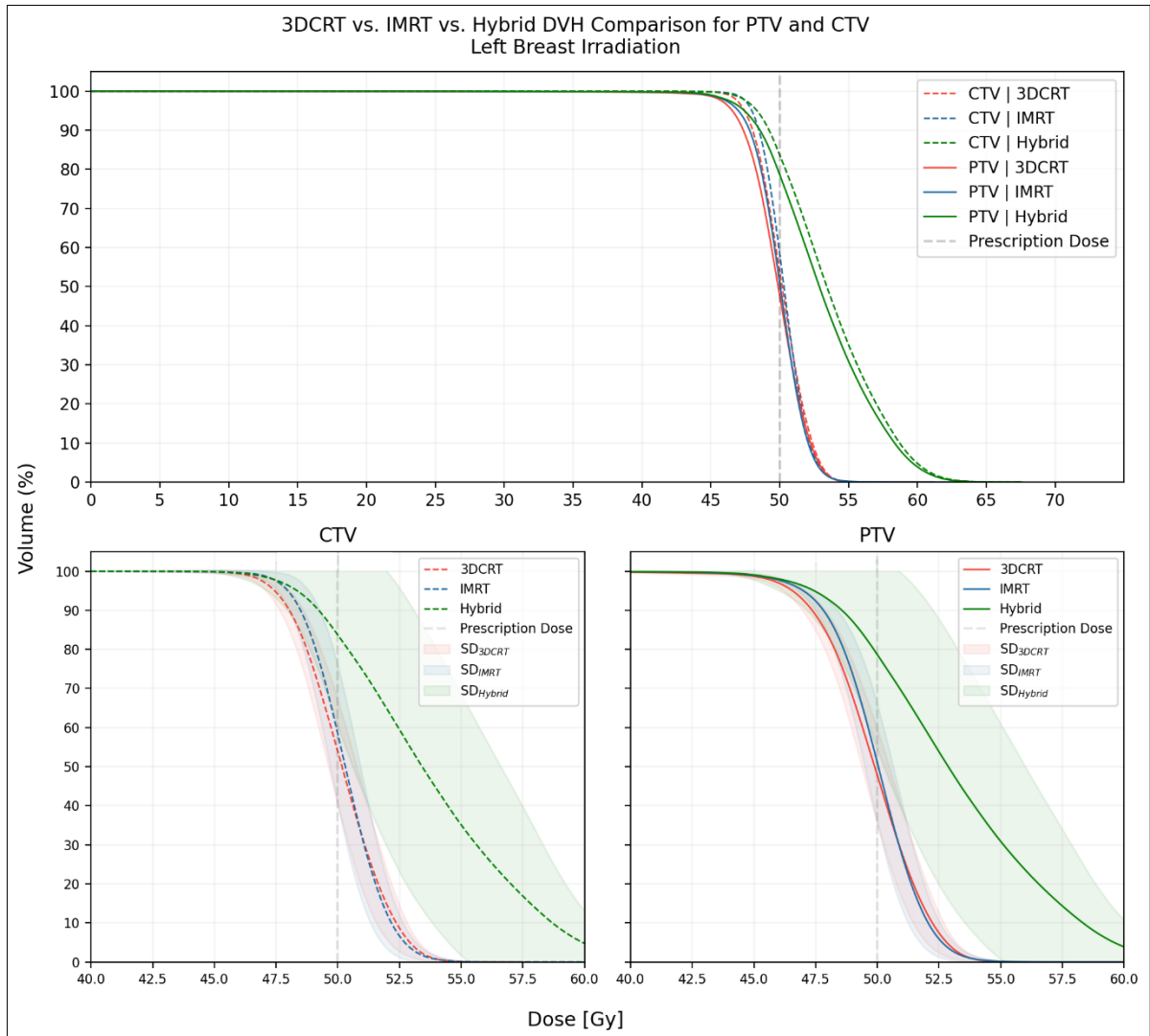
Considering the analysis performed to the TPS results, this section will present the resulting DVH plotted from the data acquired from PRIMO. Also, the box plots and numerical values for some dosimetric parameters are presented in a comparative manner. The results will give some insight about possible advantages of one technique over the others.

The mean DVH for all structures for 3D-CRT, IMRT and HT are shown below. [Graph 1]

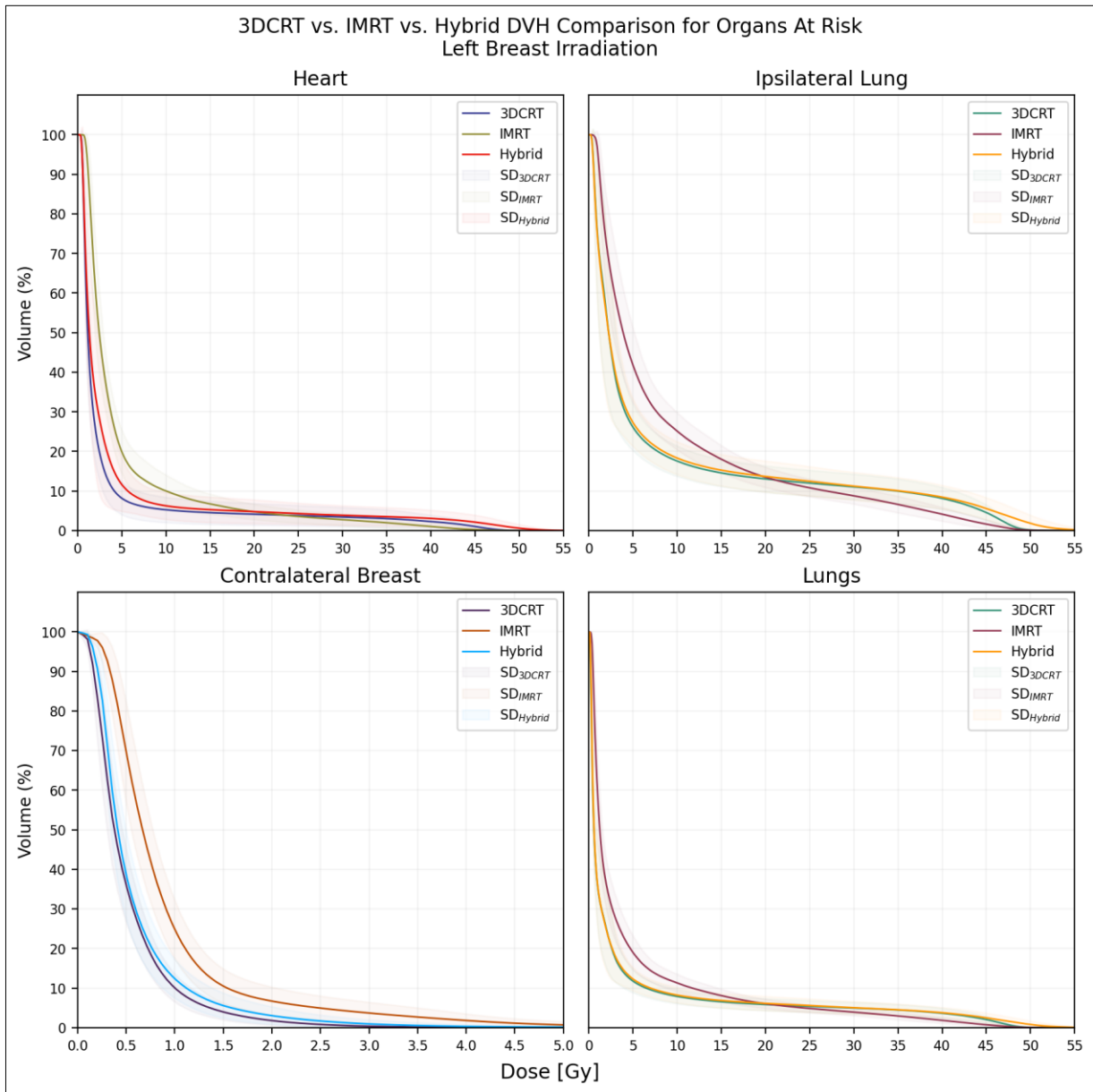


Graph 15 – Mean DVH of all structures, (a) 3D-CRT, (b) IMRT and (c) HT technique. From PRIMO.

The mean DVH comparison between techniques for the PTV and CTV, as well as for some OAR, namely the heart, contralateral breast, ipsilateral lung and both lungs, are presented below. [Graph 16, 17]

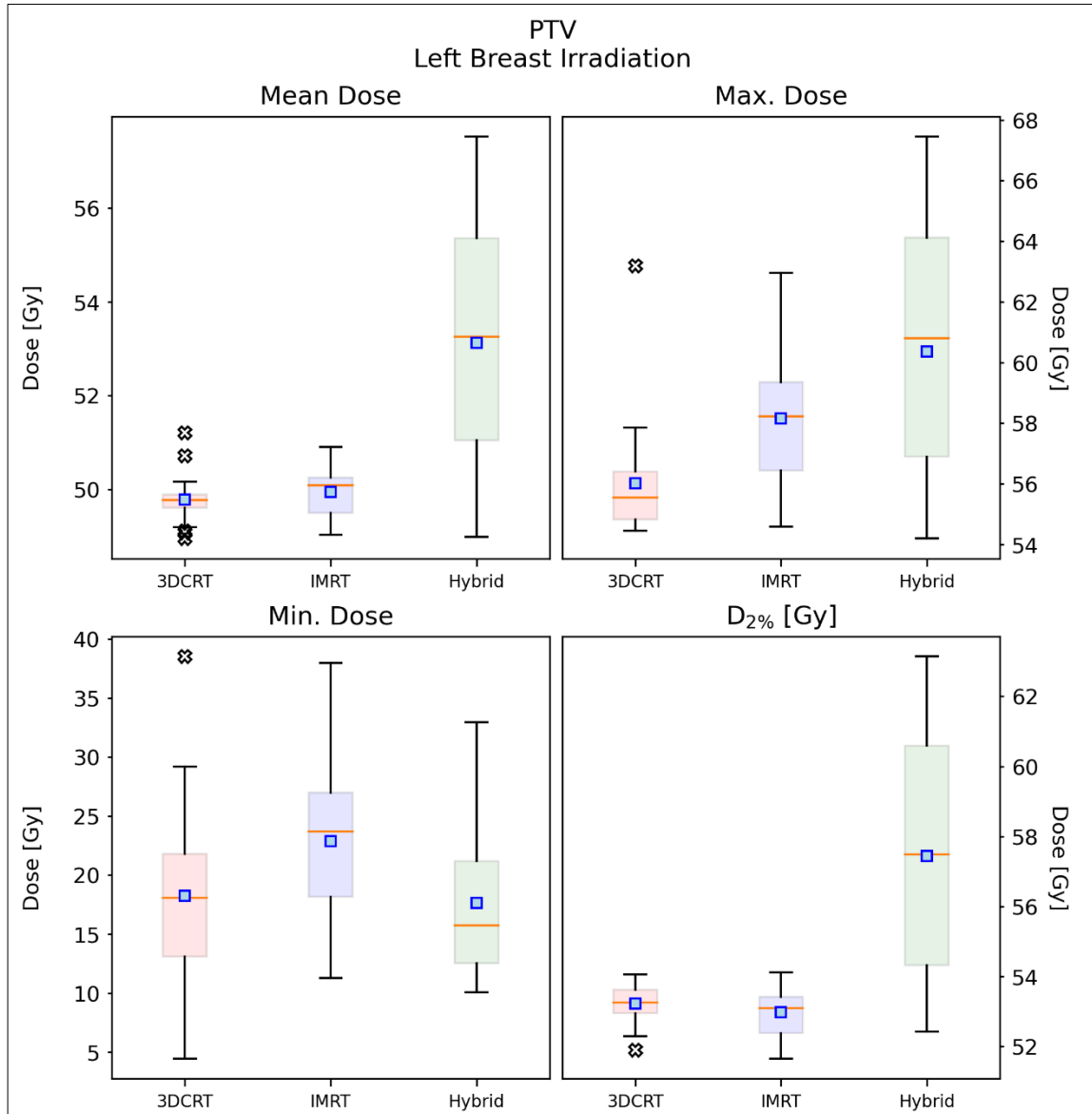


Graph 16 – Comparison of the mean DVH of the PTV and CTV between the three techniques; the bottom graphs are extracted from the graph on the top, separated by structure, zoomed in and centered on the prescribed dose of 50 Gy. Acquired with PRIMO.



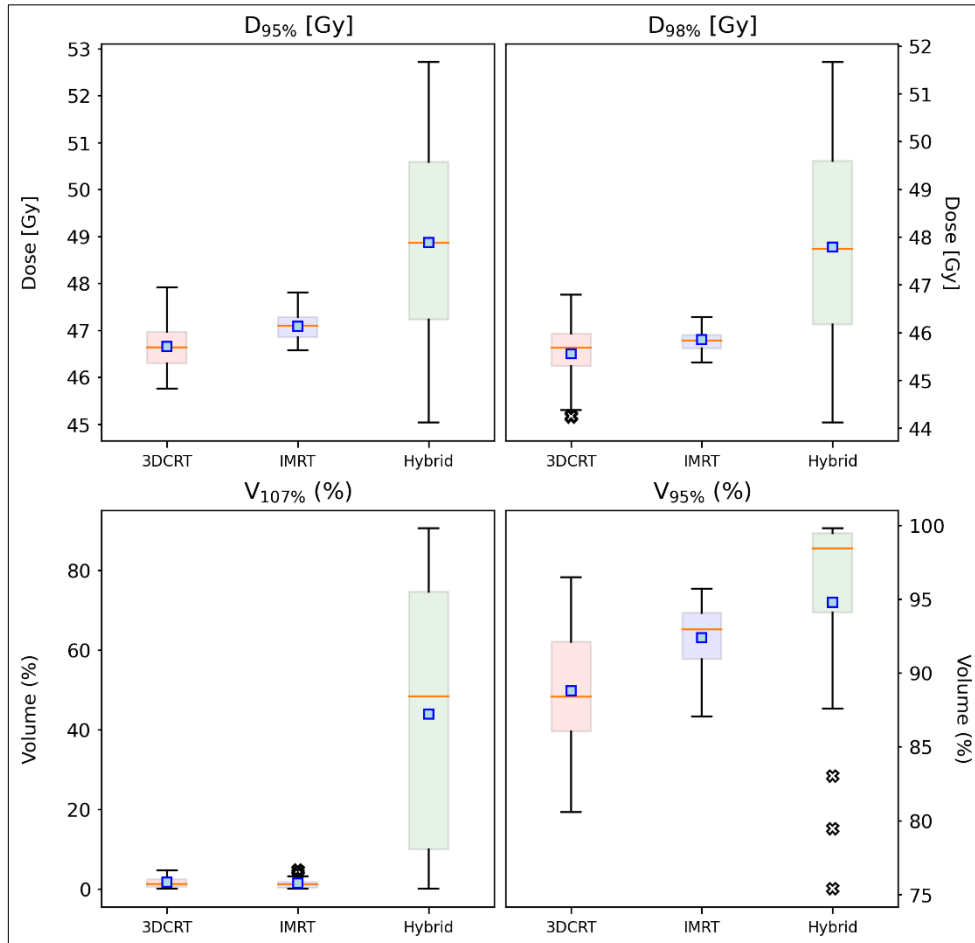
Graph 17 – Comparison of the mean DVH of the heart, contralateral breast, ipsilateral lung and both lungs, between the three techniques. Acquired with PRIMO.

For the PTV, the dosimetric parameters that were determined were the mean dose, maximum dose, minimum dose, $D_{2\%}$, $D_{95\%}$, $D_{98\%}$, $V_{107\%}$, and $V_{95\%}$. Box plots showing the distributions of the results for the three techniques are presented below. [Graph 18, 19][Table 2.1]



Graph 18 – Comparison of the box plots of the mean, maximum, and minimum doses and D_{2%} results for the PTV. Acquired with PRIMO.

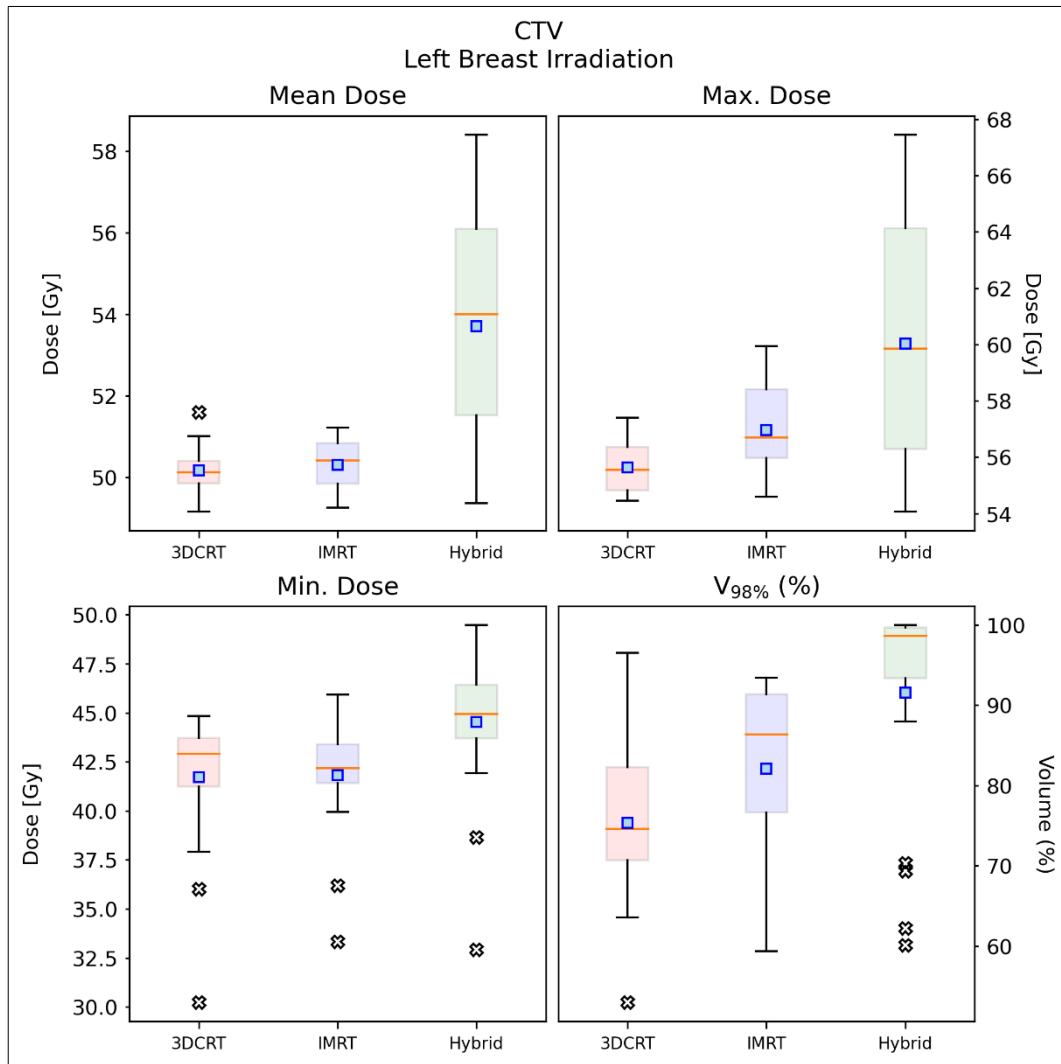
Orange dash: median; **blue square:** mean; **x mark:** outliers (points \notin [Q1 – 1.5 IQR, Q3 + 1.5 IQR])



Graph 19 – Comparison of the box plots of D_{95%}, D_{98%}, V_{107%}, and V_{95%} results for the PTV. Acquired with PRIMO.

Orange dash: median; **blue square:** mean; **x mark:** outliers (points ∉ [Q1 – 1.5 IQR, Q3 + 1.5 IQR])

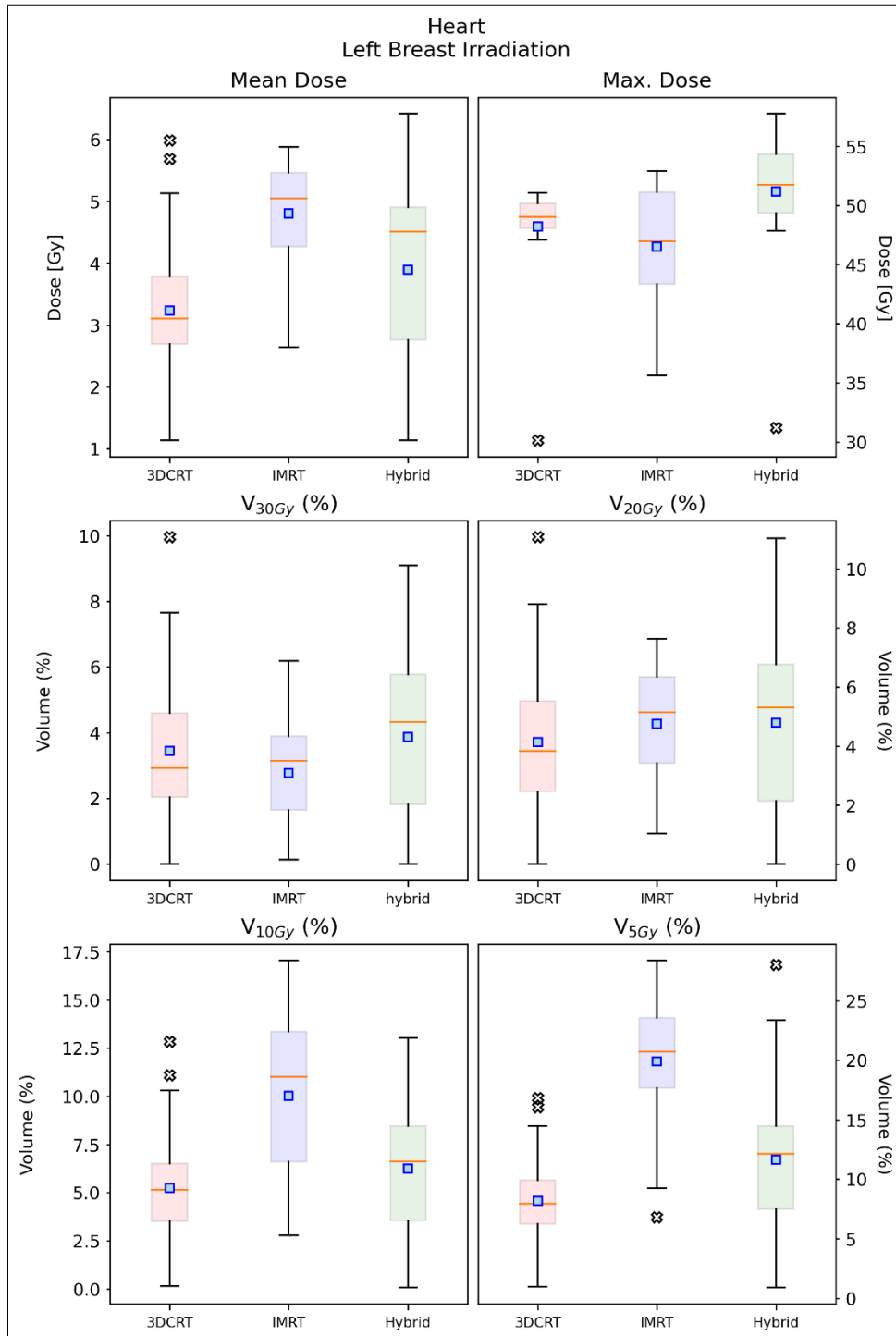
For the CTV, the dosimetric parameters that were determined were the mean dose, maximum dose, minimum dose, and V_{98%}. Box plots showing the distributions of the results for the three techniques are presented below. [Graph 20][Table 2.2]



Graph 20 – Comparison of the box plots of the results for the CTV. Acquired with PRIMO.

Orange dash: median; **blue square:** mean; **x mark:** outliers (points \notin [Q1 – 1.5 IQR, Q3 + 1.5 IQR])

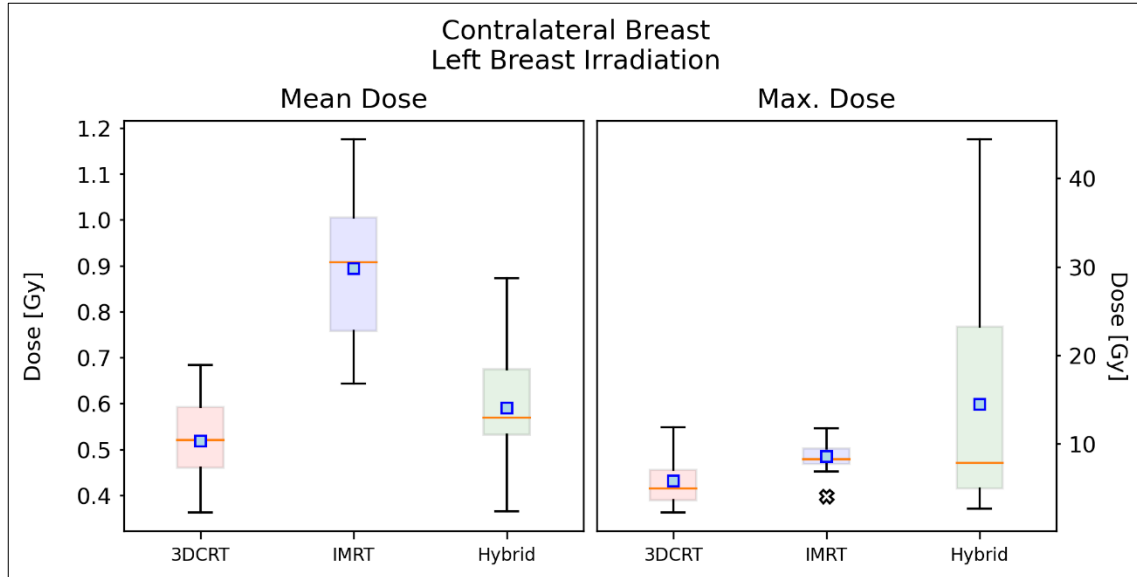
For the heart, the dosimetric parameters that were determined were the mean dose, maximum dose, V_{30Gy} , V_{20Gy} , V_{10Gy} , and V_{5Gy} . Box plots showing the distributions of the results for the three techniques are presented below. [Graph 21][Table 2.3]



Graph 21 – Comparison of the box plots of the results for the heart. Acquired with PRIMO.

Orange dash: median; **blue square:** mean; **x mark:** outliers (points $\notin [Q1 - 1.5 IQR, Q3 + 1.5 IQR]$)

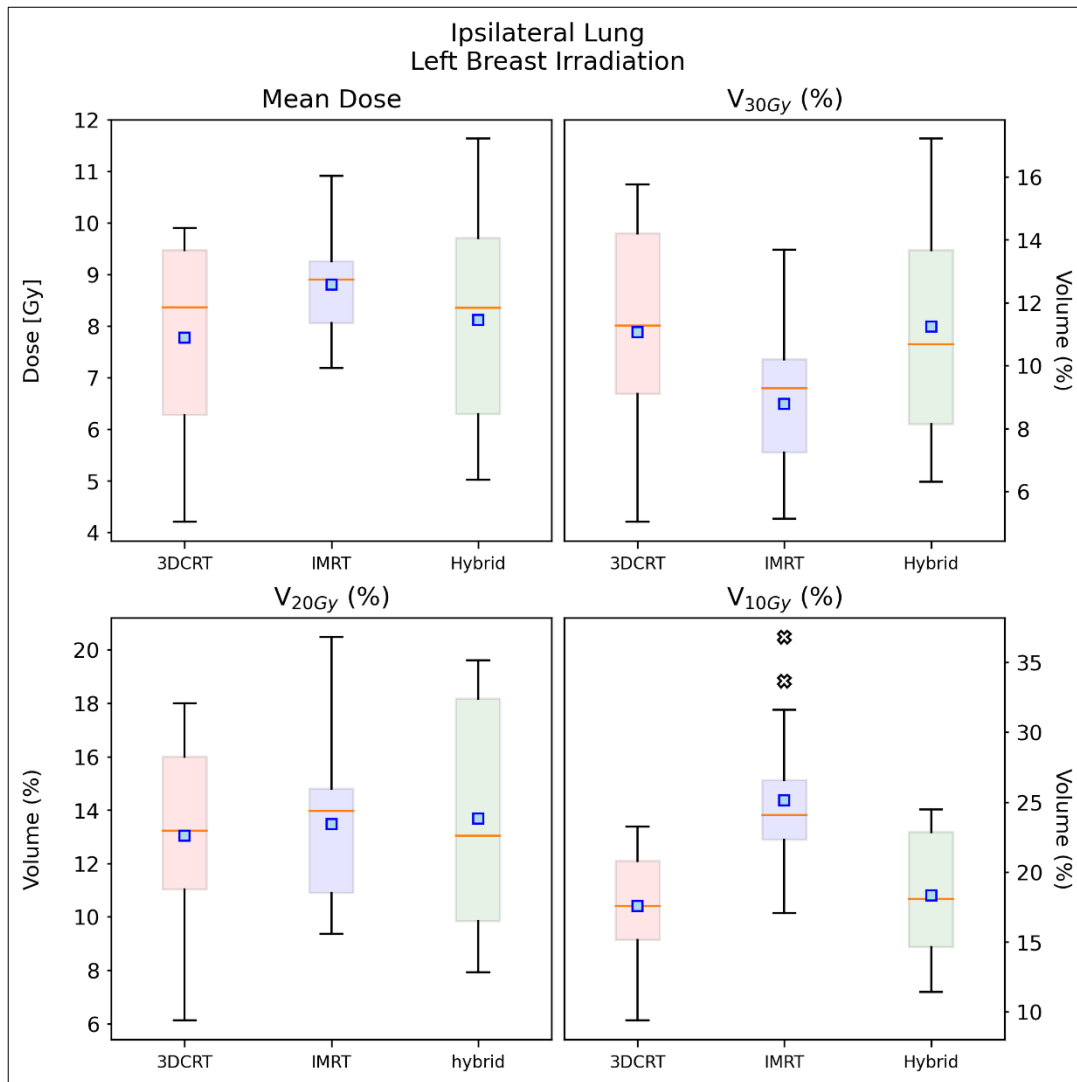
For the contralateral breast (right), the dosimetric parameters that were determined were the mean dose and maximum dose. Box plots showing the distributions of the results for the three techniques are presented below. [Graph 22][Table 2.4]



Graph 22 – Comparison of the box plots of the results for the contralateral breast. Acquired with PRIMO.

Orange dash: median; **blue square:** mean; **x mark:** outliers (points \notin [Q1 – 1.5 IQR, Q3 + 1.5 IQR])

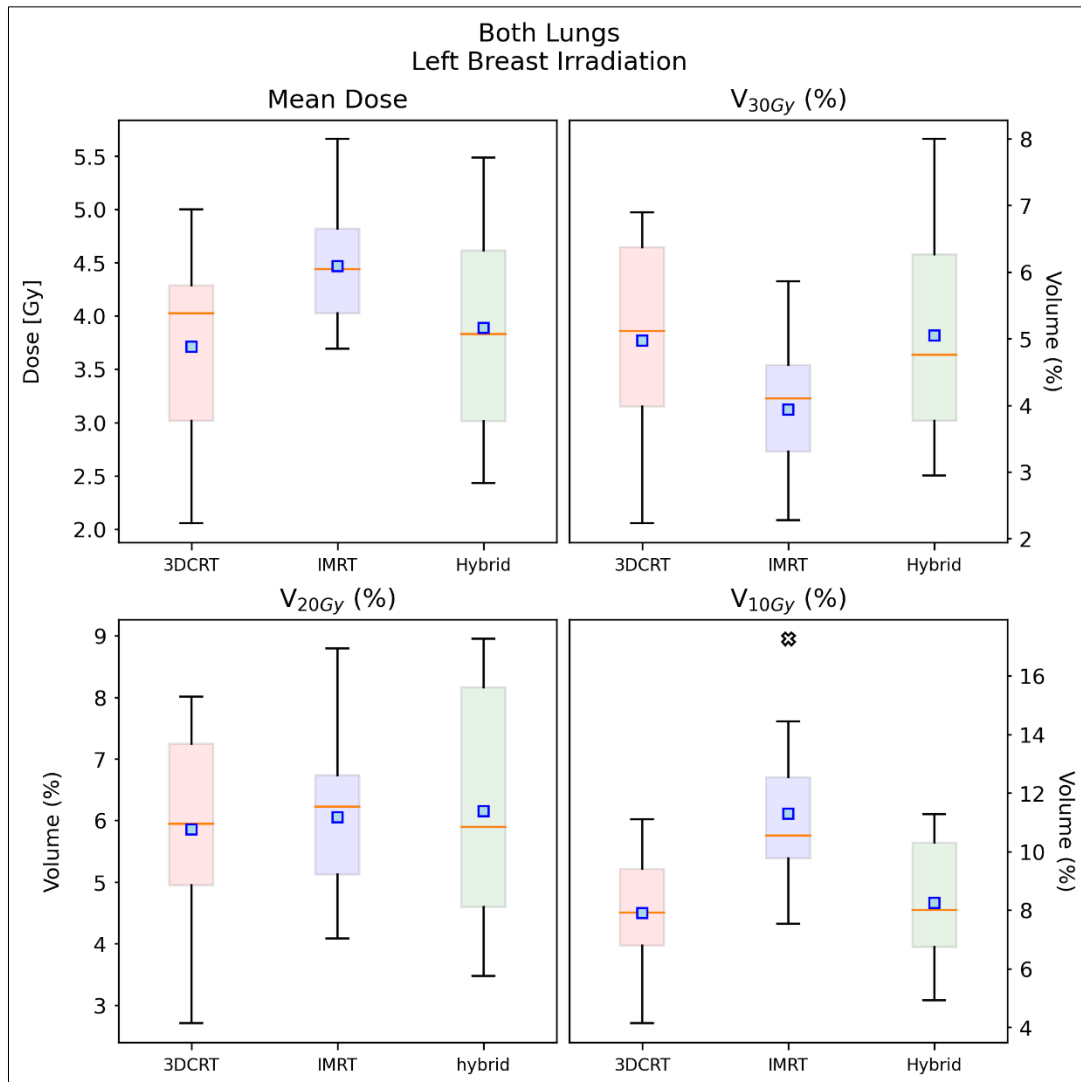
For the ipsilateral lung, the dosimetric parameters that were determined were the mean dose, V_{30Gy} , V_{20Gy} , and V_{10Gy} . Box plots showing the distributions of the results for the three techniques are presented below. [Graph 23][Table 2.5]



Graph 23 – Comparison of the box plots of the results for the ipsilateral lung. Acquired with PRIMO.

Orange dash: median; **blue square:** mean; **x mark:** outliers (points \notin [Q1 – 1.5 IQR, Q3 + 1.5 IQR])

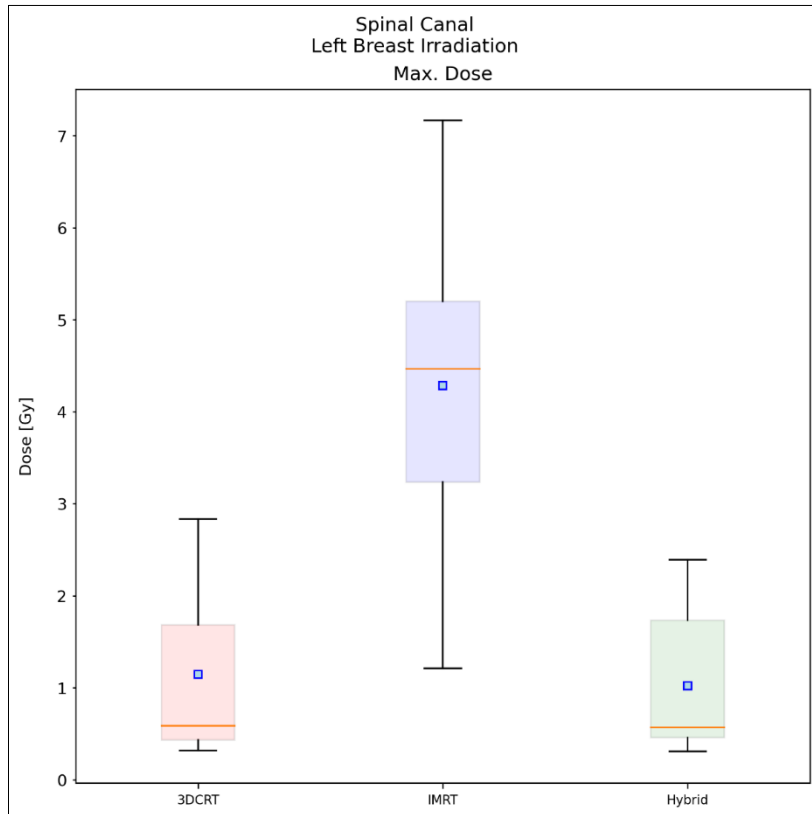
For the lungs, the dosimetric parameters that were determined were the mean dose, V_{30Gy} , V_{20Gy} , and V_{10Gy} . Box plots showing the distributions of the results for the three techniques are presented below. [Graph 24][Table 2.6]



Graph 24 – Comparison of the box plots of the results for the lungs. Acquired with PRIMO.

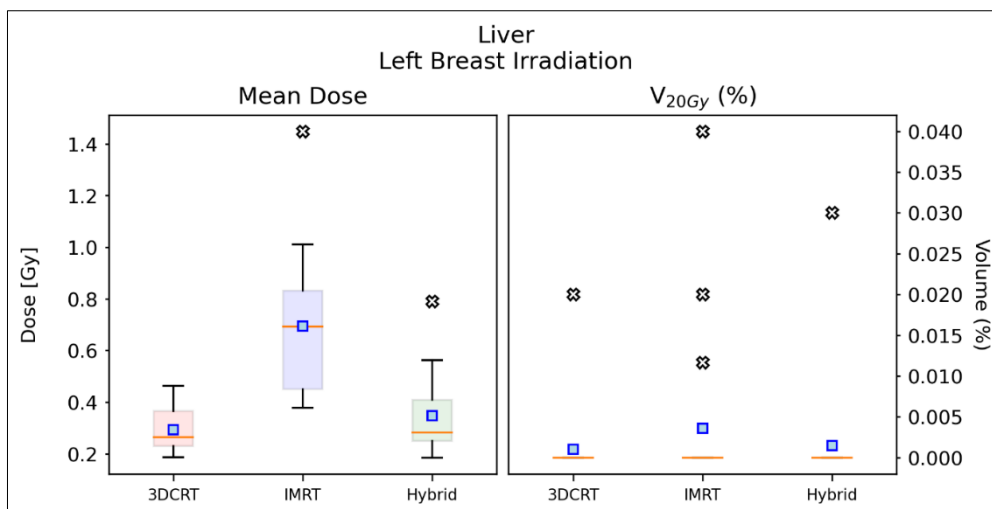
Orange dash: median; **blue square:** mean; **x mark:** outliers (points \notin [Q1 – 1.5 IQR, Q3 + 1.5 IQR])

For the spinal canal, the dosimetric parameter that was determined was the maximum dose. Box plots showing the distributions of the results for the three techniques are presented below. [Graph 25][Table 2.7]



Graph 25 – Comparison of the box plots of the results for the spinal canal. Acquired with PRIMO.

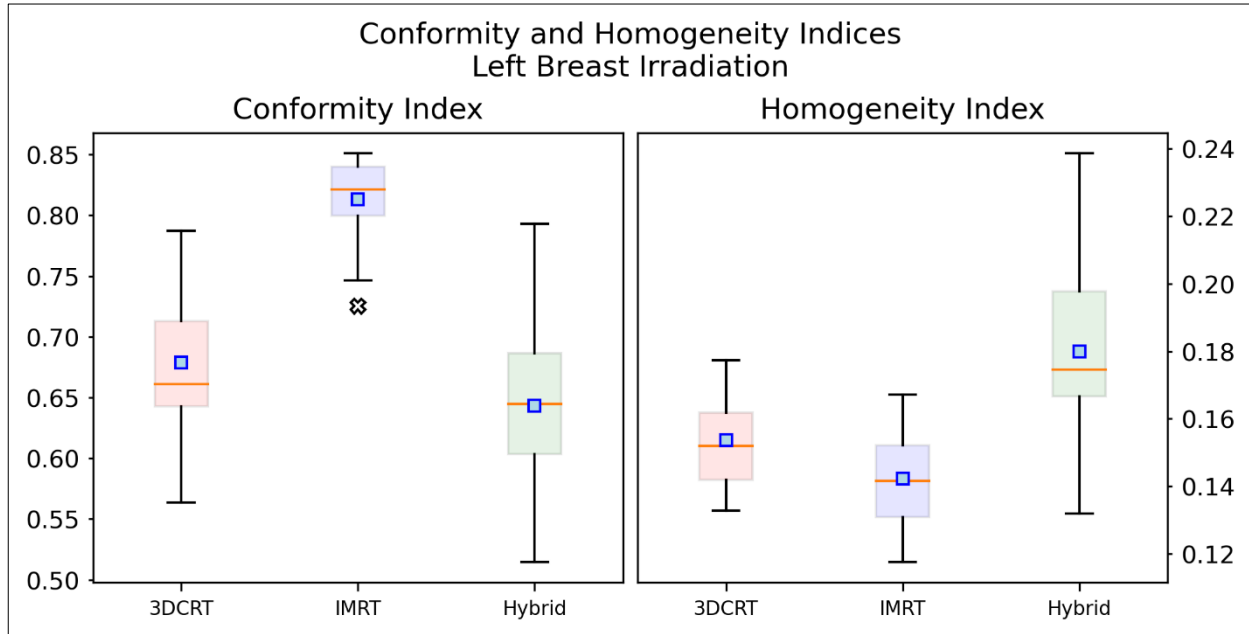
For the liver, the dosimetric parameters that were determined were the mean dose and V_{20Gy} . Box plots showing the distributions of the results for the three techniques are presented below. [Graph 26][Table 2.8]



Graph 26 – Comparison of the box plots of the results for the liver. Acquired with PRIMO.

Orange dash: median; **blue square:** mean; **x mark:** outliers (points \notin [Q1 – 1.5 IQR, Q3 + 1.5 IQR])

Box plots showing the distributions of the CI and HI for the three techniques are presented below. [Graph 27][Table 2.9]



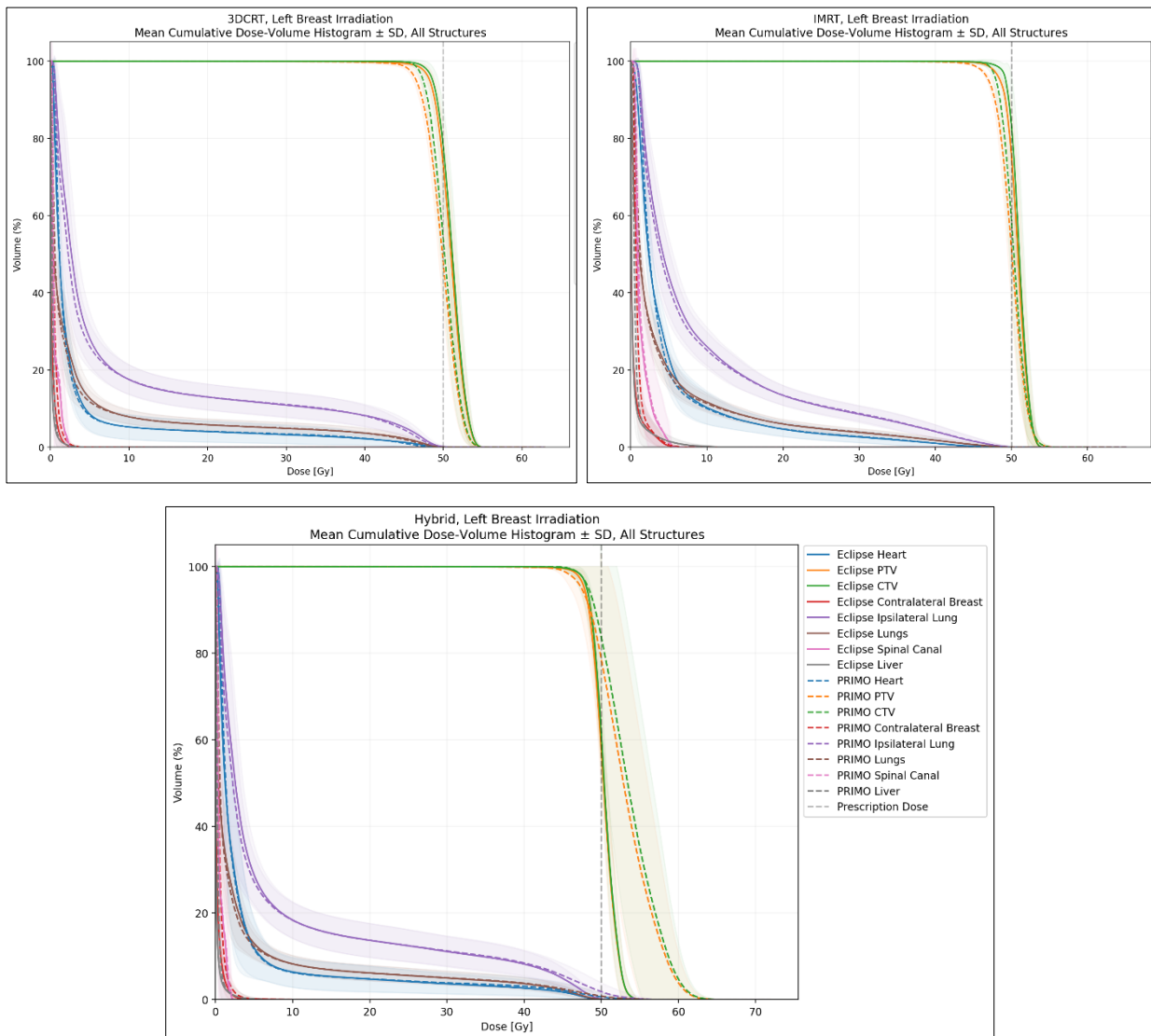
Graph 27 – Comparison of the box plots of the results for the CI and HI. Acquired with PRIMO.

Orange dash: median; **blue square:** mean; **x mark:** outliers (points \notin [Q1 – 1.5 IQR, Q3 + 1.5 IQR])

4.1.3 TPS vs. PRIMO

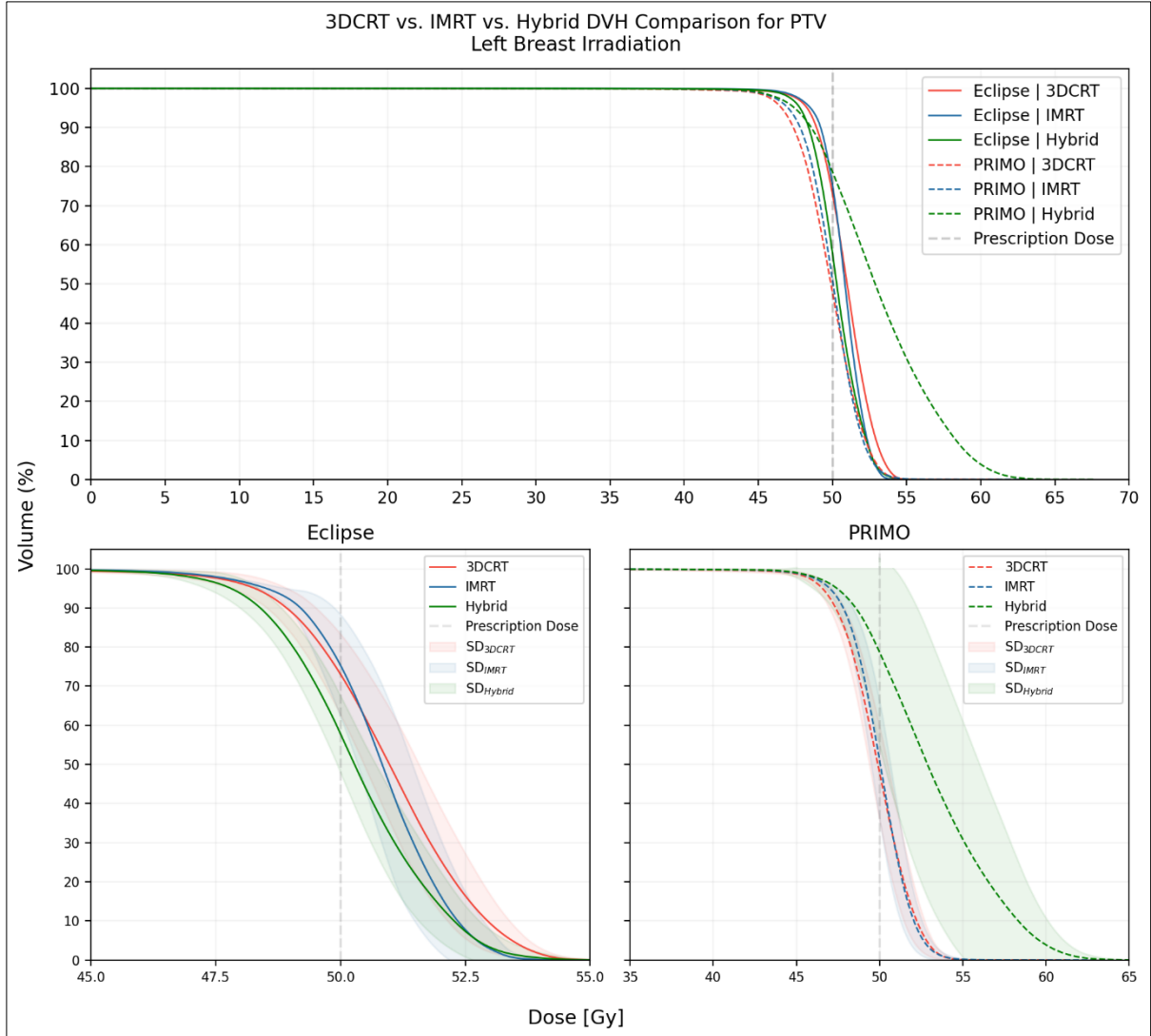
In this section, a results comparison between the two algorithms will be done. The results will be presented by DVH plot and box plots.

The mean DVH for all structures for 3D-CRT, IMRT and HT are shown below. [Graph 28]

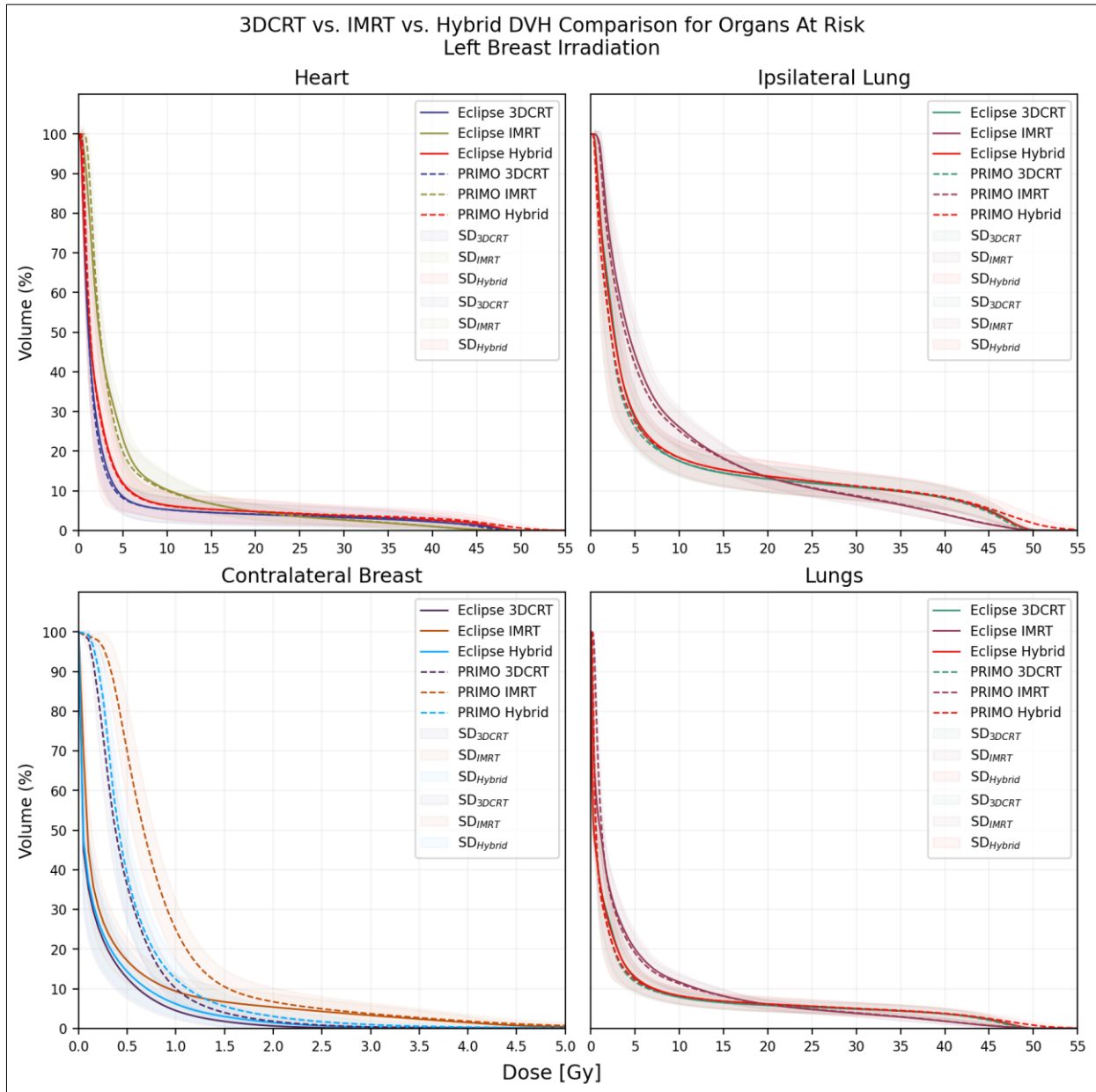


Graph 28 – Mean DVH of all structures, (a) 3D-CRT, (b) IMRT and (c) HT technique, acquired with the TPS and PRIMO.

The mean DVH comparison between techniques and tools for the PTV, as well as for some OAR, namely the heart, contralateral breast, ipsilateral lung and both lungs, are presented below. [Graph 29, 30]

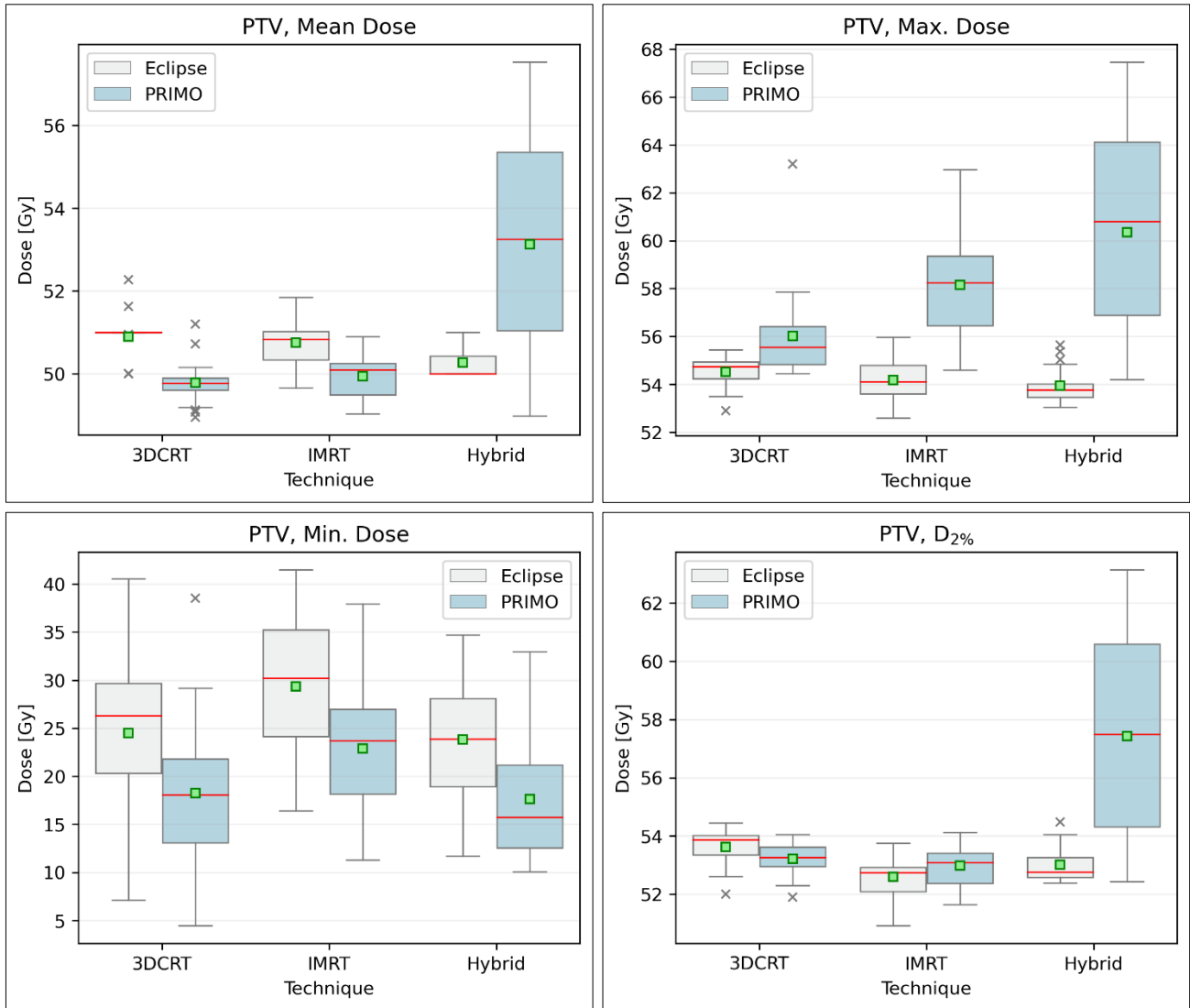


Graph 29 – Comparison of the mean DVH of the PTV among the three techniques and the two tools; the bottom graphs are extracted from the graph on the top, separated by tool, zoomed in and centered on the prescribed dose of 50 Gy.



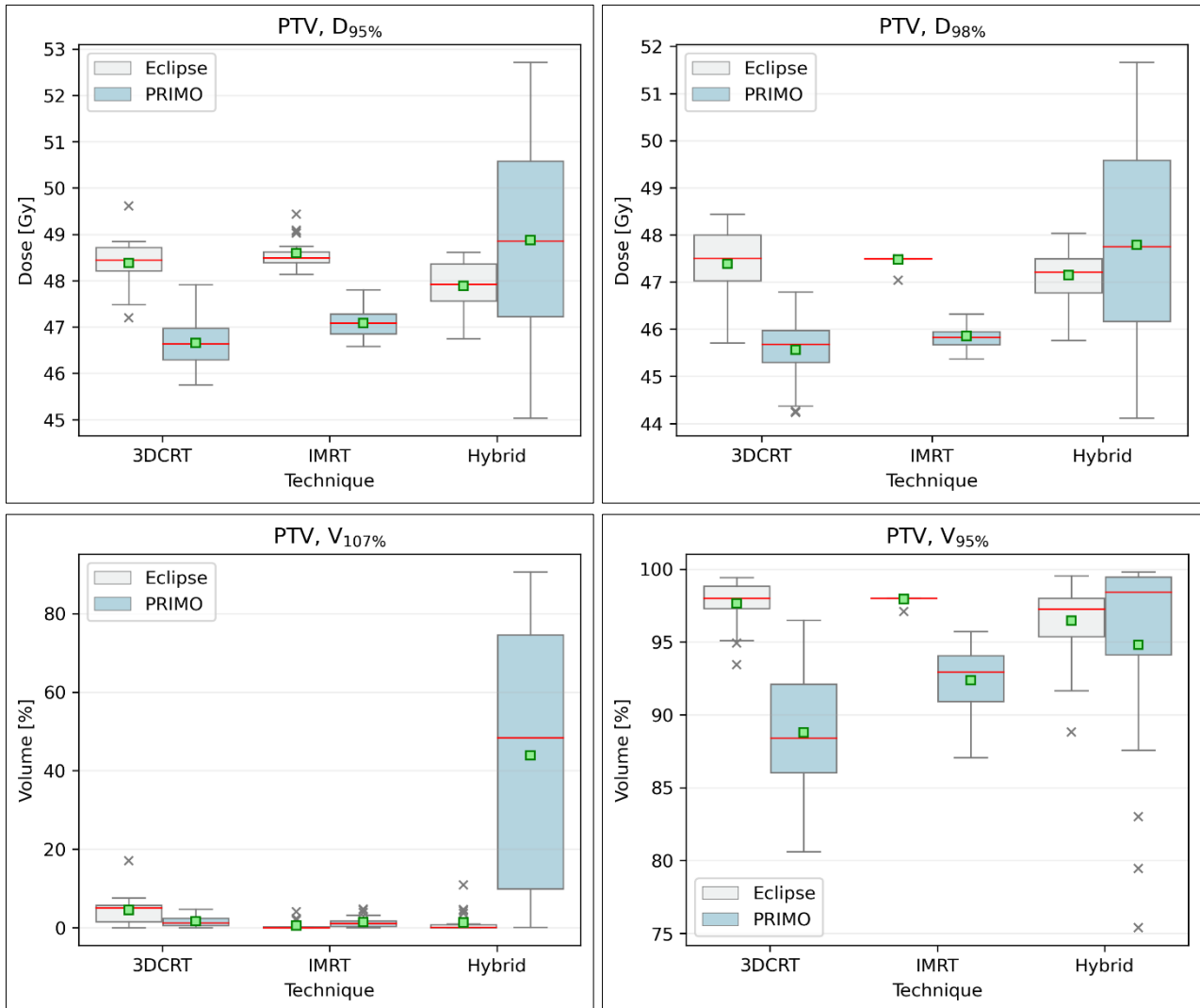
Graph 30 – Comparison of the mean DVH of the heart, contralateral breast, ipsilateral lung and both lungs, between the three techniques and two tools.

Box plots comparing all the dosimetric parameters among the three techniques and between the TPS and PRIMO are presented below.



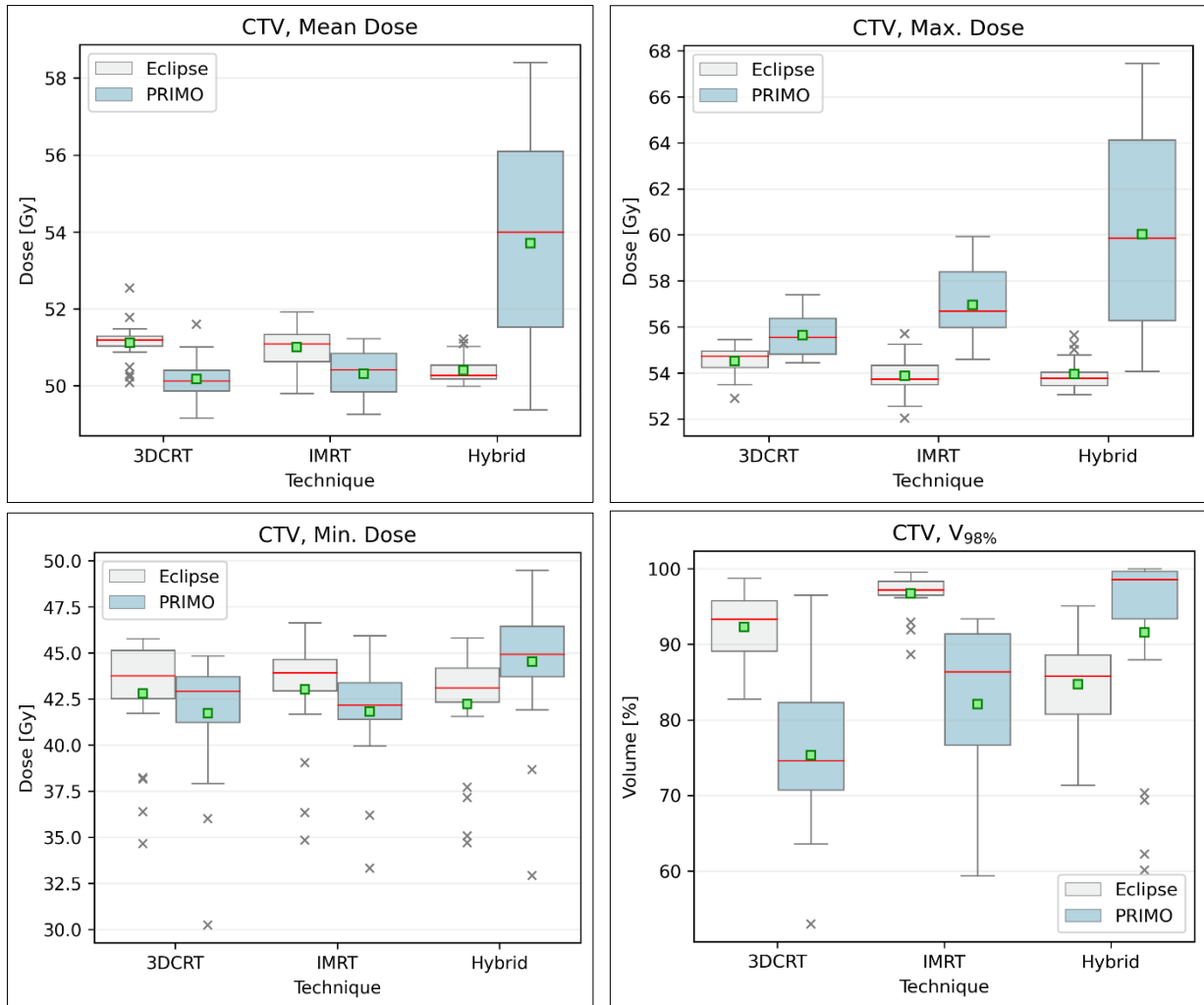
Graph 31 – Comparison of the box plots of the results for the PTV.

Orange dash: median; green square: mean; x mark: outliers (points \notin [Q1 – 1.5 IQR, Q3 + 1.5 IQR])



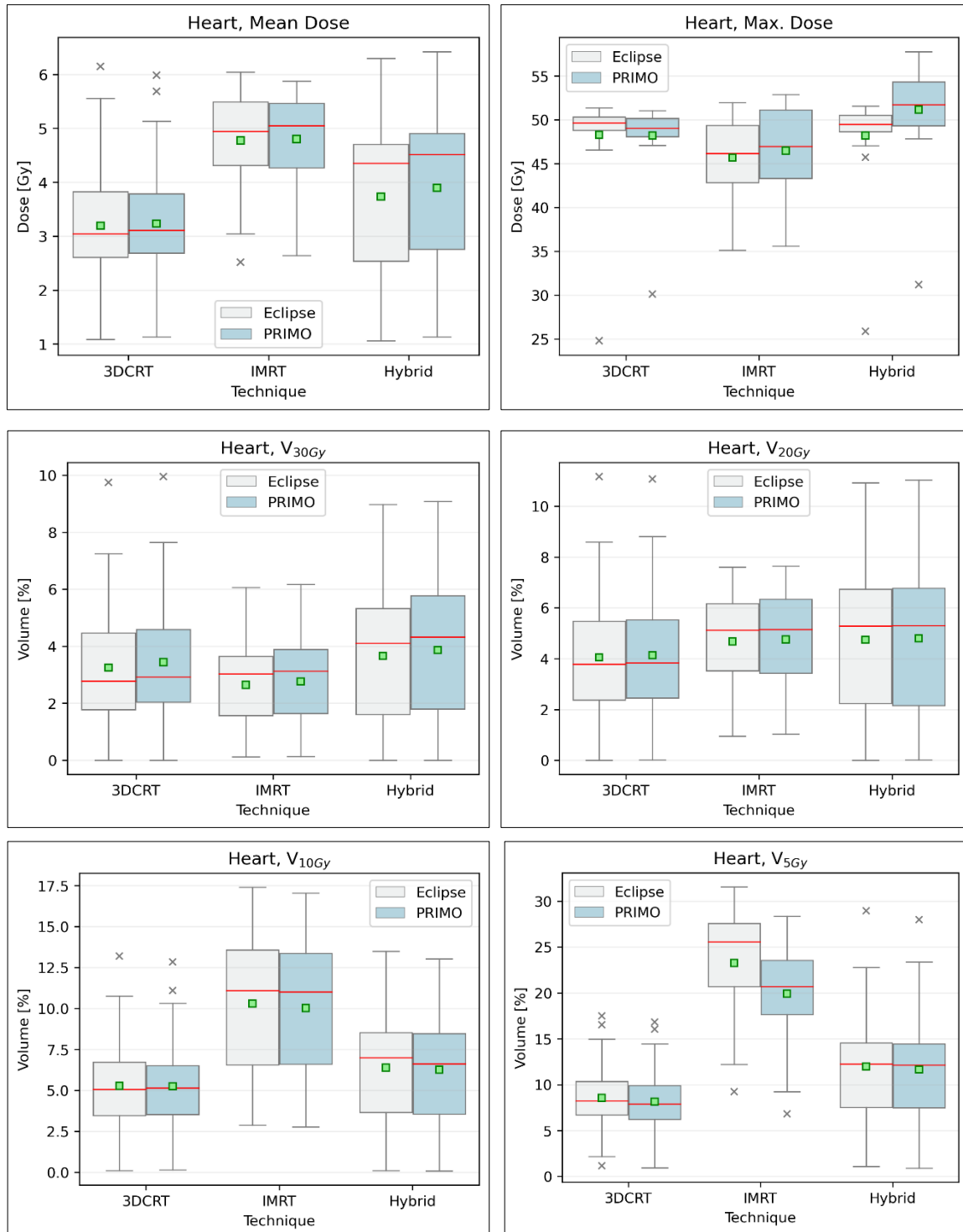
Graph 32 – Comparison of the box plots of the results for the PTV.

Orange dash: median; **green square:** mean; **x mark:** outliers (points \notin [Q1 – 1.5 IQR, Q3 + 1.5 IQR])



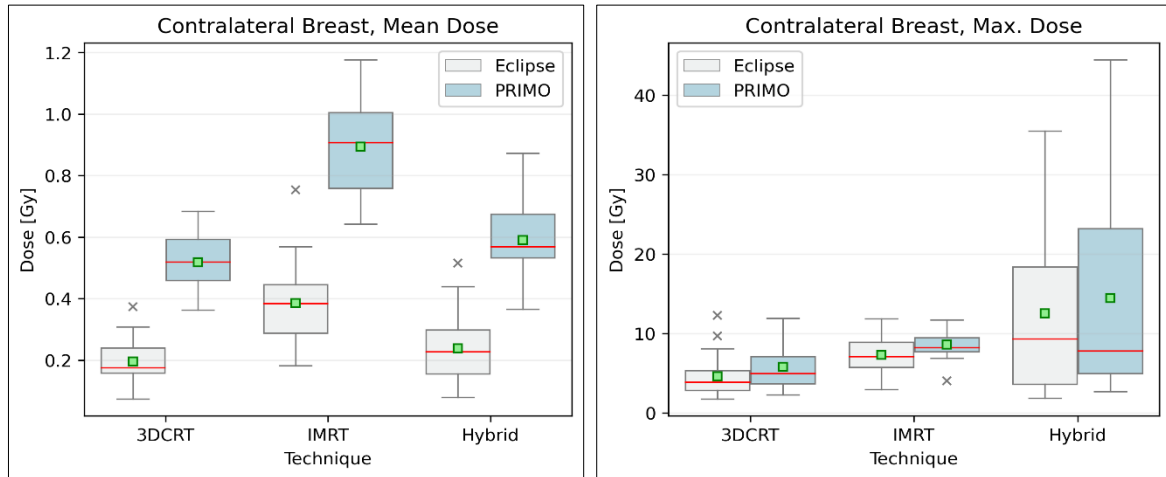
Graph 33 – Comparison of the box plots of the results for the CTV.

Orange dash: median; **green square:** mean; **x mark:** outliers (points \notin [Q1 – 1.5 IQR, Q3 + 1.5 IQR])



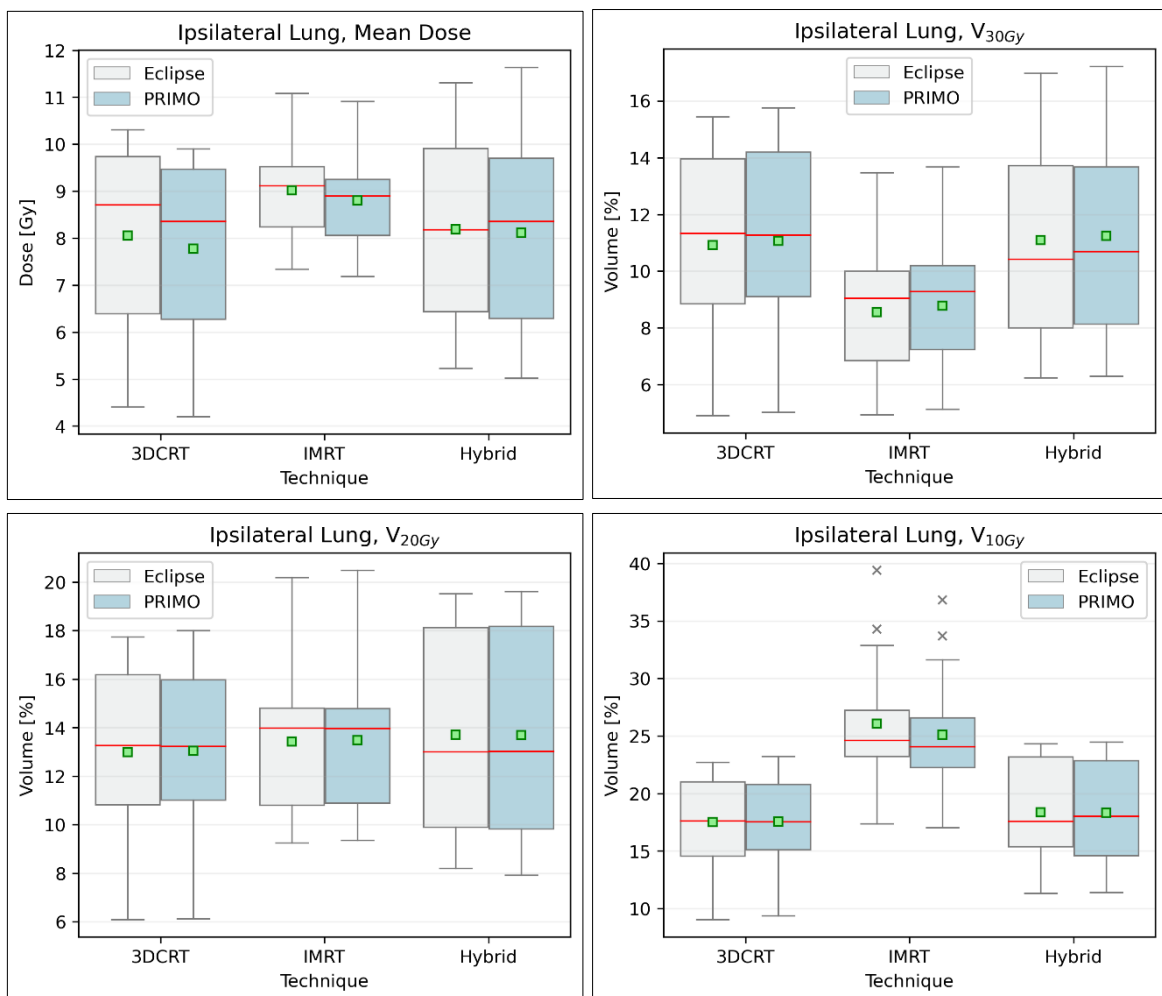
Graph 34 – Comparison of the box plots of the results for the heart.

Orange dash: median; **green square:** mean; **x mark:** outliers (points \notin [Q1 – 1.5 IQR, Q3 + 1.5 IQR])



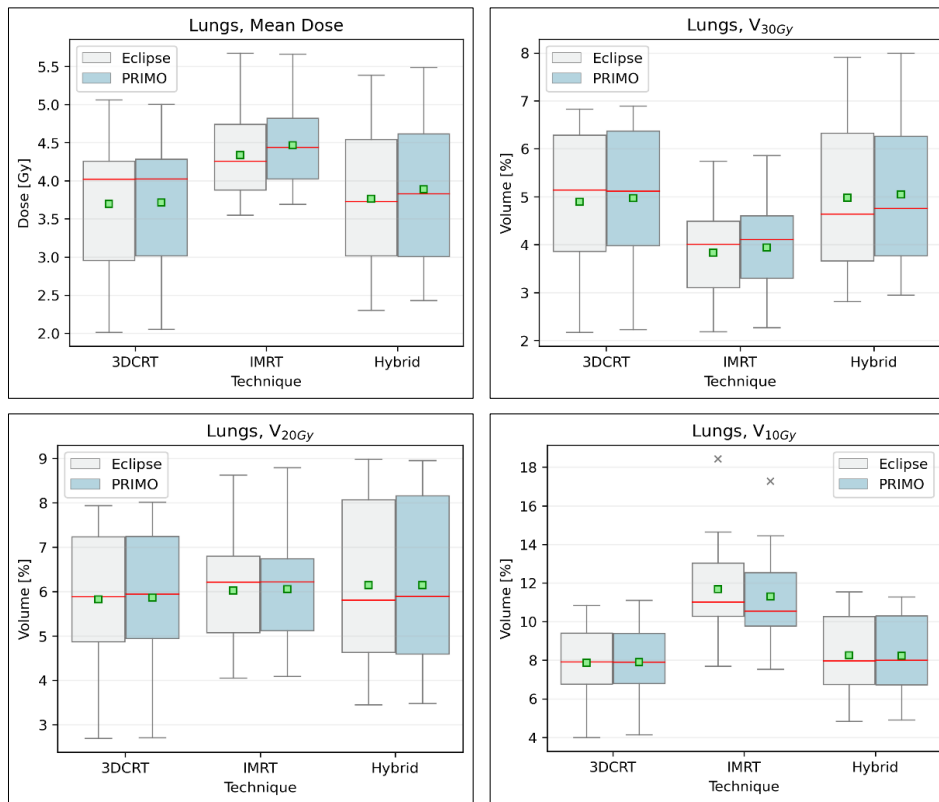
Graph 35 – Comparison of the box plots of the results for the contralateral breast.

Orange dash: median; **green square:** mean; **x mark:** outliers (points \notin [Q1 – 1.5 IQR, Q3 + 1.5 IQR])



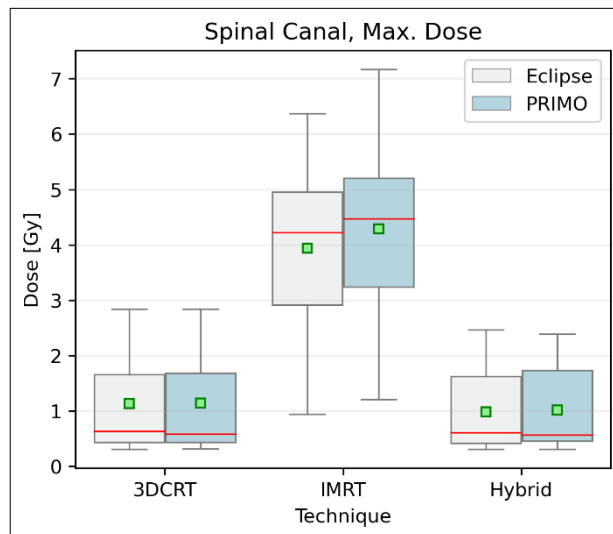
Graph 36 – Comparison of the box plots of the results for the ipsilateral lung.

Orange dash: median; **green square:** mean; **x mark:** outliers (points \notin [Q1 – 1.5 IQR, Q3 + 1.5 IQR])



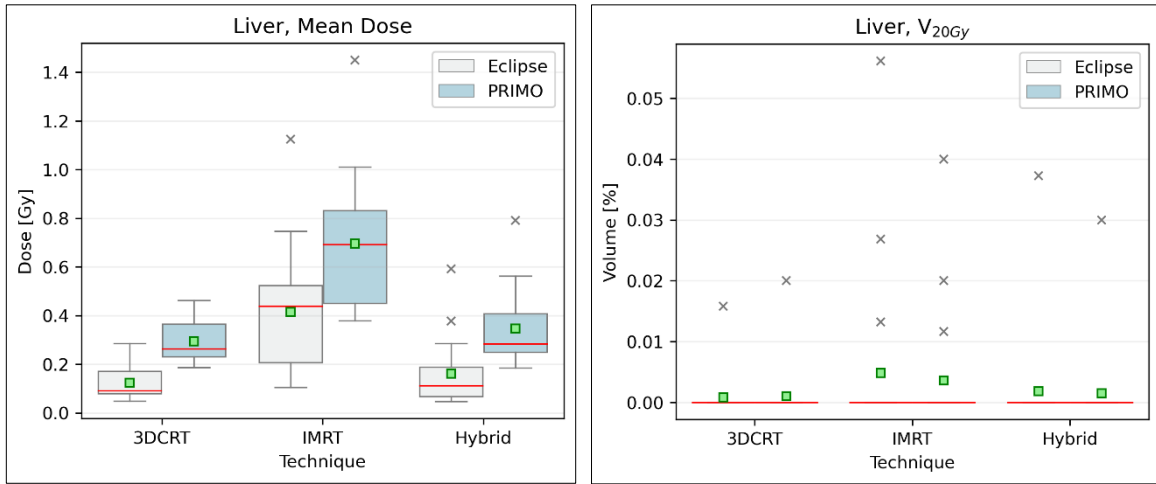
Graph 37 – Comparison of the box plots of the results for the lungs.

Orange dash: median; **green square:** mean; **x mark:** outliers (points \notin [Q1 – 1.5 IQR, Q3 + 1.5 IQR])



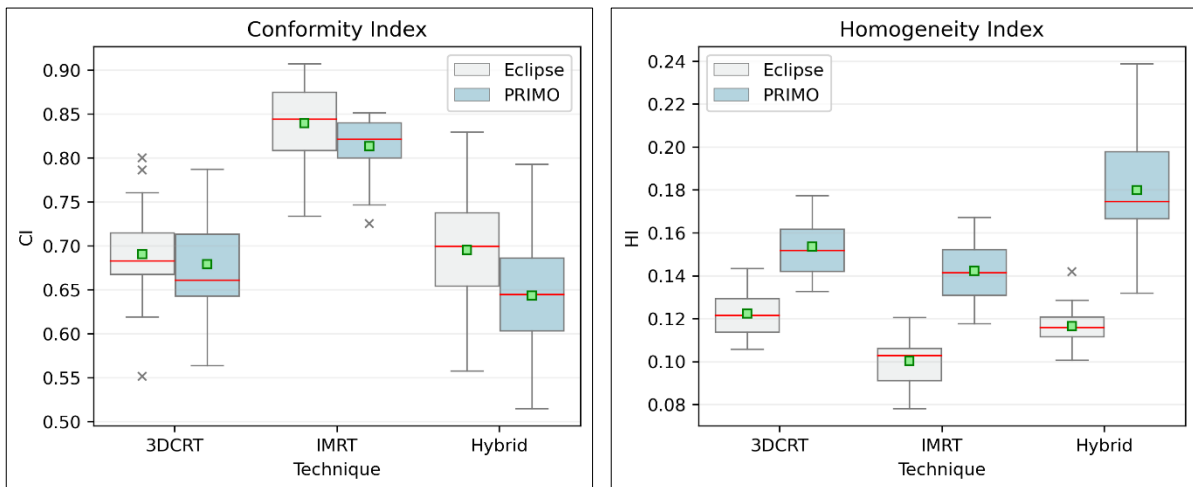
Graph 38 – Comparison of the box plots of the results for the spinal canal.

Orange dash: median; **green square:** mean; **x mark:** outliers (points \notin [Q1 – 1.5 IQR, Q3 + 1.5 IQR])



Graph 39 – Comparison of the box plots of the results for the liver.

Orange dash: median; **green square:** mean; **x mark:** outliers (points $\notin [Q1 - 1.5 IQR, Q3 + 1.5 IQR]$)



Graph 40 – Comparison of the box plots of the results for CI and HI.

Orange dash: median; **green square:** mean; **x mark:** outliers (points $\notin [Q1 - 1.5 IQR, Q3 + 1.5 IQR]$)

4.2 Discussion

4.2.1 TPS

The DVH comparisons for both the CTV and the PTV show that the HT curves were the first to decrease, followed by the 3D-CRT and then the IMRT. IMRT was able to deliver the prescribed dose of 50 Gy to a larger volume of the CTV and the PTV, compared with 3D-CRT which, in turn, delivered 50 Gy to larger portions of the target volumes than HT. The slope of the IMRT DVH was steeper than the slopes of 3D-CRT and HT, which portrayed the technique's success at reducing the percentage volume of the target structures receiving doses higher than the prescribed dose i.e., IMRT ended up resulting in smaller high dose regions than 3D-CRT and, for even higher doses, also than HT. For all values of absorbed dose, HT deposited that dose to a smaller percentage volume of the CTV and PTV than 3D-CRT: a disadvantage for doses lower than 50 Gy and an advantage for doses higher than 50 Gy.

For the heart, the DVH show that IMRT performed poorly in terms of low dose regions, resulting in larger percentage volumes receiving low doses than HT and 3D-CRT; HT delivered low doses to slightly higher percentage volumes than 3D-CRT. For higher doses, HT and 3D-CRT stayed nearly identical and IMRT was capable of delivering high doses to less heart volume compared with the other techniques. For the ipsilateral lung and both lungs, IMRT also resulted in larger low dose regions, but the slight difference between HT and 3D-CRT that appeared for the heart seemed to be almost non-existent for these structures, and IMRT was able to reduce the portion of the targets receiving high doses. For higher doses, the relative results between techniques were the same as for the heart. For the contralateral breast, IMRT resulted in larger low dose regions, and HT slightly resulted in more low dose regions than 3D-CRT.

In terms of dosimetric parameters, for the PTV, the statistically significant differences found in the results were as follows (with the respective p-value extracted from the post-hoc Nemenyi hypothesis test) : 3D-CRT resulted in a slightly higher mean dose compared with HT ($p = 0.01$); 3D-CRT deposited a higher $D_{2\%}$ compared with IMRT and HT ($p < 0.01$, $p = 0.02$); HT resulted in a lower $D_{95\%}$ compared with 3D-CRT and IMRT ($p = 0.03$, $p < 0.01$); 3D-CRT ended up forming a larger $V_{107\%}$ hot spot region compared with IMRT and HT ($p < 0.01$, $p < 0.01$); 3D-CRT achieved a wider $V_{95\%}$ than HT ($p = 0.03$).

For the CTV, HT resulted in a lower mean dose compared with 3D-CRT and IMRT ($p < 0.01$, $p < 0.01$); IMRT resulted in a larger $V_{98\%}$ compared with 3D-CRT and HT ($p = 0.01$, $p < 0.01$).

For the Heart, IMRT resulted in a higher mean dose compared with 3D-CRT ($p < 0.01$); IMRT resulted in a lower maximum dose compared with 3D-CRT ($p = 0.03$); IMRT resulted in a larger V_{10Gy} than 3D-CRT and HT ($p < 0.01$, $p < 0.01$); IMRT resulted in a larger V_{5Gy} than 3D-CRT and HT ($p < 0.01$, $p < 0.01$).

For the contralateral breast, IMRT resulted in a slightly higher mean dose compared with 3D-CRT and HT ($p < 0.01$, $p = 0.01$); IMRT resulted in higher maximum dose than 3D-CRT ($p = 0.03$).

For the ipsilateral lung, IMRT resulted in smaller V_{30Gy} compared with 3D-CRT and HT ($p = 0.01$, $p = 0.02$); IMRT resulted in larger V_{10Gy} compared with 3D-CRT and HT ($p < 0.01$, $p < 0.01$).

For the lungs, IMRT resulted in smaller V_{30Gy} compared with 3D-CRT ($p = 0.01$), and larger V_{10Gy} with IMRT compared with 3D-CRT and HT ($p < 0.01$, $p < 0.01$).

For the spinal canal, IMRT resulted in higher maximum dose compared with 3D-CRT and HT ($p < 0.01$, $p < 0.01$).

For the liver, IMRT resulted in higher mean dose compared with 3D-CRT and HT ($p < 0.01$, $p < 0.01$).

The conformity index had its best (highest, closest to 1) result with IMRT, compared with 3D-CRT and HT ($p < 0.01$, $p < 0.01$). The homogeneity index also had its best (lowest, closest to 0) result with IMRT, compared with 3D-CRT and HT ($p < 0.01$, $p = 0.02$).

In terms of MU, all three techniques showed statistically significant differences among themselves, with 3D-CRT, HT and IMRT employing a number of MU by ascending order (all pair-wise $p < 0.01$); IMRT used a particularly high number of MU, while the difference between 3D-CRT and HT wasn't so large.

4.2.2 PRIMO

The DVH comparisons for both the CTV and the PTV show that the HT curves were the last to decrease and there were very high doses delivered to large volumes of

the targets; also, the results were very dispersed, which can be noted by the high standard deviation. Clearly, something about the HT results is wrong and extremely different from the Eclipse results. We found a pattern that indicated PRIMO does not handle the presence of wedges well, as the HT plans without wedges were acceptable, while the plans with wedges resulted in very high doses to the targets. One plan with wedges and one without wedges were calculated for the same patient and this issue was verified. This case will be presented later, but it is being mentioned here to warn the reader about the unreliability of the HT results that are being shown here. IMRT was able to deliver the prescribed dose of 50 Gy to a larger volume of the CTV and the PTV, compared with 3D-CRT. The slope of the IMRT DVH was steeper than the slope of 3D-CRT, which portrayed the technique's success at reducing the percentage volume of the target structures receiving doses higher than the prescribed dose i.e., IMRT ended up resulting in smaller high dose regions than 3D-CRT.

For the heart, the DVH show that IMRT performed poorly in terms of low dose regions, resulting in larger percentage volumes receiving low doses than HT and 3D-CRT; HT delivered low doses to slightly higher percentage volumes than 3D-CRT. For higher doses, HT showed larger percentage volumes receiving high doses than 3D-CRT, and IMRT was capable of delivering high doses to less heart volume compared with the other techniques. For the ipsilateral lung and both lungs, IMRT also resulted in larger low dose regions, but the slight difference between HT and 3D-CRT that appeared for the heart seemed to be almost non-existent for these structures. For higher doses, HT showed larger percentage volumes receiving high doses than 3D-CRT, and IMRT was able to reduce the portion of the targets receiving high doses. For the contralateral breast, IMRT resulted in larger low dose regions, and HT slightly resulted in more low dose regions than 3D-CRT.

In terms of dosimetric parameters, for the PTV, the statistically significant differences found in the results were as follows (with the respective p-value extracted from the post-hoc Nemenyi hypothesis test) : HT resulted in a higher mean dose compared with 3D-CRT and IMRT ($p = 0.01$, $p = 0.01$); 3D-CRT resulted in a lower maximum dose compared with IMRT and HT ($p = 0.03$, $p < 0.01$); IMRT resulted in a higher minimum dose compared with 3D-CRT ($p = 0.02$); HT resulted in a higher $D_{2\%}$ than IMRT ($p < 0.01$); HT resulted in a higher $D_{95\%}$ than 3D-CRT ($p < 0.01$); HT resulted in a higher $D_{98\%}$ than 3D-CRT and IMRT ($p < 0.01$, $p = 0.02$); HT resulted in a much larger $V_{107\%}$ compared with 3D-CRT and IMRT ($p = 0.03$, $p < 0.01$); HT resulted in a larger $V_{95\%}$ than 3D-CRT ($p < 0.01$).

For the CTV, HT resulted in a higher mean dose compared with 3D-CRT and IMRT ($p = 0.01$, $p = 0.02$); HT resulted in a higher maximum dose than 3D-CRT ($p = 0.01$); HT resulted in a higher minimum dose than 3D-CRT and IMRT ($p < 0.01$, $p = 0.01$); HT resulted in a larger $V_{98\%}$ than 3D-CRT ($p < 0.01$).

For the heart, IMRT resulted in a higher mean dose than 3D-CRT ($p < 0.01$); HT resulted in a higher maximum dose than 3D-CRT and IMRT ($p = 0.02$, $p = 0.01$); IMRT resulted in a larger V_{10Gy} than 3D-CRT ($p = 0.01$); IMRT resulted in a larger V_{5Gy} than 3D-CRT ($p < 0.01$).

For the contralateral breast, IMRT resulted in a higher mean dose than 3D-CRT and HT ($p < 0.01$, $p < 0.01$).

For the ipsilateral lung, IMRT resulted in a larger V_{10Gy} compared with 3D-CRT and HT ($p < 0.01$, $p < 0.01$).

For the lungs, IMRT resulted in a larger V_{10Gy} compared with 3D-CRT and HT ($p < 0.01$, $p < 0.01$).

For the spinal canal, IMRT resulted in a much higher maximum dose compared with 3D-CRT and HT ($p < 0.01$, $p < 0.01$).

For the liver, IMRT resulted in a higher mean dose compared with 3D-CRT and HT ($p < 0.01$, $p < 0.01$).

The conformity index had its best (highest, closest to 1) result with IMRT, compared with 3D-CRT and HT ($p < 0.01$, $p < 0.01$). The homogeneity index had its worst (furthest from 0) result with HT, compared with 3D-CRT and IMRT ($p = 0.01$, $p < 0.01$).

4.2.3 Comparison with the literature

According to the literature, statistically significant differences that some authors found for the PTV were as follows: *Xiaoxue Xie et al.*¹⁶ found that their approach to HT resulted in larger $V_{95\%}$ than 3D-CRT and IMRT, which contradicts our results from the TPS and partially agrees with the results from PRIMO; *Yi-Chi Liu et al.*¹⁸ found higher maximum dose with HT compared with IMRT, higher minimum dose with IMRT compared with HT, larger $V_{95\%}$ with IMRT compared with HT, larger $V_{107\%}$ with HT compared with IMRT, agreeing with the results from PRIMO, although the results we got stem from a simulation problem, and higher $D_{98\%}$ with IMRT compared with HT,

disagreeing with our results from PRIMO; *William Rodriguez*²⁷ found lower $D_{2\%}$ and $D_{95\%}$ with IMRT compared with 3D-CRT.

For the heart, *Gamal Elhusseiny, MD et al.*²⁸ found smaller V_{5Gy} , V_{20Gy} , V_{30Gy} , and V_{40Gy} with IMRT compared with 3D-CRT, and the V_{5Gy} contradicts our results from the TPS and PRIMO; *Xiaoxue Xie et al.*¹⁶ found smaller V_{5Gy} with 3D-CRT than with IMRT and HT, with the IMRT resulting in larger low dose regions than 3D-CRT agreeing with our results from the TPS and PRIMO, larger V_{10Gy} with IMRT compared with 3D-CRT and HT, agreeing with our results from the TPS and partially agreeing with the results from PRIMO, and narrower V_{40Gy} with IMRT than with 3D-CRT and HT; *Jackie Yim et al.*¹⁷ found lower mean dose with 3D-CRT than with HT; *Yi-Chi Liu et al.*¹⁸ found higher mean dose with IMRT than with HT, higher maximum dose with IMRT compared with HT, disagreeing with our results from PRIMO, and larger V_{5Gy} with IMRT than with HT, agreeing with our results from the TPS; *William Rodriguez*²⁷ found a higher mean dose with IMRT *step-and-shoot* than with 3D-CRT, which in turn was higher than *dynamic MLC* IMRT, contradicting our results from the TPS and PRIMO.

For the contralateral breast, *Attallah, H.S. et al.*²⁹ found lower mean dose with 3D-CRT compared with IMRT, agreeing with our results from the TPS and PRIMO; *Gamal Elhusseiny, MD et al.*²⁸ found higher mean dose with 3D-CRT than with IMRT, contradicting our results from the TPS and PRIMO; *Xiaoxue Xie et al.*¹⁶ found greater mean dose with IMRT compared with 3D-CRT and HT, agreeing with our results from the TPS and PRIMO; *Jackie Yim et al.*¹⁷ found higher maximum dose with 3D-CRT than with HT; *Yi-Chi Liu et al.*¹⁸ found higher mean dose with IMRT than with HT, agreeing with our results from the TPS and PRIMO, and higher maximum dose with IMRT than with HT; *William Rodriguez*²⁷ found higher maximum dose with 3D-CRT compared with IMRT, disagreeing with our results, and higher mean dose with IMRT compared with 3D-CRT, agreeing with our results from the TPS and PRIMO.

For the ipsilateral lung, *Gamal Elhusseiny, MD et al.*²⁸ found lower mean dose with IMRT than with 3D-CRT, smaller V_{20Gy} with IMRT than with 3D-CRT, and smaller V_{30Gy} with IMRT than with 3D-CRT, the latter agreeing with our results; *Xiaoxue Xie et al.*¹⁶ found larger V_{13Gy} with IMRT than with 3D-CRT and HT, agreeing with our results from the TPS and PRIMO for V_{10Gy} (low dose regions), and smaller V_{30Gy} and V_{40Gy} with IMRT compared with 3D-CRT and HT, agreeing with our results; *Yi-Chi Liu et al.*¹⁸ found higher mean dose with IMRT than with HT, larger V_{5Gy} and V_{10Gy} with IMRT than with HT, agreeing with our results from the TPS and PRIMO for low dose regions, wider V_{20Gy} with

IMRT than with HT, and larger $V_{30\text{Gy}}$ with IMRT than with HT, contradicting our results; *William Rodriguez*²⁷ found higher $V_{20\text{Gy}}$ with dynamic IMRT than with 3D-CRT.

For the indices, *Attallah, H.S. et al.*²⁹ found better HI with IMRT than with 3D-CRT, agreeing with our results from the TPS; *Gamal Elhousseiny, MD et al.*²⁸ found better HI with 3D-CRT than with IMRT, disagreeing with our results from the TPS; *Xiaoxue Xie et al.*¹⁶ found better HI and CI with IMRT and HT than with 3D-CRT, partially agreeing with our results from the TPS and PRIMO; *Jackie Yim et al.*¹⁷ found better HI with HT than with 3D-CRT, disagreeing with our results from PRIMO; *Yi-Chi Liu et al.*¹⁸ found better CI with HT than with IMRT, disagreeing with our results from the TPS and PRIMO, and better HI with IMRT compared with HT, agreeing with our results from the TPS and PRIMO; *William Rodriguez*²⁷ found better CI with IMRT compared with 3D-CRT, agreeing with our results from the TPS and PRIMO.

*Xiaoxue Xie et al.*¹⁶ found that the average MU required for 3D-CRT was nearly 2.2 and 1.75-fold less than for IMRT and HT, respectively; *Yi-Chi Liu et al.*¹⁸ found less MU usage with HT than with IMRT; *William Rodriguez*²⁷ found immensely higher MU with IMRT than with 3D-CRT. The order of ascending MU usage reported by these authors agree with our results, but our IMRT results seem to have used an exaggerate amount of MU.

4.2.4 TPS vs. PRIMO

Comparing our results from the TPS and PRIMO, the statistically significant differences that were found (evaluated by the p-value of the Wilcoxon Signed Rank test with a significance level of $p < 0.05$) are stated below.

For the PTV, the mean dose was higher with the TPS for the 3D-CRT and IMRT, but higher with PRIMO for the HT ($p < 0.01$, $p < 0.01$, $p < 0.01$); the maximum dose was higher with PRIMO for all three techniques ($p < 0.01$, $p < 0.01$, $p < 0.01$); the minimum dose was higher with the TPS for all three techniques ($p = 0.04$, $p = 0.02$, $p = 0.01$); $D_{2\%}$ was higher with PRIMO for the HT ($p < 0.01$); $D_{95\%}$ was higher with the TPS for 3D-CRT and IMRT ($p < 0.01$, $p < 0.01$); $D_{98\%}$ was higher with the TPS for 3D-CRT and IMRT ($p < 0.01$, $p < 0.01$); $V_{107\%}$ was larger with the TPS for 3D-CRT, but larger with PRIMO for IMRT and HT ($p = 0.01$, $p = 0.02$, $p < 0.01$); $V_{95\%}$ was larger with the TPS for 3D-CRT and IMRT ($p < 0.01$, $p < 0.01$).

For the CTV, the mean dose was higher with the TPS for 3D-CRT and IMRT, but higher with PRIMO for the HT ($p < 0.01$, $p < 0.01$, $p < 0.01$); the maximum dose was

higher with PRIMO for all three techniques ($p < 0.01$, $p < 0.01$, $p < 0.01$); the minimum dose was higher with PRIMO for the HT ($p = 0.02$); $V_{98\%}$ was larger with the TPS for 3D-CRT and IMRT ($p < 0.01$, $p < 0.01$).

For the heart, the maximum dose was higher with PRIMO for the HT ($p = 0.01$).

For the contralateral breast, the mean dose was higher with PRIMO for all three techniques ($p < 0.01$, $p < 0.01$, $p < 0.01$).

For the ipsilateral lung, no significant differences were spotted.

For the lungs, no significant differences were spotted.

For the spinal canal, no significant differences were found.

For the liver, the mean dose was higher with PRIMO for all three techniques ($p < 0.01$, $p < 0.01$, $p < 0.01$).

The CI was better with the TPS for IMRT and HT ($p = 0.03$, $p = 0.03$), and HI was better with the TPS for all three techniques ($p < 0.01$, $p < 0.01$, $p < 0.01$).

4.2.5 The wedge issue

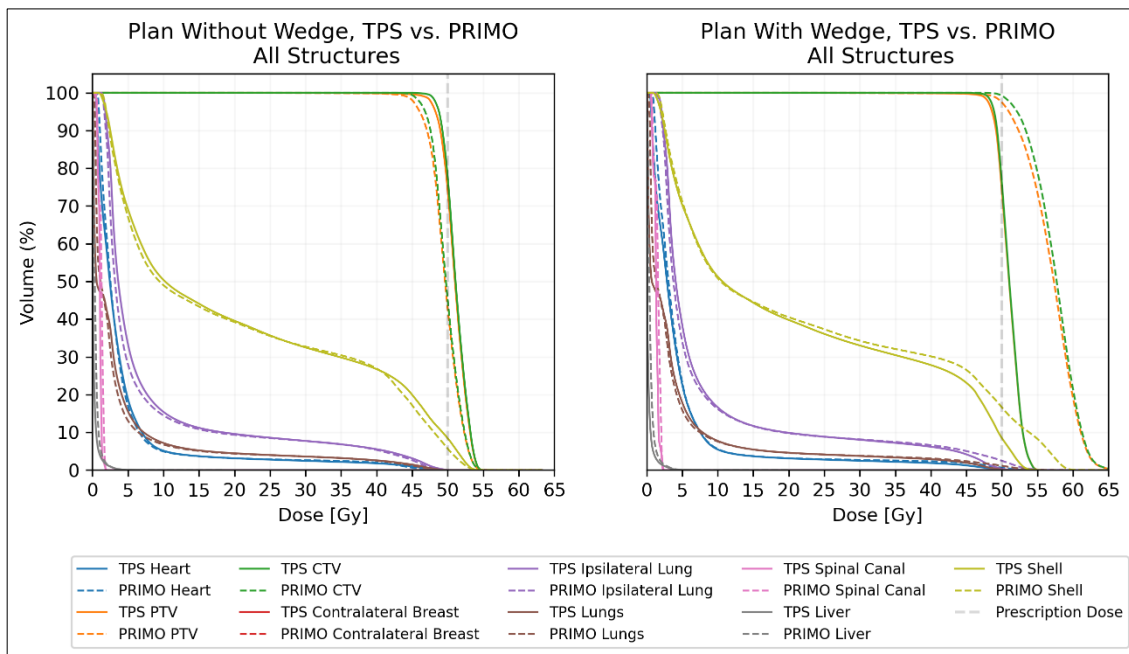
The dosimetric results for the target volumes and, consequently, for the homogeneity and conformity indices suggest PRIMO had some trouble simulating HT plans. After inspecting some plans, a pattern was noticed: the plans that had wedges seemed to disagree with the results from the TPS by a large degree, resulting in higher doses to the target volumes and larger *hot spots*; also, the distribution of the results showed a very noticeable dispersion, ending up in a larger than desired plan-wise variability. On the other hand, PRIMO simulations of plans without wedges seemed to behave well and have acceptable results.

Picking one patient as an example, two plans were designed: one with wedges and one without. Each of those plans provided results from the TPS and PRIMO.

The DVH and lateral dose profiles on the isocentre of the plans are compared below. [Graph 41, 42, 43, 44]

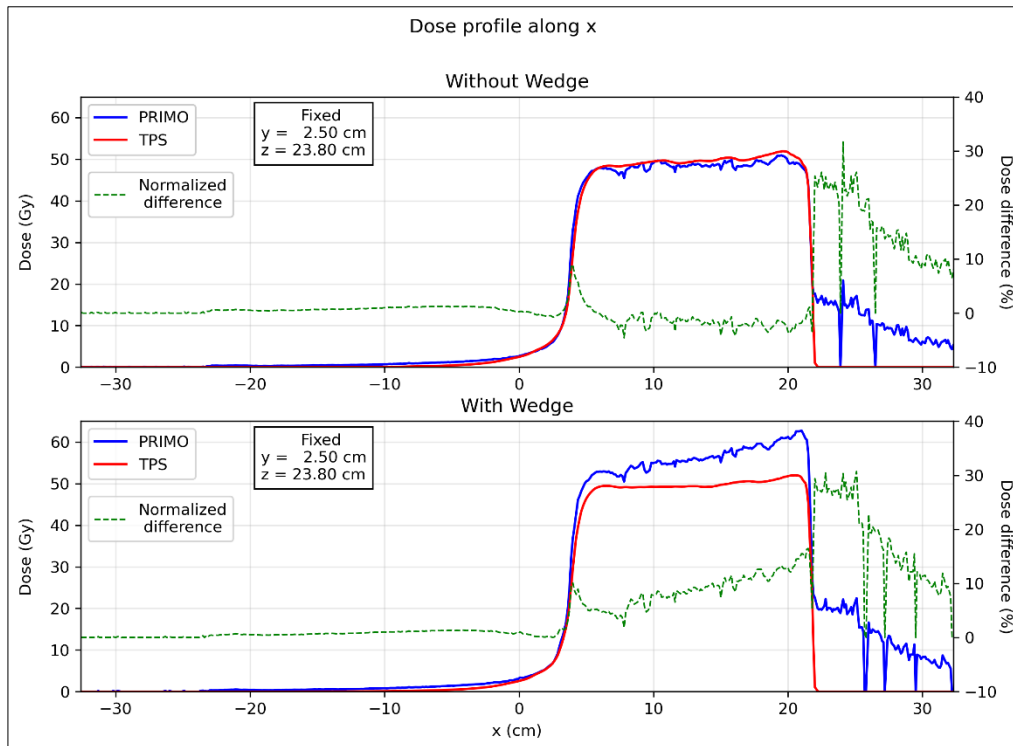
By looking at the DVH, it is noticeable that differences regarding the OAR are practically negligible, but the differences for the CTV and PTV are significant. The TPS handled both plans well, but the PRIMO simulation of the plan with wedge resulted in

large high dose volumes, while the TPS and PRIMO curves of the plan without wedges were much closer to each other.

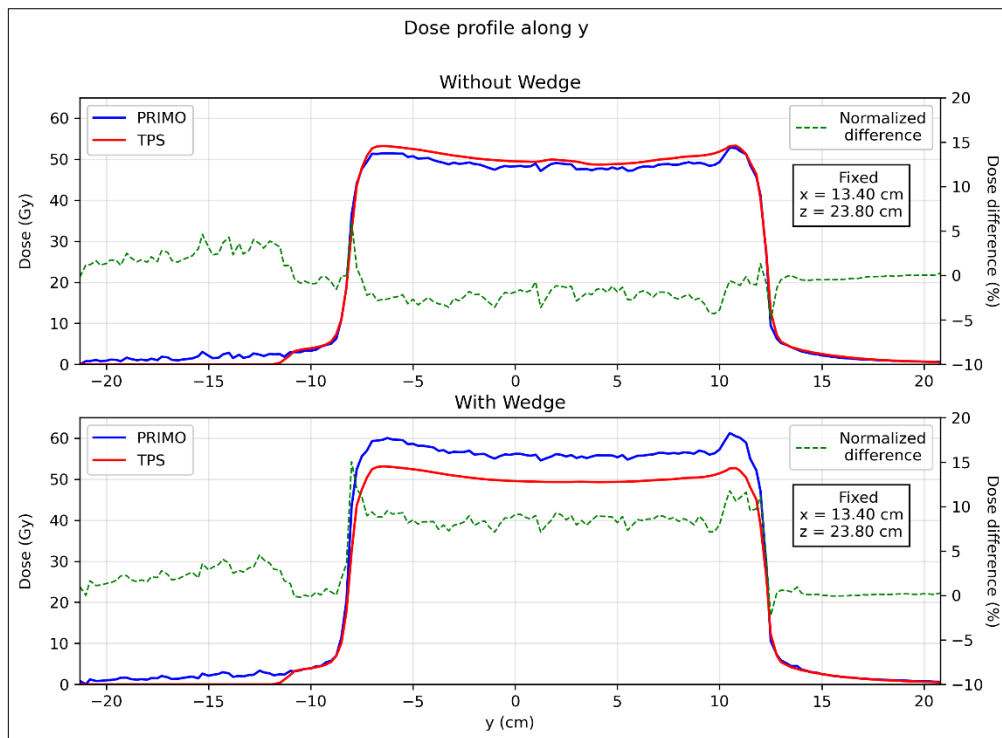


Graph 41 – Comparison of the DVH as provided by the TPS and PRIMO between the plan without wedges and the plan with wedge.

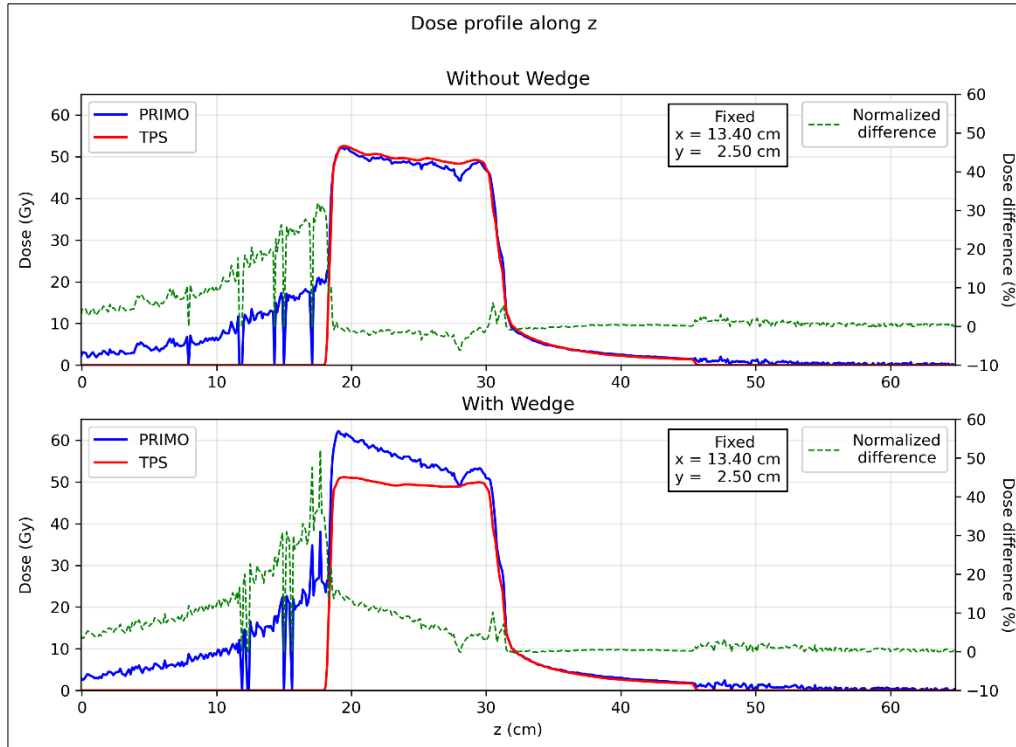
Analysing the lateral dose profiles on the isocentre [Graph 42, 43, 44], it's shown that while the curves of the TPS and PRIMO for the plan without wedges are very close, the distance between them enlarges for the plan with wedge, with PRIMO sometimes surpassing the prescribed dose; also, for x and z, the TPS and PRIMO profiles for the plan without wedge are nearly “flat”, while the PRIMO profiles for the plan with wedge show a significant slope, suggesting PRIMO ignores the presence of wedges and, thus, homogeneity was lost. Especially in the profiles along x and z, on the right and left side of the curves, respectively, the PRIMO curves appear to display some noisy readings, while the TPS curves are flat at 0; this happens because those regions correspond to the extremity of the breast and while the TPS does not calculate the radiation absorption outside delineated structures, PRIMO does and the values shown for the blue curves most likely represent dose absorption in air voxels. The normalized difference is calculated as the percentage difference between the PRIMO and TPS doses, normalized at the maximum dose from PRIMO (the reference curve).



Graph 42 – Comparison between the dose profiles along x from the TPS and PRIMO, for the plan without wedge and the plan with wedge.



Graph 43 – Comparison between the dose profiles along y from the TPS and PRIMO, for the plan without wedge and the plan with wedge.



Graph 44 – Comparison between the dose profiles along z from the TPS and PRIMO, for the plan without wedge and the plan with wedge.

5 Conclusions and future work

The DVH resulting from the TPS calculations showed that IMRT achieved better target coverage than the other two techniques and although 3D-CRT achieved better coverage than HT, it also resulted in larger high dose areas compared with HT. Regarding OAR, IMRT resulted in larger low dose volumes compared with the other techniques, but was better at sparing those OAR from high doses; HT resulted in slightly larger low dose volumes compared with 3D-CRT for the heart, but other than that those two techniques behaved similarly for the OAR. In terms of dosimetric parameters extracted from the TPS results, for the PTV, HT achieved the best mean dose, IMRT and HT resulted in the best $D_{2\%}$, IMRT and 3D-CRT resulted in the best $D_{95\%}$, IMRT and HT formed smaller $V_{107\%}$ *hot spot* regions than 3D-CRT, and 3D-CRT and IMRT resulted in the best $V_{95\%}$ coverage; for the CTV, HT resulted in the best mean dose and IMRT resulted in the best $V_{98\%}$ coverage; for the heart, 3D-CRT and HT resulted in the lowest mean doses, IMRT resulted in the lowest maximum dose, and 3D-CRT and HT resulted in smaller low dose volumes V_{5Gy} and V_{10Gy} ; for the contralateral breast, 3D-CRT and HT resulted in the lowest mean doses, and 3D-CRT resulted in the lowest maximum dose; for the ipsilateral lung, IMRT resulted in the smallest V_{30Gy} , and 3D-CRT and HT resulted in the smallest V_{10Gy} ; for the lungs, the results were analogous; for the spinal canal, 3D-CRT and HT were the best at reducing the maximum dose to the spinal canal; for the liver, 3D-CRT and HT resulted in lower mean doses. IMRT achieved the best homogeneity and conformity indices, while 3D-CRT and HT achieved practically identical results. IMRT used almost 4 times as much MU as 3D-CRT and around 3 times as much as HT, which is a problem for IMRT since there is an augmented risk of radiation originating from leakage from the linac's head and from scattering in the collimators that can end up absorbed by the patient and lead to radiation-induced long-term complications.

Regarding the PRIMO results, reliable conclusions cannot be stated as the obtained HT results come from deficient calculations due to the presence of wedges in some plans.

Taking only into account the 3D-CRT and IMRT techniques, for the PTV, the TPS resulted in higher mean doses with 3D-CRT and IMRT, the maximum dose was higher with PRIMO for all techniques, the minimum dose was higher with the TPS for all techniques, $D_{95\%}$ and $D_{98\%}$ were higher with the TPS for 3D-CRT and IMRT, $V_{107\%}$ was

larger with the TPS for 3D-CRT, but larger with PRIMO for IMRT, $V_{95\%}$ was larger with the TPS for 3D-CRT and IMRT; for the CTV, the mean dose was higher with the TPS for 3D-CRT and IMRT, the maximum dose was higher with PRIMO for all techniques, $V_{98\%}$ was larger with the TPS for 3D-CRT and IMRT; for the contralateral breast, the mean dose was higher with PRIMO for all techniques; for the liver, the mean dose was higher with PRIMO for all techniques; for the heart, the ipsilateral lung, the lungs and the spinal canal, no significant differences were found. IMRT resulted in a better CI with the TPS, compared with PRIMO, and the TPS calculations resulted in better HI for all techniques.

One patient was treated with the developed HT. A 3D-CRT was calculated, but it failed a constraint in the ipsilateral lung, $V_{20\text{Gy}} < 20\%$. To solve the issue, an approach to a HT plan was made and combining the advantages of both IMRT and 3D-CRT, that ipsilateral lung constraint was met, and the target coverage was acceptable.

For future work, the HT plans with wedges could be calculated from scratch, this time without wedges and clinically equivalent, and the comparative study redone. Other idea would be to report this issue to the PRIMO developers and, if the problem is recognized, design the best HT plans possible regardless of the presence of wedges. Also, it is thought that the HT plans could improve if the weight of the IMRT beams increased, as it would enhance the PTV coverage and the detrimental consequence to the OAR would probably be minimal. Looking for the heart and breast volumes and breast separation of the patients and relating them to the HT treatment success could be an option, as those structure volumes are likely criteria for the outcome of the treatment. An approach with a physical phantom and linac could be made and those results could be compared with the TPS and PRIMO calculations.

References

- 1 – (2021, March 26). *Breast cancer*. World Health Organization. <https://www.who.int/news-room/fact-sheets/detail/breast-cancer>

- 2 – Instituto Português de Oncologia do Porto Francisco Gentil, E.P.E. (janeiro 2020) Registo Oncológico 2018

- 3 – Ferrão, F. (2022, January 28). *Pandemia deixou quase 5 mil cancros por diagnosticar*. Diário de Notícias. <https://www.dn.pt/sociedade/pandemia-deixou-quase-5-mil-cancros-por-diagnosticar-14534510.html>

- 4 – Casey, Dana L., Gaorav P. Gupta, e David W. Ollila. «The Role of Intraoperative Radiation in Early-Stage Breast Cancer». *Clinical Breast Cancer* 21, n. 2 (abril de 2021): 103–11. <https://doi.org/10.1016/j.clbc.2020.12.007>.

- 5 – Harris, Eleanor E. R., e William Small. «Intraoperative Radiotherapy for Breast Cancer». *Frontiers in Oncology* 7 (22 de dezembro de 2017): 317. <https://doi.org/10.3389/fonc.2017.00317>.

- 6 – Hensley, Frank W. «Present State and Issues in IORT Physics». *Radiation Oncology* 12, n. 1 (dezembro de 2017): 37. <https://doi.org/10.1186/s13014-016-0754-z>.

- 7 – Wang, Lin, Minmin Zhu, Yuelong Cui, Xudong Zhang, e Guowen Li. «Efficacy Analysis of Intraoperative Radiotherapy in Patients with Early-Stage Breast Cancer». *Cancer Cell International* 20, n. 1 (dezembro de 2020): 446. <https://doi.org/10.1186/s12935-020-01533-z>.

- 8 – Benson, Rony, e Supriya Mallick. «Therapeutic Index and Its Clinical Significance». Em *Practical Radiation Oncology*, editado por Supriya Mallick, Goura K. Rath, e Rony Benson, 191–92. Singapore: Springer Singapore, 2020. https://doi.org/10.1007/978-981-15-0073-2_31.

- 9 – ICRU (1999) ICRU Report 62: Prescribing, Recording and Reporting Photon Beam Therapy (Supplement to ICRU Report 50). ICRU, Bethesda.

10 – Journal of the ICRU Vol 10 No 1 (2010) Report 83 – Prescribing, Recording, and Reporting Photon-Beam Intensity-Modulated Radiation Therapy (IMRT)

11 – *Functional subunits*. ICRPaedia. http://icrpaedia.org/Functional_subunits

12 – Mathieu, Dominique & Shahvary, Nazanin & Côté, Nicolas & Boulva, Kerianne & Meloche-Dumas, Léamarie & Vu, Toni & Patocskai, Erica & Bernier, Christina & Roberge, David & Fortin, Israël. (2017). Helical Tomotherapy for Postmastectomy Radiotherapy after Immediate Left Breast Reconstruction: A Case Study. *Cureus*. 9. 10.7759/cureus.1462.

13 – Harms, Joseph, Jiahan Zhang, Oluwatosin Kayode, Jonathan Wolf, Sibotian, Neal McCall, Kristin A. Higgins, Richard Castillo, and Xiaofeng Yang. 'Implementation of a Knowledge-Based Treatment Planning Model for Cardiac-Sparing Lung Radiation Therapy'. *Advances in Radiation Oncology* 6, no. 6 (November 2021): 100745. <https://doi.org/10.1016/j.adro.2021.100745>.

14 – ICRU (1993) ICRU Report 50: Prescribing, Recording and Reporting Photon Beam Therapy. ICRU, Bethesda.

15 – Otto, K. (2008), Volumetric modulated arc therapy: IMRT in a single gantry arc. *Med. Phys.*, 35: 310-317. <https://doi.org/10.1118/1.2818738>

16 – Xie, Xiaoxue, Shuyu Ouyang, Hui Wang, Wenjuan Yang, Hekun Jin, Bingqiang Hu, and Liangfang Shen. 'Dosimetric Comparison of Left-Sided Whole Breast Irradiation with 3D-CRT, IP-IMRT and Hybrid IMRT'. *Oncology Reports* 31, no. 5 (May 2014): 2195–2205. <https://doi.org/10.3892/or.2014.3058>.

17 – Yim, Jackie, Clare Suttie, Regina Bromley, Marita Morgia, and Gillian Lamoury. 'Intensity Modulated Radiotherapy and 3D Conformal Radiotherapy for Whole Breast Irradiation: A Comparative Dosimetric Study and Introduction of a Novel Qualitative Index for Plan Evaluation, the Normal Tissue Index'. *Journal of Medical Radiation Sciences* 62, no. 3 (September 2015): 184–91. <https://doi.org/10.1002/jmrs.126>.

18 – Liu, Yi-Chi, Hung-Ming Chang, Hsin-Hon Lin, Chia-Chun Lu, and Lu-Han Lai. 'Dosimetric Comparison of Intensity-Modulated Radiotherapy, Volumetric Modulated Arc Therapy and Hybrid Three-Dimensional Conformal Radiotherapy/Intensity-Modulated Radiotherapy Techniques for Right Breast Cancer'. *Journal of Clinical Medicine* 9, no. 12 (29 November 2020): 3884. <https://doi.org/10.3390/jcm9123884>.

- 19 – Saw, Cheng B., SiCong Li, Frank Battin, Janice McKeague, and Christopher A. Peters. 'External Beam Planning Module of Eclipse for External Beam Radiation Therapy'. *Medical Dosimetry* 43, no. 2 (2018): 195–204. <https://doi.org/10.1016/j.meddos.2018.03.003>.
- 20 – Rodriguez, M., J. Sempau, and L. Brualla. 'PRIMO: A Graphical Environment for the Monte Carlo Simulation of Varian and Elekta Linacs'. *Strahlentherapie Und Onkologie* 189, no. 10 (October 2013): 881–86. <https://doi.org/10.1007/s00066-013-0415-1>.
- 21 – Rodriguez, M., J. Sempau, and L. Brualla. 'PRIMO User Manual' (2019)
- 22 – Wollschlaeger, Daniel, Karle, Heiko. "Analyzing dose-volume histograms using DVHmetrics for R" University Medical Center Mainz, Germany (2021)
- 23 – R Core Team (2021). R: A language and environment for statistical computing. R Foundation for Statistical Computing, Vienna, Austria. <https://www.R-project.org/>
- 24 – Guido Van Rossum and Fred L. Drake. 2009. Python 3 Reference Manual. CreateSpace, Scotts Valley, CA
- 25 – Radiation Therapy Oncology Group. "RTOG 1005 – A Phase III Trial Of Accelerated Whole Breast Irradiation With Hypofractionation Plus Concurrent Boost Versus Standard Whole Breast Irradiation Plus Sequential Boost For Early-Stage Breast Cancer" (2011)
- 26 – Paddick I. A simple scoring ratio to index the conformity of radiosurgical treatment plans. Technical note. *J Neurosurg.* 2000 Dec;93 Suppl 3:219-22. doi: 10.3171/jns.2000.93.supplement. PMID: 11143252
- 27 – Rodriguez, William Vladimir Ona. 'Comparison between 3D-CRT and Modulated Techniques for Head-and-Neck and Breast', 020008. Riobamba, Ecuador, 2018. <https://doi.org/10.1063/1.5050360>
- 28 – Elhousseiny, Gamal, Waleed O. Arafat, Azza Helal and Saad Elkomy. "IMRT treatment plans of left breast cancer: Comparison with 3 DCRT." (2015).
- 29 – Attallah, Hany S., Radwa M. Hamed, Haytham A. Abdelkader, Mahmoud M. Abdallah, Aliaa Mahmoud, Ibraheem Haggag, Bassam E. Makram, and Ahmed M. El-Saeed. 'Radiotherapy to the Left Breast with 3DCRT, IMRT or VMAT: International Medical Center Experience'. *Journal of Cancer Therapy* 12, no. 03 (2021): 107–15. <https://doi.org/10.4236/jct.2021.123012>

Attachments

1. TPS results

Table 1.1. – Dosimetric parameters for the PTV, for the different techniques, with the Friedman’s p-value. TPS results.

Metric	3D-CRT (Mean ± SD Median)	IMRT (Mean ± SD Median)	HT (Mean ± SD Median)	p-value
D _{mean}	50.892 ± 0.537 51.000 Gy	50.747 ± 0.527 50.830 Gy	50.271 ± 0.425 50.000 Gy	0.01
D _{max}	54.524 ± 0.659 54.734 Gy	54.179 ± 0.865 54.117 Gy	53.953 ± 0.704 53.776 Gy	0.09
D _{min}	24.498 ± 8.327 26.303 Gy	29.349 ± 7.031 30.191 Gy	23.837 ± 5.967 23.876 Gy	0.05
D _{2%}	53.624 ± 0.654 53.869 Gy	52.592 ± 0.725 52.747 Gy	53.010 ± 0.580 52.765 Gy	< 0.01
D _{95%}	48.380 ± 0.544 48.444 Gy	48.594 ± 0.314 48.490 Gy	47.883 ± 0.499 47.928 Gy	< 0.01
D _{98%}	47.383 ± 0.741 47.508 Gy	47.477 ± 0.101 47.500 Gy	47.151 ± 0.603 47.208 Gy	0.09
V _{107%}	4.464 ± 3.885 5.036 %	0.541 ± 1.091 0.006 %	1.308 ± 2.648 0.061 %	< 0.01
V _{95%}	97.649 ± 1.536 98.015 %	97.954 ± 0.198 98.000 %	96.458 ± 2.607 97.282 %	0.02

Table 1.2. – Dosimetric parameters for the CTV, for the different techniques, with the Friedman’s p-value. TPS results.

Metric	3D-CRT (Mean ± SD Median)	IMRT (Mean ± SD Median)	HT (Mean ± SD Median)	p-value
D _{mean}	51.117 ± 0.538 51.193 Gy	51.005 ± 0.540 51.087 Gy	50.410 ± 0.376 50.273 Gy	< 0.01
D _{max}	54.524 ± 0.659 54.734 Gy	53.866 ± 0.871 53.739 Gy	53.938 ± 0.689 53.776 Gy	0.05
D _{min}	42.797 ± 3.197 43.761 Gy	43.004 ± 2.883 43.916 Gy	42.207 ± 3.248 43.093 Gy	0.52
V _{98%}	92.328 ± 4.811 93.357 %	96.749 ± 2.616 97.204 %	84.710 ± 6.338 85.815 %	< 0.01

Table 1.3 – Dosimetric parameters for the heart, for the different techniques, with the Friedman’s p-value. TPS results.

Metric	3D-CRT (Mean ± SD Median)	IMRT (Mean ± SD Median)	HT (Mean ± SD Median)	p-value
D _{mean}	3.195 ± 1.287 3.045 Gy	4.774 ± 0.958 4.942 Gy	3.737 ± 1.457 4.355 Gy	< 0.01
D _{max}	48.293 ± 5.496 49.654 Gy	45.674 ± 4.479 46.182 Gy	48.221 ± 5.310 49.491 Gy	0.02
V _{30 Gy}	3.254 ± 2.389 2.782 %	2.645 ± 1.485 3.030 %	3.658 ± 2.388 4.103 %	0.12
V _{20 Gy}	4.058 ± 2.736 3.787 %	4.674 ± 1.929 5.130 %	4.739 ± 2.954 5.283 %	0.26
V _{10 Gy}	5.269 ± 3.211 5.062 %	10.283 ± 4.254 11.100 %	6.382 ± 3.504 7.002 %	< 0.01
V _{5 Gy}	8.581 ± 4.207 8.220 %	23.245 ± 6.131 25.556 %	11.981 ± 6.800 12.239 %	< 0.01

Table 1.4 – Dosimetric parameters for the contralateral breast, for the different techniques, with the Friedman’s p-value. TPS results.

Metric	3D-CRT (Mean ± SD Median)	IMRT (Mean ± SD Median)	HT (Mean ± SD Median)	p-value
D _{mean}	0.196 ± 0.075 0.175 Gy	0.386 ± 0.138 0.384 Gy	0.238 ± 0.108 0.227 Gy	< 0.01
D _{max}	4.643 ± 2.677 3.907 Gy	7.340 ± 1.997 7.083 Gy	12.535 ± 10.601 9.325 Gy	0.02

Table 1.5 – Dosimetric parameters for the ipsilateral lung, for the different techniques, with the Friedman’s p-value. TPS results.

Metric	3D-CRT (Mean ± SD Median)	IMRT (Mean ± SD Median)	HT (Mean ± SD Median)	p-value
D _{mean}	8.054 ± 1.828 8.716 Gy	9.018 ± 1.042 9.123 Gy	8.187 ± 1.854 8.179 Gy	0.25
V _{30 Gy}	10.913 ± 3.270 11.340 %	8.561 ± 2.150 9.050 %	11.099 ± 3.517 10.430 %	< 0.01
V _{20 Gy}	12.991 ± 3.374 13.275 %	13.424 ± 2.578 13.980 %	13.703 ± 3.908 13.013 %	0.64
V _{10 Gy}	17.524 ± 3.885 17.637 %	26.070 ± 4.965 24.624 %	18.386 ± 4.240 17.586 %	< 0.01

Table 1.6 – Dosimetric parameters for the lungs, for the different techniques, with the Friedman’s p-value. TPS results.

Metric	3D-CRT (Mean ± SD Median)	IMRT (Mean ± SD Median)	HT (Mean ± SD Median)	p-value
D _{mean}	3.697 ± 0.893 4.023 Gy	4.337 ± 0.538 4.256 Gy	3.766 ± 0.903 3.730 Gy	0.09
V _{30 Gy}	4.891 ± 1.481 5.139 %	3.833 ± 0.944 4.009 %	4.977 ± 1.606 4.639 %	0.01
V _{20 Gy}	5.823 ± 1.540 5.889 %	6.020 ± 1.187 6.214 %	6.145 ± 1.785 5.810 %	0.70
V _{10 Gy}	7.868 ± 1.840 7.924 %	11.693 ± 2.360 11.025 %	8.258 ± 1.996 7.979 %	< 0.01

Table 1.7 – Dosimetric parameters for the spinal canal, for the different techniques, with the Friedman’s p-value. TPS results.

Metric	3D-CRT (Mean ± SD Median)	IMRT (Mean ± SD Median)	HT (Mean ± SD Median)	p-value
D _{max}	1.131 ± 0.822 0.637 Gy	3.940 ± 1.411 4.223 Gy	0.981 ± 0.697 0.613 Gy	< 0.01

Table 1.8 – Dosimetric parameters for the liver, for the different techniques, with the Friedman’s p-value. TPS results.

Metric	3D-CRT (Mean ± SD Median)	IMRT (Mean ± SD Median)	HT (Mean ± SD Median)	p-value
D _{mean}	0.123 ± 0.067 0.090 Gy	0.414 ± 0.250 0.439 Gy	0.160 ± 0.131 0.111 Gy	< 0.01
V _{20 Gy}	0.001 ± 0.003 0.000 %	0.005 ± 0.013 0.000 %	0.002 ± 0.008 0.000 %	0.23

Table 1.9 – CI and HI, for the different techniques, with the Friedman’s p-value. TPS results.

Metric	3D-CRT (Mean ± SD Median)	IMRT (Mean ± SD Median)	HT (Mean ± SD Median)	p-value
CI	0.691 ± 0.054 0.683	0.840 ± 0.045 0.844	0.695 ± 0.067 0.699	< 0.01
HI	0.122 ± 0.011 0.122	0.100 ± 0.012 0.103	0.116 ± 0.010 0.116	< 0.01

Table 1.10 – MU, for the different techniques, with the Friedman’s p-value.

Metric	3D-CRT (Mean ± SD Median)	IMRT (Mean ± SD Median)	HT (Mean ± SD Median)	p-value
MU	242.870 ± 8.335 241.300	894.120 ± 136.153 864.050	287.215 ± 35.476 288.350	< 0.01

2. PRIMO results

Table 2.1. – Dosimetric parameters for the PTV, for the different techniques, with the Friedman’s p-value. PRIMO results.

Metric	3D-CRT (Mean ± SD Median)	IMRT (Mean ± SD Median)	HT (Mean ± SD Median)	p-value
D _{mean}	49.782 ± 0.512 49.770 Gy	49.939 ± 0.528 50.088 Gy	53.128 ± 2.821 53.252 Gy	< 0.01
D _{max}	56.024 ± 1.879 55.544 Gy	58.160 ± 2.283 58.234 Gy	60.360 ± 4.331 60.797 Gy	< 0.01
D _{min}	18.231 ± 7.705 18.069 Gy	22.886 ± 6.085 23.713 Gy	17.616 ± 5.586 15.747 Gy	0.02
D _{2%}	53.226 ± 0.549 53.258 Gy	52.981 ± 0.753 53.088 Gy	57.436 ± 3.647 57.490 Gy	< 0.01
D _{95%}	46.658 ± 0.502 46.636 Gy	47.087 ± 0.335 47.090 Gy	48.874 ± 2.263 48.856 Gy	< 0.01
D _{98%}	45.561 ± 0.669 45.685 Gy	45.582 ± 0.242 45.833 Gy	47.786 ± 2.217 47.754 Gy	< 0.01
V _{107%}	1.662 ± 1.392 1.171 %	1.447 ± 1.450 1.060 %	43.899 ± 33.503 48.392 %	< 0.01
V _{95%}	88.785 ± 3.987 88.395 %	92.380 ± 2.444 92.947 %	94.794 ± 7.222 98.437 %	< 0.01

Table 2.2 – Dosimetric parameters for the CTV, for the different techniques, with the Friedman’s p-value. PRIMO results.

Metric	3D-CRT (Mean ± SD Median)	IMRT (Mean ± SD Median)	HT (Mean ± SD Median)	p-value
D _{mean}	50.175 ± 0.516 50.132 Gy	50.314 ± 0.601 50.415 Gy	53.704 ± 2.911 54.003 Gy	< 0.01
D _{max}	55.644 ± 0.860 55.544 Gy	56.958 ± 1.504 56.698 Gy	60.028 ± 4.306 59.860 Gy	0.01
D _{min}	41.720 ± 3.443 42.909 Gy	41.809 ± 2.749 42.168 Gy	44.529 ± 3.606 44.935 Gy	< 0.01
V _{98%}	75.323 ± 9.551 74.611 %	82.068 ± 11.279 86.402 %	91.564 ± 13.432 98.615 %	< 0.01

Table 2.3 – Dosimetric parameters for the heart, for the different techniques, with the Friedman’s p-value. PRIMO results.

Metric	3D-CRT (Mean ± SD Median)	IMRT (Mean ± SD Median)	HT (Mean ± SD Median)	p-value
D _{mean}	3.233 ± 1.272 3.107 Gy	4.803 ± 0.927 5.047 Gy	3.894 ± 1.527 4.512 Gy	< 0.01
D _{max}	48.205 ± 4.300 49.047 Gy	46.499 ± 4.699 46.977 Gy	51.152 ± 5.433 51.722 Gy	< 0.01
V _{30 Gy}	3.439 ± 2.437 2.922 %	2.769 ± 1.522 3.135 %	3.862 ± 2.452 4.327 %	0.39
V _{20 Gy}	4.135 ± 2.756 3.833 %	4.755 ± 1.944 5.147 %	4.793 ± 3.008 5.307 %	0.52
V _{10 Gy}	5.255 ± 3.195 5.136 %	10.017 ± 4.074 11.002 %	6.257 ± 3.408 6.611 %	0.01
V _{5 Gy}	8.178 ± 4.123 7.914 %	19.902 ± 5.509 20.710 %	11.640 ± 6.757 12.142 %	< 0.01

Table 2.4 – Dosimetric parameters for the contralateral breast, for the different techniques, with the Friedman’s p-value. PRIMO results.

Metric	3D-CRT (Mean ± SD Median)	IMRT (Mean ± SD Median)	HT (Mean ± SD Median)	p-value
D _{mean}	0.519 ± 0.092 0.520 Gy	0.894 ± 0.152 0.908 Gy	0.590 ± 0.132 0.569 Gy	< 0.01
D _{max}	5.802 ± 2.755 4.973 Gy	8.595 ± 1.689 8.249 Gy	14.450 ± 13.225 7.855 Gy	0.14

Table 2.5 – Dosimetric parameters for the ipsilateral lung, for the different techniques, with the Friedman’s p-value. PRIMO results.

Metric	3D-CRT (Mean ± SD Median)	IMRT (Mean ± SD Median)	HT (Mean ± SD Median)	p-value
D _{mean}	7.771 ± 1.767 8.360 Gy	8.806 ± 1.028 8.898 Gy	8.117 ± 1.881 8.357 Gy	0.39
V _{30 Gy}	11.067 ± 3.220 11.281 %	8.785 ± 2.066 9.283 %	11.241 ± 3.499 10.690 %	0.21
V _{20 Gy}	13.047 ± 3.336 13.236 %	13.480 ± 2.566 13.971 %	13.683 ± 3.928 13.033 %	0.95
V _{10 Gy}	17.559 ± 3.835 17.548 %	25.127 ± 4.699 24.086 %	18.320 ± 4.160 18.053 %	< 0.01

Table 2.6 – Dosimetric parameters for the lungs, for the different techniques, with the Friedman’s p-value. PRIMO results.

Metric	3D-CRT (Mean ± SD Median)	IMRT (Mean ± SD Median)	HT (Mean ± SD Median)	p-value
D _{mean}	3.713 ± 0.865 4.028 Gy	4.466 ± 0.524 4.441 Gy	3.887 ± 0.914 3.830 Gy	0.16
V _{30 Gy}	4.969 ± 1.457 5.118 %	3.939 ± 0.908 4.106 %	5.048 ± 1.600 4.761 %	0.21
V _{20 Gy}	5.859 ± 1.521 5.948 %	6.056 ± 1.180 6.224 %	6.148 ± 1.798 5.893 %	0.64
V _{10 Gy}	7.898 ± 1.812 7.909 %	11.293 ± 2.238 10.554 %	8.243 ± 1.960 8.011 %	< 0.01

Table 2.7 – Dosimetric parameters for the spinal canal, for the different techniques, with the Friedman’s p-value. PRIMO results.

Metric	3D-CRT (Mean ± SD Median)	IMRT (Mean ± SD Median)	HT (Mean ± SD Median)	p-value
D _{max}	1.144 ± 0.824 0.586 Gy	4.286 ± 1.484 4.468 Gy	1.021 ± 0.717 0.569 Gy	< 0.01

Table 2.8 – Dosimetric parameters for the liver, for the different techniques, with the Friedman’s p-value. PRIMO results.

Metric	3D-CRT (Mean ± SD Median)	IMRT (Mean ± SD Median)	HT (Mean ± SD Median)	p-value
D _{mean}	0.294 ± 0.083 0.264 Gy	0.695 ± 0.267 0.693 Gy	0.347 ± 0.148 0.283 Gy	< 0.01
V _{20 Gy}	0.001 ± 0.004 0.000 %	0.004 ± 0.010 0.000 %	0.002 ± 0.007 0.000 %	0.45

Table 2.9 – CI and HI, for the different techniques, with the Friedman’s p-value. PRIMO results.

Metric	3D-CRT (Mean ± SD Median)	IMRT (Mean ± SD Median)	HT (Mean ± SD Median)	p-value
CI	0.679 ± 0.057 0.661	0.813 ± 0.034 0.821	0.643 ± 0.074 0.645	< 0.01
HI	0.154 ± 0.013 0.122	0.142 ± 0.013 0.142	0.180 ± 0.028 0.175	< 0.01

3. ECMP e-poster



IPOPORTO
INSTITUTO PORTUGUÊS DE ONCOLOGIA DO PORTO FG, EPE

José Mesquita^{3,*}, N. Pereira², A. R. Pinho², J. Lencart^{1,2}, A. G. Dias^{1,2}

(1)Medical Physics, Radiobiology, and Radiation Protection Group, IPO Porto Research Center (CI-IPOP), Portuguese Oncology Institute of Porto (IPO Porto), Porto, Portugal
 (2)Medical Physics Department, Portuguese Oncology Institute of Porto (IPO Porto), Porto, Portugal
 (3)Departamento de Física e Astronomia, Faculdade de Ciências, Universidade do Porto, Porto, Portugal
 * josemesquita_outlook.pt

INTRODUCTION

There are different approaches to employ radiotherapy for conservative breast cancer treatment. The purpose of this work was to analyze and compare cumulative dose-volume histograms (DVH) and dosimetric parameters of treatment plans calculated in the treatment planning system (TPS) Eclipse using three delivery techniques; Conformal Radiotherapy (3DCRT), Intensity Modulated Radiotherapy (IMRT), and a hybrid technique (HT), currently under development.

MATERIALS & METHODS

3DCRT, IMRT and HT treatment plans for 15 left-sided (LS) breast cancer patients were calculated on the TPS. A dose of 50 Gy in 25 fractions to the Planning Target Volume (PTV) was prescribed. The first stage of this comparative study consisted on a thorough statistical analysis of the 3DCRT, IMRT and HT plans performed using Python scripts, in order to assess the impact of each technique on the plan, namely PTV coverage and dose homogeneity, and dose to critical organs at risk (OAR).

The DVH were exported from the TPS in tabular format and, for each technique and structure, the DVH of all patients were converted into a single point-wise mean histogram and its respective standard-deviation (SD). Depending on the analyzed structure, the dosimetric parameters retrieved from the data were the mean dose (D_{mean}), maximum dose (D_{max}), minimum dose (D_{min}), minimum dose absorbed by a percentage volume of 2%, 50%, 95% and 98% ($D_{2\%V}$, $D_{50\%V}$, $D_{95\%V}$, $D_{98\%V}$), volume receiving at least 95%, 98%, and 107% of prescribed dose ($V_{95\%}$, $V_{98\%}$, $V_{107\%}$) and 5, 10, 20, and 30 Gy (V_5 , V_{10} , V_{20} , V_{30}). Also, conformity and homogeneity indices (CI and HI) were calculated and defined as suggested by Paddick (2000) and ICRU Report 83 (2010).

The legitimacy of the results was determined by the Friedman hypothesis test, which evaluates the trueness of the statement «there is at least one technique that yields a statistically significant difference in the results when compared with the others», and a further pairwise scope was provided by the post-hoc Nemenyi test, which pinpoints which plans are different. Both consecutive tests were performed with a significance level of 0.05.

REFERENCES

Paddick I. A simple scoring ratio to index the conformity of radiosurgical treatment plans. Technical note. J Neurosurg. 2000 Dec;93 Suppl. 3:219-22.
 Journal of the ICRU Vol 10 No 1 (2010) Report 83 – Prescribing, Recording, and Reporting Photon-Beam Intensity-Modulated Radiation Therapy (IMRT)

ECMP 2022
17th-20th August 2022, Dublin - Ireland

3DCRT vs. IMRT vs. Hybrid – A Comparative Study In Breast Cancer Patients

RESULTS

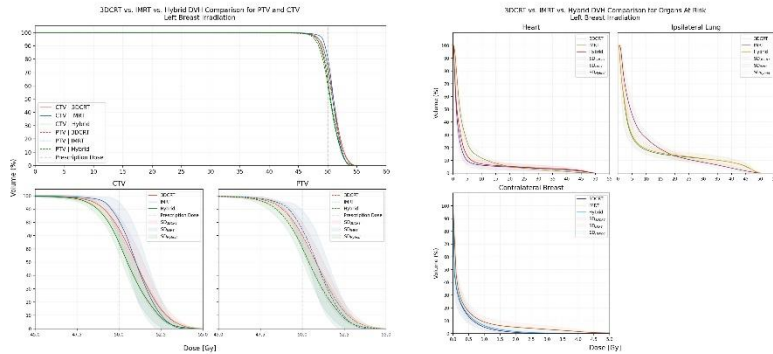


Figure 1 – DVH comparison for PTV and CTV treated with 3DCRT, IMRT and HT. Below, a zoomed view of the curves. **Figure 2** – DVH comparison for some OAR treated with 3DCRT, IMRT and HT.

Table 1 – Dosimetric parameters for different structures and techniques, with the Friedman's p-value.

Metric	3DCRT (Mean ± SD Median)	IMRT (Mean ± SD Median)	HT (Mean ± SD Median)	P-value
PTV				
D_{mean}	50.729 ± 0.440 51.000 Gy	50.763 ± 0.589 50.848 Gy	50.361 ± 0.456 50.000 Gy	0.13
D_{max}	54.423 ± 0.698 54.720 Gy	54.354 ± 0.875 54.248 Gy	53.977 ± 0.807 53.550 Gy	0.42
D_{min}	24.165 ± 8.684 25.096 Gy	28.497 ± 7.570 28.868 Gy	24.706 ± 6.356 24.072 Gy	0.63
$D_{2\%}$	53.467 ± 0.684 53.899 Gy	52.024 ± 0.783 52.833 Gy	53.033 ± 0.658 52.718 Gy	0.03
$D_{50\%}$	48.245 ± 0.507 48.390 Gy	48.029 ± 0.362 48.449 Gy	47.507 ± 0.562 48.034 Gy	0.01
$D_{95\%}$	47.223 ± 0.771 47.399 Gy	47.469 ± 0.116 47.500 Gy	47.179 ± 0.671 47.497 Gy	0.26
$V_{107\%}$	3.377 ± 2.587 4.867 %	0.715 ± 1.211 0.010 %	1.640 ± 2.978 0.003 %	0.007
$V_{95\%}$	97.350 ± 1.651 97.846 %	97.693 ± 0.226 98.000 %	96.383 ± 2.933 97.982 %	0.25
Heart				
D_{mean}	3.559 ± 1.209 3.252 Gy	5.054 ± 0.773 5.330 Gy	4.088 ± 1.270 4.477 Gy	0.005
D_{max}	49.664 ± 0.965 49.673 Gy	46.425 ± 4.228 47.570 Gy	49.566 ± 1.232 49.858 Gy	0.07
V_{30} Gy	3.851 ± 2.404 3.071 %	2.911 ± 1.375 3.329 %	4.091 ± 2.294 4.176 %	0.16
V_{20} Gy	4.792 ± 2.685 3.868 %	6.211 ± 1.866 5.517 %	5.206 ± 2.810 5.324 %	0.94
V_{10} Gy	6.166 ± 3.082 5.346 %	11.860 ± 3.011 12.656 %	7.195 ± 3.197 7.162 %	<0.001
V_5 Gy	9.876 ± 3.838 9.187 %	24.191 ± 4.981 25.498 %	13.601 ± 6.498 12.821 %	<0.001
Contralateral Breast (Right)				
D_{mean}	0.207 ± 0.080 0.193 Gy	0.381 ± 0.147 0.375 Gy	0.240 ± 0.112 0.220 Gy	<0.001
D_{max}	5.249 ± 2.832 4.333 Gy	7.395 ± 2.157 7.293 Gy	13.074 ± 10.374 11.974 Gy	0.02
Ipsilateral Lung (Left)				
D_{mean}	8.218 ± 1.690 8.693 Gy	9.203 ± 0.981 9.207 Gy	8.450 ± 1.781 8.483 Gy	0.34
V_{30} Gy	11.314 ± 3.137 11.987 %	8.498 ± 2.009 8.977 %	11.440 ± 3.669 10.254 %	0.002
V_{20} Gy	13.543 ± 3.131 13.641 %	13.587 ± 2.746 14.348 %	14.170 ± 3.825 13.282 %	0.94
V_{10} Gy	18.088 ± 3.582 17.263 %	27.438 ± 4.763 28.448 %	19.038 ± 4.053 19.678 %	<0.001

For the PTV, IMRT delivered the lowest D_{max} , being significantly different from 3DCRT ($P = 0.03$); IMRT deposited the greatest $D_{95\%}$, different from HT ($P = 0.01$); 3DCRT resulted in the largest $V_{107\%}$, different from both IMRT and HT ($P = 0.03$ and $P = 0.02$, respectively).

For the heart, IMRT resulted in the highest and more detrimental mean dose, compared with both 3DCRT and HT ($P = 0.005$ and $P = 0.046$); IMRT was a lot worse in terms of volume inside the 10 and 5 Gy isodose curves (low dose regions), compared with both 3DCRT and HT ($P = 0.001$ and $P = 0.002$ for V_{10} Gy, $P = 0.001$ and $P = 0.005$ for V_5 Gy).

For the contralateral breast, IMRT deposited a higher mean dose, compared with 3DCRT and HT ($P = 0.001$ and $P = 0.03$); 3DCRT was more conservative in terms of maximum dose, compared with IMRT and HT ($P = 0.046$ and $P = 0.03$).

For the ipsilateral lung, IMRT deposited at least 30 Gy to a narrower volume, compared with 3DCRT and HT ($P = 0.005$ and $P = 0.01$); for lower dose regions (namely, inside the 10 Gy isodose line), IMRT behaved worse than 3DCRT and HT, irradiating a much larger volume ($P = 0.001$ and $P = 0.003$).

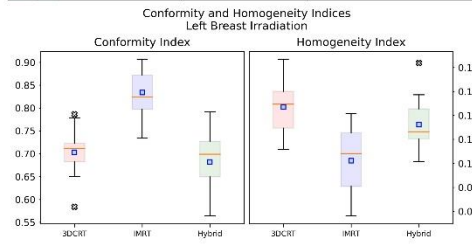


Figure 3 – Boxplot distributions of the conformity and homogeneity indices achieved with the three techniques: Orange dash: median; blue square: mean; x mark: outliers (points \notin [Q1 – 1.5 IQR, Q3 + 1.5 IQR]).

DISCUSSION & CONCLUSIONS

IMRT indeed provided better target coverage, retaining the dose delivery to desired levels of homogeneity and conformity: there were no significant differences between 3DCRT and HT. Also, considerable hotspots on the PTV that are present when 3DCRT is applied shrink with HT and nearly disappear with IMRT. In general, the results show that IMRT may end up causing late radiation exposure complications since it is the technique that yields wider low-dose regions on the OAR (3DCRT and HT do not seem to differ significantly in low-dose volumes, though); on the other hand, e.g. IMRT was more conservative in terms of high-dose regions on the ipsilateral lung, evidenced by the smaller size of the 30 Gy isodose region when compared to 3DCRT and HT (these two techniques did not show significant differences). Both for the heart and the contralateral breast, 3DCRT and HT also did not show evidence of any kind of divergence regarding mean dose, while IMRT delivered higher doses to those organs, imposing a need for proper and careful deliberation prior to going ahead with IMRT for its advantages in terms of conformity, homogeneity and smaller low-dose regions. It is also important to note that 3DCRT resulted in a lower maximum dose to the contralateral breast, compared with IMRT and HT. With this sample of 15 patients, HT did not prove itself to be a major improvement in any aspect, 3DCRT remains a very good technique and a worthy standard, while IMRT can be beneficial in specific cases.

Figure 3.1 – e-poster for the fourth European Congress in Medical Physics 2022, Dublin. Early version of this work, without PRIMO results.